SCINTILLATION TIME COMPONENT STUDIES IN THALLIUM - ACTIVATED SODIUM IODIDE

A Thesis

Submitted to

the Faculty of Graduate Studies

University of Manitoba

In Partial Fulfillment

of the Requirements for the Degree

Doctor of Philosophy

by

William Robert Wall

August 1968

ABSTRACT

An experimental system has been constructed in which the photon sampling technique is used to investigate the scintillation pulse shape of NaI(Tl) under gamma ray stimulation. The effect of temperature on crystals of various thallium concentrations has been studied, resulting in a considerably more detailed description of the time processes involved than has been previously available.

Analysis of the data indicates that the first two microseconds of the scintillation is characterized by at least twelve distinct decay processes, four of which are reported here for the first time. Of the twelve time components four are attributed to one radiative and three metastable states associated with a Tl^+ luminescent centre. Four others are characteristic of the pure sodium iodide crystal, one of which may indicate the presence of a stoichiometric excess of iodine. Three processes are ascribed to the thallium dimer or other multiple thallous ion centres. Energy transport in the crystal is suggested as the twelfth process.

A simple empirical model for the kinetics of the Tl^+ luminescence is suggested although the complexity of the gamma luminescence is shown to be difficult to interpret unambiguously. The thermal equilibrium theory of kinetics that has recently been advanced seems to be inappropriate for the case of NaI(Tl).

ACKNOWLEDGEMENTS

The author wishes to express sincere thanks to his research director, Dr. K. I. Roulston, the University of Manitoba. Throughout the whole period of this study his friendly guidance and discerning criticism have proved invaluable.

Thanks are also extended to Dr. I. Cooke and the members of his research group for the many fruitful discussions we have had.

The author is indebted to the Harshaw Chemical Co. for supplying some of the crystals used in this study.

The financial assistance of the Defence Research Board, the National Research Council and St. Paul's College is gratefully acknowledged.

CONTENTS

LIST OF FIGURES

LIST OF TABLES

CHAPTER I

INTRODUCTION

Of fundamental concern in the study of luminescence is the determination of the time dependence of the emission. Since the scintillation pulse shape contains the past history of energy transfer and storage in the crystal, it can be expected to yield information not only on the characteristic mean lives of the various states present but also details concerning the interrelations between such states. In practice it is not possible to describe completely the nature of the scintillation process from the behaviour of the pulse shape since the latter cannot be determined exactly. It is this lack of precision in the determination of the pulse shape that has, until quite recently, severely limited the use of the time dependence as a predictor of the scintillation mechanism.

The experimental problem that is of concern in this work is the measurement of the time dependence of the rate of emission of photons produced by a scintillator crystal which has been excited through the absorption of a gamma ray. The total absorption of a one MeV gamma ray in a crystal of sodium iodide doped with approximately 0.1% molar thallium will result in the production, at room temperature, of roughly fifty thousand visible and near-visible photons (Pertsev et al, 1965). This emission refers to the fluorescence and short-lived phosphorescence which is virtually complete in a time of a few microseconds and ignores the presence of long-lived phosphorescence which may take hours to disappear (Cameron et al, 1962; Emigh and Megill, 1954). The purpose of the experiment is to obtain the time of emission of each of these photons with respect to the time of absorption of the incident gamma ray.

Measurements of luminescence lifetimes have been made on various materials for more than forty years. What the early experimenters lacked in the way of sophisticated electronics was almost made up by their ingenuity. In a review article, Perrin (1929) makes mention of several techniques. A synchronous spark was used to illuminate a radial strip of anthracene deposited on a rotating wheel. An upper limit to the lifetime of anthracene was found to be 6 microseconds. A related method was the photographic recording of the luminous path length of a high speed jet of luminescent solution. Gaviola (1926) used a Kerr-cell technique to determine that the fluorescence lifetime of Rhodamine B in water was 2.5 nanoseconds. Perrin (1926) used an indirect technique to infer that the lifetime of fluorescein dye was 4.3 nanoseconds. This involved a calculation based on the disorientation that is characteristic of Brownian movement and predicted the effect of the viscosity of the solvent on the degree of polarization of the emission (in which the decay time of the excited state is a parameter). Delorme and Perrin (1929) describe a modification of Becquerel's phosphoroscope with which fluorescent lifetimes of uranium salts were measured in the 100 microsecond region.

The removal of the shrouds of secrecy from the World War II development of the photomultiplier (PM) tube resulted in the resurrection of the scintillation counter technique which, in its visual form, was a mainstay of research in nuclear physics for the first thirty years of this century. The introduction of the photomultiplier not only ushered in a new era in experimental nuclear physics but also resulted in equally radical modifications to techniques in the study of luminescence. As well, under the spur of practical applications in nuclear physics, research on a vastly expanded scale in the field of new scintillators produced, as a byproduct, a wealth of data in the field of luminescence.

The classical technique for luminescence time studies developed during this past twenty years around the observation of the emission by a photomultiplier whose output is displayed on an oscilloscope. Because of the nature of the emission, the N photons of a scintillation are not emitted simultaneously. For monomolecular processes, the photon emission intensity has a function form F(t) (in photons/sec) which can be expressed as a sum of exponential time functions:

$$(1.1) \qquad F(t) = \sum_j A_j \exp(-t/\tau_j)$$

$$(1.2) \qquad N = \int_0^\infty F(t)\, dt$$

where τ_j is the lifetime of the j^{th} component.

The continuous function (1.1) represents the intensity at any time t, averaged over many scintillations. The PM converts this flux of N photons into a time correlated current pulse containing M electrons. Although the photoelectric and secondary emission processes in the PM tube are virtually instantaneous (less than 10^{-10} sec), relatively long variable times are involved in electron transit down the tube (about 36 ± 2 ns total transit time for the 56AVP at 2500 V). Statistical fluctuations in the transit time have been extensively investigated.

These fluctuations determine the time distribution of the arrival at the anode of the M electrons relative to t = 0, the time of excitation of the crystal. Further modification of the electron pulse shape is due to the time constant of the PM anode circuit and to the final display on the oscilloscope. For a successful application of the photomultiplier/oscilloscope technique, not only must the distortions of

the measuring system be negligible (or removable) but as well signal averaging is generally required to smooth statistical fluctuations.

In the simplest version of the technique (Bonanomi and Rossel, 1951) a large load resistor is used in the anode of the PM with the result that the voltage pulse displayed on the oscilloscope is effectively the time integral of the PM current. It is presumed that the scintillation emission intensity, equation (1.1), has but one exponential term. Then the rise time (10% to 90%) of the oscilloscope trace is equal to 2.2 τ. A variation of this version, used, for example, by Storey et al (1958), involves photographing the integrated single scintillation traces, enlarging them, and carefully differentiating the enlargements to obtain the form of the emission intensity. A second version, used, for example, by Eby and Jentschke (1954) involves the use of a very small PM load resistor (170 ohm). In this case the resultant voltage pulse will follow the PM current pulse if the anode time constant is much less than any of the time constants present in the current pulse (i,e less than any of the τ_j in equation 1.1). Signal averaging was obtained by photographing single traces and summing some 75 traces at 20 ns intervals. Other versions more specifically designed to study nanosecond fluorescence may be found in the literature. These include the pulse amplitude method of Bittman et al (1952) and Wall (1956), the pulsed crystal method of Phillips and Swank (1953), and the pulsed multiplier method of Singer et al (1956).

In all of these experiments, the weak link in the measurement chain has been the oscilloscope, either because of its insufficient frequency response or because of its relatively small dynamic range. The amplitude of the PM pulse can be measured with fair precision over

at most one decade. Time information, at best, is good to one or two percent. The necessary statistical averaging can be accomplished in one of two ways. In the first way individual traces are summed. This is tedious unless done photographically, in which case the measurement is hampered by the resultant broad trace. The second way is to use a long time constant at the PM anode. This integration suppresses statistical fluctuation but unfortunately also masks any fine details present in the emission. In general only the lifetime of the main emission component is obtainable with perhaps an indication of other mean lives if they are sufficiently strong.

Despite these limitations the photomultiplier/oscilloscope technique has produced most of the data currently available on alkali-halide scintillation lifetimes. A representative selection of the results of such experiments is found in Table 1.1.

The introduction of the photon sampling by Bollinger and Thomas (1961) resulted in an order of magnitude improvement in the determination of scintillation pulse shapes. This technique, which essentially determines the time of emission of each photon in a scintillation, is a modification of the method of delayed coincidences used by Lundby (1950). Because of its extremely good time resolution, the photon sampling method has been extensively used in studies of the fast emissions in plastic and liquid scintillators (Koechlin, 1964; McGuire et al, 1965; Kirkbride et al, 1967; Kuchnir and Lynch, 1968) but has not seen much application in the case of the longer emissions characteristic of the alkali-halides.

Table 1.1

Summary of the Results of Previous NaI(Tl) Investigations

(room temperature unless otherwise noted)

AUTHOR	EXCITATION	DECAY TIME (ns)	COMMENTS
Hofstadter (1949)	γ	250 ± 25%	
Bonanomi and Rossel (1951)	γ	320$^{\Delta}$	$(5 \times 10^{12}:0.38)^{\S}$ Monocrystal
			$(8 \times 10^{11}:0.30)^{\S}$ Powder
Bonanomi and Rossel (1952)	α	130	$(3.2 \times 10^{13}:0.41)^{\S}$ Y_2
Eby and Jentschke (1954)	α,γ,d	I 240	dependent on Tl concentration
		II 59	rise time component
Plyavin' (1958)	spark	220 ± 10	$(13 \times 10^{6}:0.026)^{\S}$
Plyavin' (1959)	spark	220	$(15 \times 10^{6}:0.028)^{\S\Delta}$
	γ	I 330	$(11 \times 10^{7}:0.099)^{\S\Delta}$
		II	$(4.5 \times 10^{7}:0.054)^{\S\Delta}$
Owen (1959)	γ	250	
	α	250	noted a complex front
Koch et al (1959)	γ	250	time for 63% of total light
	α	180	
Startsev et al (1960)	γ	I 250	
		II 700 to 1200	5 to 10% of total light
Robertson and Lynch (1961)	γ	I 230 ± 10	
		II 1500 ± 80	43% of total light
Bollinger and Thomas (1961)	γ	I 230	noted multiple components
Bergsøe et al (1966)	γ	200	
Lynch (1966)	spark	6.2 ± 1.5	spike at 77°K in 325 nm emission band

§ – (frequency factor in sec^{-1}: activation energy in eV)

Δ – estimates from published graphs

CHAPTER II

THE PHOTON SAMPLING TECHNIQUE

2.1 Introduction

The determination of the scintillation pulse shape ideally involves the measurement of the time of emission of each of the photons of a single pulse. Since it is not practical to deal with each photon, the photon sampling technique severely attenuates the light flux from the crystal so that the probability of the attenuated pulse having more than one photon per scintillation is small. The time of arrival of a single photon in the attenuated pulse relative to the start of the unattenuated pulse can be measured with good precision. Thus the problem of determining the time of emission of several thousand photons in a single pulse is replaced by the equivalent problem of determining the time of emission of single photons statistically sampled from millions of pulses.

Although the technique was first introduced by Lundby in 1950, the efficient use of the method required the development of two electronic devices, the multichannel pulse height analyser (PHA) and the time-to-amplitude converter (TAC). The essential parts of the photon sampling experiment are shown in the block diagram of fig. 2.1. In this figure the scintillator under test is in good optical contact with PM 1 which produces trigger signals coincident with the rising front edge of gamma induced scintillations. PM 2 is shielded from the scintillator so that it receives rather less than one photon, on the average, for each scintillation in the crystal. This photomultiplier has sufficient gain to produce trigger pulses from single photoelectrons ejected from its photocathode. The time interval between the zero-time trigger from PM 1 ('Start' signal) and the trigger from PM 2 ('Stop' signal) is transformed into an analogue voltage pulse by the TAC. These voltage pulses are analysed and stored in the PHA and the

Figure 2.1

Simplified Block Diagram of the Photon Sampling Experiment

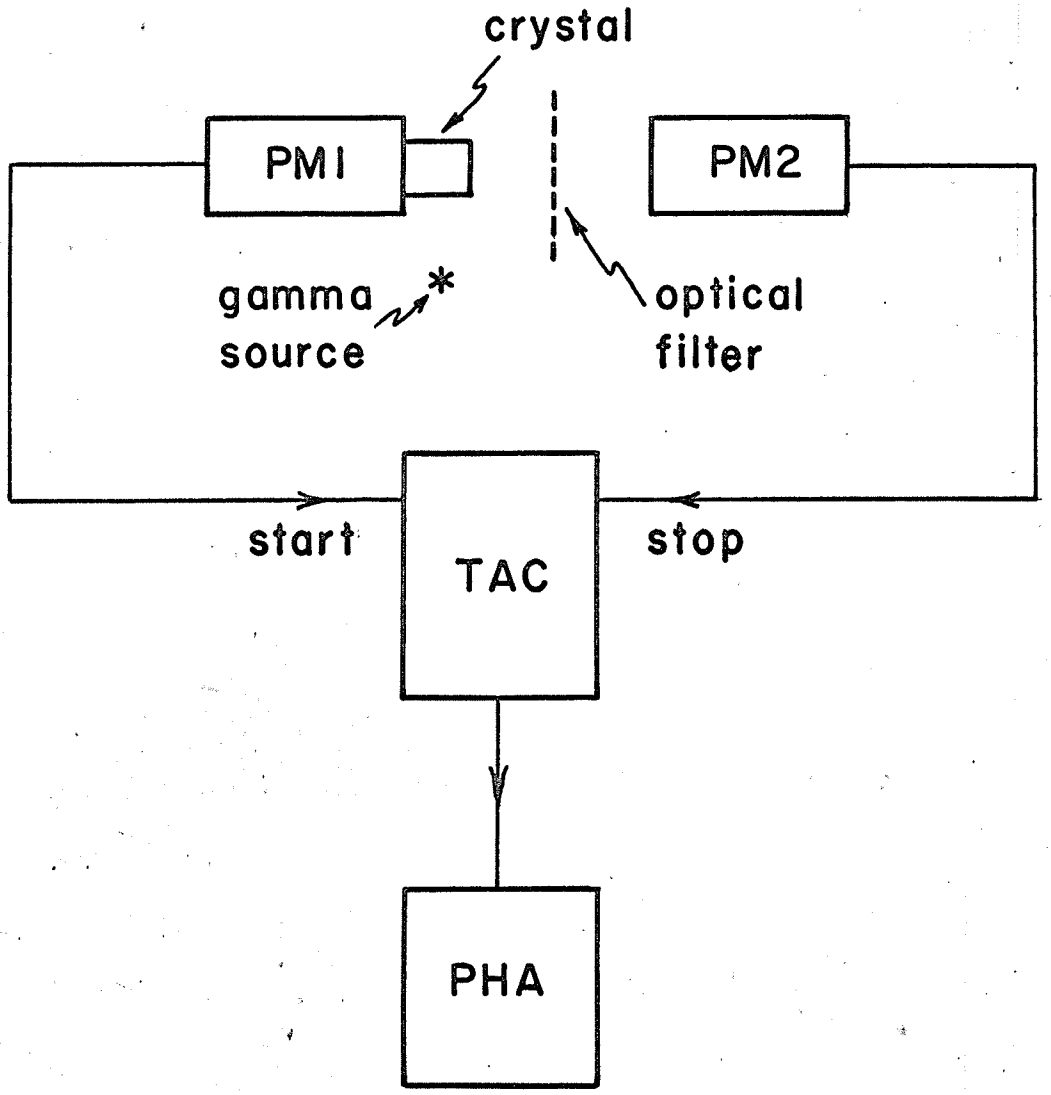
crystal
PM1
PM2
gamma
source
optical
filter
start
stop
TAC
PHA

spectrum obtained is essentially the shape of the average gamma-induced scintillation. A more detailed description of the apparatus will be given in Chapter III.

This type of measuring system produced a representation of the time variation being investigated. We are interested in the differences between this representation and the true time variation. Four distinct properties of the measuring system result in a representation which is a distortion of the true time variation.

2.2 Factors Affecting Distortion

Most time-to-amplitude converters are capable of measuring only one event at a time, i.e., they will produce an output more or less proportional to the time interval between a start signal and a stop signal. In the case of a phenomenon where an initial start is to be correlated with possibly more than one stop, the TAC will measure the time interval to the first stop and will ignore the possible presence of subsequent stops. As a result the observed time variation will, in general, differ from the true time variation. This type of distortion is commonly referred to as being due to "dead time losses".

The analogue to digital conversion and storage in multichannel pulse height analysers introduces another effect. In the conversion process all pulses in a certain range of heights are stored in a single channel, i.e. the channel width is finite. Thus the time spectrum being analysed is effectively integrated over small time regions and a histogram is produced which is usually not the same form as the time variation. We refer to this as a distortion to finite channel width.

Inherent in any measuring system is the presence of nonlinearity. It is apparent that the presence of a nonlinear analogue conversion of the

time interval in the TAC or a nonlinearity in the subsequent multichannel analyser conversion will result in a distortion of the representation of the time spectrum being studied.

The final system property resulting in a distortion is that of time jitter in the measurement. By this we mean, if the system were called upon to measure an exactly constant time interval between start and stop the measured representation would be a distribution of times centred on the true single time interval. This effect is said to be due to the finite width of the system response function.

In the subsequent subsections of this chapter each of the above system characteristics is examined in some detail. The nature of the resultant distortion is obtained so as to allow for its removal when necessary.

2.3 Dead Time Losses

The property of the time analysis that is central to the discussion of this section is the fact that the apparatus cannot measure two time differences simultaneously. This characteristic is a defect when the phenomenon under investigation inherently involves the possibility that two or more time intervals require simultaneous analysis. If this is the usual state of affairs the system may not be of much use but if the probability of multiple measurements is sufficiently small and random, then elementary statistical theory can be used to predict the form of the distortion due to the missing measurements.

To further describe the problem we define an event to consist of a start signal together with zero, one or more correlated stop signals. Note that if the probability of multiple stops is to be small, this implies

that the probability of having an event consisting of a start and no stop is quite high. Fig. 2.2 indicates the classification of events according to multiplicity. Fig 2.2 (a) shows an event of multiplicity one, in which case the measuring system records the time t_1. Fig. 2.2 (b) shows an event of multiplicity zero wherein no time measurement is made. Fig 2.2(c) is an example of a higher multiplicity event in which case the time interval t_2 is recorded but t_3 is lost. In these figures T represents the maximum analysis of the measuring system.

Suppose that a large number of events is studied. Let this number, which is the number of starts, be denoted by S. In these S events there will have occurred a number of stops, say N, and a number of analyses, M. Note that a system capable of measuring multiple events would have analysed N intervals and not the smaller number M. Also note that M is the number of non - zero events. We presume that $S >> N > M$.

For any event let the probability of getting a stop in the time dt after a time interval t be denoted by p(t) dt. It is the purpose of the experiment to measure this true time variation p(t). Because of dead time losses the system will produce a distorted representation which is referred to as q(t). We wish to obtain the relation between the two distributions p(t) and q(t).

Let w represent the probability of obtaining a stop anywhere in the time interval T. Then:

$$(2.1) \qquad w = \int_0^T p(t)\, dt$$

If one presumes that the events are independent of each other and that the probability of more than one stop in an event is small, then the probability distribution of event types will be the Poisson distribution.

Figure 2.2

Classification of Events

(a) Multiplicity One

(b) Multiplicity Zero

(c) Multiplicity Two

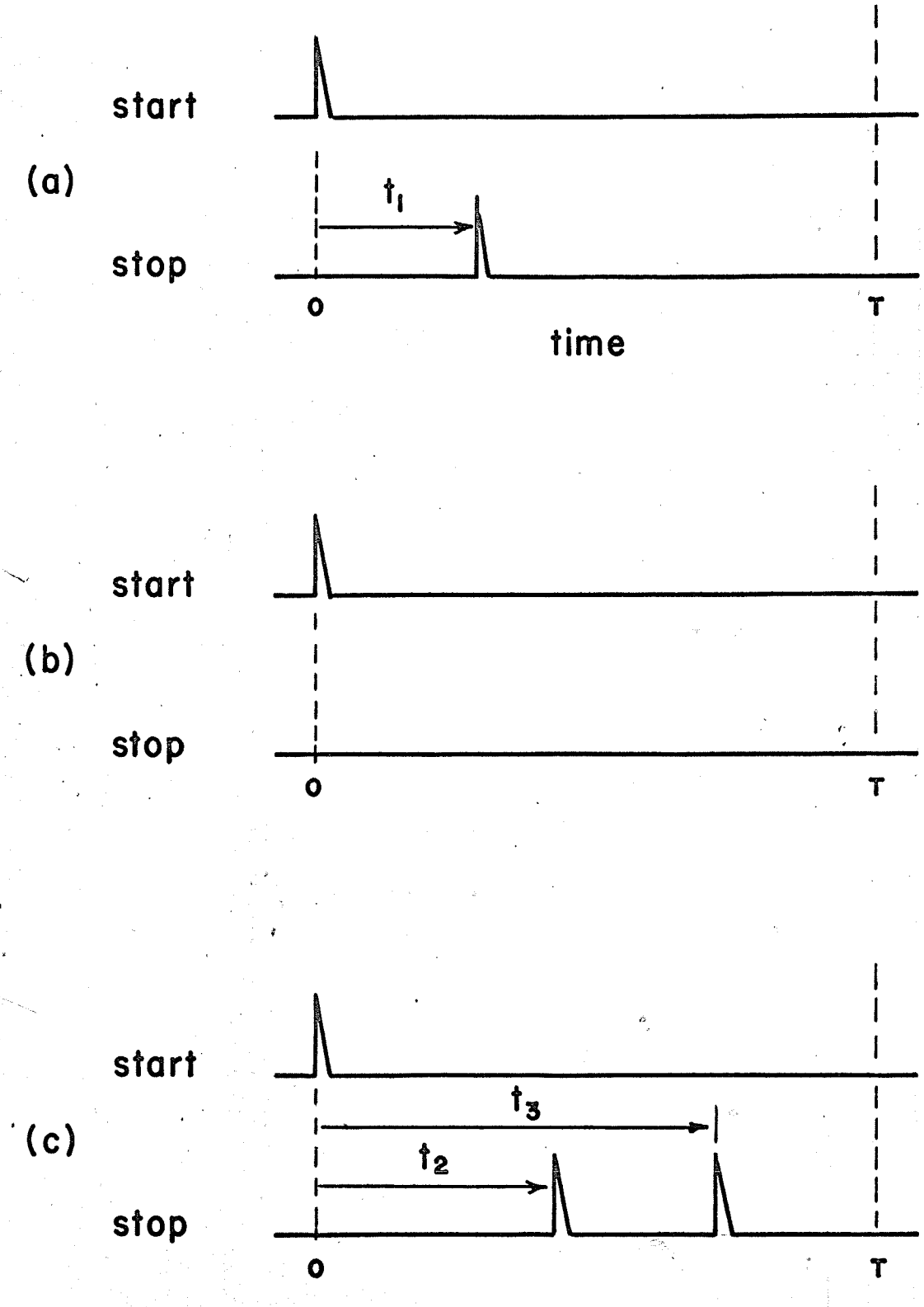
start
(a)
t_1
stop
0
T
time
start
(b)
stop
0
T
start
t_3
(c)
t_2
stop
0
T

Then, in the time interval up to T,

(2.2)
e^{-w} is the probability of occurence of a zero event,

$w\, e^{-w}$ is the probability of occurrence of a single event,

$w^2\, e^{-w}/2!$ is the probability of occurrence of a double event,

$w^x\, e^{-w}/x!$ is the probability of occurrence of an event of multiplicity x.

Then w can be expressed as:

(2.3)
$$w = 0\ (e^{-w}) + 1\ (w\, e^{-w}) + 2\ (w^2\, e^{-w}/2!) + \ldots\ldots$$
$$= \Sigma \times w^x\, e^{-w}/x! \qquad x = 0, \infty .$$

In the form of equation (2.3), w is expressed as a sum of contributions each of the form: the probability of an event of multiplicity x times x, the number of stops in such an event.

In the time interval up to t, the probability of not having a stop is simply given by the probability of a zero event in this smaller time interval, i.e. is:

(2.4) $$\exp\ (-\int_0^t p(t)\ dt)$$

Then the probability, q(t) of measuring a stop in the time dt after a time interval t will be given by the probability of there being no earlier stop times the probability of a stop arriving in the range dt, i.e.:

$$q(t)\ dt = \exp\ (-\int_0^t p(t)\ dt)\ p(t)\ dt$$

Thus the required relationship is:

(2.5) $$q(t) = p(t)\ \exp\ (-\int_0^t p(t)\ dt)$$

It is to be noted that the probability of not having an earlier stop can be obtained from the q(t) distribution since it is the distribution of first stops. That is:

(2.6) $$\exp\ (-\int_0^t p(t)\ dt) = 1 - \int_0^t q(t)\ dt$$

Then equation (2.5) becomes:

$$q(t) = p(t)\ (1 - \int_o^t q(t)\ dt)$$

or:

$$p(t) = q(t)/(1 - \int_o^t q(t)\ dt) \tag{2.7}$$

Relation (2.5) and its inverse (2.7) are useful, the former to predict a distortion, and the latter to correct an experimental distribution for distortion. Since it is generally more convenient to express these relations in terms of the distribution of multichannel analyser pulses which would be obtained in the analysis of S events, let us denote the spectrum displayed by the analyser by r(t). Then:

$$q(t) = r(t)/S$$

If the corresponding true distribution function is f(t), then:

$$p(t) = f(t)/S$$

Also: $w = N/S$

Then equations (2.5) and (2.7) become, respectively:

$$r(t) = f(t)\ \exp\ (-\frac{1}{S}\int_o^t f(t)\ dt), \tag{2.8}$$

$$f(t) = r(t)/(1 - \frac{1}{S}\int_o^t r(t)\ dt). \tag{2.9}$$

To be more precise, the integrals in the above equations should be replaced by discrete summations since multichannel analyser displays are in terms of channels. Thus:

$$\frac{1}{S}\int_0^t f(t)\,dt \rightarrow \frac{1}{S}\left(\sum_{j=1}^{i-1} f_j + f_i/2\right)$$

wherein the indices refer to time in terms of channel number. Thus equations (2.8) and (2.9) become, respectively:

$$(2.10) \qquad r_i = f_i \exp\left[-\frac{1}{S}\left(\frac{1}{2} f_i + \sum_{j=1}^{i-1} f_j\right)\right]$$

$$(2.11) \qquad f_i = r_i/\left[1 - \frac{1}{S}\left(\frac{1}{2} r_i + \sum_{j=1}^{i-1} r_j\right)\right]$$

Relation (2.11) has been used by Bollinger and Thomas (1961), by McGuire et al (1965) and by most other experimenters engaged in this form of experiment to correct their experimental curves for dead time losses. Relation (2.10) has been reported by Wall and Roulston (1965) and has been found useful in the assessment of the characteristics of dead time distortions.

2.4 Applications

It is of some interest to examine the effects of dead time losses on two particular types of time distributions.

The example of the distribution f(t) being a constant in time has application in the study of noise and also in the calibration of the measuring system. If f(t) = A, a constant, then, using equation (2.8):

$$(2.12) \qquad f(t) = A \exp(-A\,t/S)$$

Thus if the real time variation is a horizontal straight line in time, the measured distribution will be exponential of time constant S/A.

This prediction has been subjected to experimental verification. To achieve a time distribution in which all time intervals are equally probable, a random source of pulses (from a PM tube) was used to

activate the stop input of a time converter system. A second source of pulses, completely uncorrelated with the stop source was used to activate the start input of the system. Since a random time stop source is used, the presence of dead time losses is insured. One observes a time distribution r(t) which is exponential and of time constant S/A (within the limits of experimental precision).

In most experiments, noise will be present on the stop input and, as the above theory shows, will result in the presence of an exponential term in the observed r(t). However, in most cases, S, the total number of events analysed, will be much larger than A, the number of random background measurements in an initial channel of the distribution r(t). In typical experiments S/A is of the order of 10^5. Thus the time constant of the noise spectrum would be 10^5 channels. This would be observable in analysers having 400 channels as a 0.4% drop in background over the range of the analyser.

The obtaining of a random spectrum is frequently used to determine the nonlinearity of the system and/or determine the time calibration, i.e. the width of a channel in seconds. There is a distinct danger that the exponential distribution that results will cause significant errors in the results. Bollinger and Thomas (1961) for example, fed periodic pulses into the start of their system and random counts into the stop. If useful statistics were obtained in reasonably short times, in all probability fairly high random count rates were used. It is not inconceivable that the 10% variation in channel widths which they observed was due partially or totally to the exponential nature of r(t) inherent in this technique.

This danger can be completely circumvented by interchanging the two inputs to the TAC, that is, feed the random pulses into the start and the periodic pulses into the stop. Since the stop period must be larger than the maximum analysis time of the system (t), it is categorically impossible to have two or more stops in a single event and dead time losses cannot occur. In this case r(t) would theoretically be a horizontal straight line and any deviation from this can be interpreted unambiguously as being due to system nonlinearity. This form of nonlinearity determination has been used by Weber et al (1956), Chase and Higinbotham (1957), Lefevre and Russel (1959) and others. It is unfortunate that the danger of using random stops in calibration experiments has not been emphasized in the literature.

Another theoretical time distribution of interest, especially in this work, is the exponential one. If one examines the case where:

$$f(t) = a\, e^{-\alpha t} \tag{2.13}$$

then an application of equation (2.8) results in the measured distribution taking the form:

$$r(t) = A\, e^{-\alpha t} \exp\left[-\frac{A}{\alpha S}(1 - e^{-\alpha t})\right]. \tag{2.14}$$

Note that the strength of the distortion term is given by $\exp(-A/\alpha S)$, and if this is to be small then $A/\alpha S$ must be small. The size of this term can be used in a particular experiment to determine whether, or not, a correction for dead time losses is necessary.

2.5 Finite Channel Width

The property of the time analysis system which is central to the discussion of this section is the analogue-to-digital conversion and storage characteristic of the PHA. In this process all pulses in ad-

jacent ranges of heights are stored in consecutive channels. To examine this in more detail let us presume that the width of a time channel is λ seconds and that λ is constant. The case where λ is not constant is dealt with in section 2.6. Let the time spectrum under analysis be denoted by f(t). Then the number of counts in channel number i, r_i, will be given by:

$$(2.15) \qquad r_i = \int_{(i-1)\lambda}^{i\lambda} f(t)\, dt$$

Of particular interest is the case where $f(t) = A\, e^{-t/\tau}$. In this case equation (2.15) becomes:

$$(2.16) \qquad r_i = A\, \tau\, e^{-i\lambda/\tau}\, (e^{\lambda/\tau} - 1),\ i = 1,2,3, \ldots\ldots$$

$$(2.17) \quad \text{or} \qquad r_i = A'\, e^{-i\lambda/\tau}$$

$$(2.18) \quad \text{where} \qquad A' = A\tau\, (e^{\lambda/\tau} - 1).$$

Note that the histogram representation maintains the exponential character of f(t) with an unchanged time constant but that the amplitude A' of the representation is not a simple multiple of A. It may be possible, in certain experiments, to approximate:

$$(2.19) \qquad e^{\lambda/\tau} - 1 \approx \lambda/\tau$$

Then: $\qquad A' \approx A\lambda$

and the histogram representation is faithful since A' is simply a constant times A. However, this approximation may not be very good. For example, if τ were ten machine channels, the error in the approximation would be over 5%. In an experiment where f(t) is made up of sums of exponentials, and measurements of relative intensities are made,

equation (2.18) may be required to remove the effects of finite channel width. Pursuing this a bit further, let us find the area under the histogram representation for N points:

$$I_N = \Sigma A' e^{-i\lambda/\tau} \qquad i = 1, N$$

$$= A' (1 - e^{-N\lambda/\tau})/(e^{\lambda/\tau} - 1) \tag{2.20}$$

If N is effectively infinite:

$$I_\infty = A'/(e^{\lambda/\tau} - 1) = A\tau \tag{2.21}$$

2.6 System Nonlinearity

Following from the discussion in the preceding section we consider next the effects of time scale nonlinearity. The channels of the measuring system have, in general, time widths which are not completely uniform. If λ_i denotes the width of the $i^{\underline{th}}$ channel and λ_1 the width of the first channel then:

$$\lambda_i = \lambda_1 + a_1(i - 1) + a_2(i - 1)^2 + \ldots, \quad i = 1,2,\ldots. \tag{2.22}$$

That is, the variation can be expressed by some sort of polynomial in i. The time to be associated with the $i^{\underline{th}}$ channel is

$$t_i = \Sigma\lambda_j, \quad j = 1, i. \tag{2.23}$$

The measuring system produces a rèpresentation, r_i, of the input function, f(t), which is linear in i and therefore nonlinear in the time t. If the exponential function, $f(t) = A\, e^{-t/\tau}$, is again used as a particular example of an input to the measuring system, then the number of counts in the $i^{\underline{th}}$ channel will be given by:

$$r_i = \int_{t_{i-1}}^{t_i} A\, e^{-t/\tau}\, dt$$

(2.24)

$$= A\, \tau\, e^{-t_i/\tau}\, (e^{\lambda i/\tau} - 1)$$

Both of the exponentials in (2.24) give rise to distortions, the first being the cumulative effect of nonlinearities in all channels up to the $i^{\underline{th}}$, while the second contains only the nonuniformity of the $i^{\underline{th}}$ channel itself.

As to the problem of correcting this distortion, one technique that has been employed (for example by Bollinger and Thomas, 1961; McGuire et al, 1965) is to divide the measured number of counts in a channel by the channel width. If approximation (2.19) is valid, then (2.24) becomes:

(2.25) $$r_i = A\, \lambda_i\, e^{-t_i/\tau}\ .$$

Thus division by λ_i will remove part of the nonlinearity present in (2.25). What is not so apparent is the danger of applying only this correction in the case of a monotonic variation of channel width. If equation (2.22) is a monotonic function of i, then the nonlinearities in the two exponential terms of (2.24) are in opposite senses. The removal of one of them, say by dividing r_i by λ_i results in a worse distortion than was present originally. Hence both terms must be corrected for if a correction is deemed necessary. To remove the nonlinearity in the exponential term of (2.25) requires the association of the data point r_i, not with channel number i, but rather with the t_i of equation (2.23).

Note that if the two corrections mentioned above are applied, the result will still not be quite right in that the division by channel width rests on the validity of approximation (2.19).

In general, considerable care must be taken if a system is sufficiently nonlinear to warrant corrections.

2.7 System Response Effects

The final feature of the measuring system of interest in the study of distortions is that of system response. As was outlined earlier in this chapter, the experimental measurement of a single time interval is characterized by statistical time jitter. This results in a blurring or smearing of the time distribution under analysis.

A physical system can be thought of as a device by which an input function $f(t)$ is transformed into an output function $r(t)$. The system can be characterized by an operator, L, such that L operating on $f(t)$ produces the function $r(t)$, i.e.

$$L[f(t)] = r(t) \tag{2.26}$$

The operator L is presumed to be bounded and linear. We introduce the Dirac delta "function", $\delta(t)$, defined by:

$$\delta(t) = 0 \text{ for } t \neq 0$$
$$\int_{-\infty}^{\infty} \delta(t)\, dt = 1 \tag{2.27}$$

If this delta function is applied to the input of the system, the output function that results is called the system response function (SRF) and will be denoted by $g(t)$. That is:

$$L[\delta(t)] = g(t) \tag{2.28}$$

In other disciplines the SRF will be referred to as a spread function, or as an impulse response function. Note that the SRF, $g(t)$, effectively defines the properties of the operator L, i.e. the behaviour of the system. From its definition in (2.27), it is evident that the delta function plays the role of an identity function in a convolution product, that is:

$$(2.29) \qquad f(t) = \int_{-\infty}^{\infty} \delta(t - y)\ f(y)\ dy = \delta(t) * f(t)$$

Equation (2.26) can be written as:

$$L\left[\int_{-\infty}^{\infty} \delta(t - y)\ f(y)\ dy\right] = r(t)$$

Since L is linear and bounded it can be taken in under the integral:

$$\int_{-\infty}^{\infty} L[\delta(t - y)]\ f(y)\ dy = r(t)$$

If use is made of equation (2.28) then:

$$(2.30a) \qquad r(t) = \int_{-\infty}^{\infty} g(t - y)\ f(y)\ dy$$

Since the convolution product is commutative:

$$(2.30b) \qquad r(t) = g(t) * f(t) = f(t) * g(t)$$

$$= \int_{-\infty}^{\infty} f(t - y)\ g(y)\ dy$$

We have then the well known general result that the response, $r(t)$, of a linear system, to an arbitrary input function, $f(t)$, is given by the convolution product of $f(t)$ and $g(t)$.

It is useful to approximate the integral of equation (2.30b) by a sum. For some suitably small time interval, λ, we can write the approximation:

$$r(t) = \Sigma\lambda\ g(n\lambda)\ f(t - n\lambda), \quad n = 1, \infty.$$

In this expression it is assumed that g(t) is zero for negative times since a real system cannot respond before it is stimulated. If g(t) is small when t is large, as is usually the case, the tail of the infinite series can be discarded:

$$(2.31) \qquad r(t) = \Sigma\lambda\ g(n\lambda)\ f(t - n\lambda), \quad n = 1, M$$

where M is a sufficiently large integer. In this form the system output is given approximately by a certain linear combination of the input and a number of its past values. In other words, r(t) is given approximately by a weighted sum of a set of past values of the input. If r(t) and f(t) are described by their values at $t = i\lambda$, then (2.31) becomes:

$$(2.32) \qquad r_i = \Sigma\ g_n\ f_{i-n}\ , \ n = 1, M.$$

This relation is useful for the particular system of this work since the output is in the form of a histogram.

Of concern is the distorting effect of the SRF on a theoretical distribution. The problem facing the experimenter is the inversion of equation (2.30), i.e. the input function is to be deduced from experimental data on the functions r(t) and g(t).

Of the various inversion methods, one of the most popular can be aptly described by "cut and try". In this method the theoretical form of f(t) is known (or assumed). The parameters in f(t) are varied

judiciously so that f(t) * g(t) fits the experimental r(t) with some precision. Computations for the folding are generally performed on a computer. This procedure has been followed by Bollinger and Thomas (1961), Falk and Katz, (1962), McGuire et al, (1965), Wenzelburger, (1967) and Lynch, (1968). In essence, the same technique was followed by Gold, (1965) to compute pulse amplitude spectral distortions due to pile-up effects.

Perhaps a more useful approach was taken by Herget et al (1962) in which an approximate f(t) is obtained from the experimentally known r(t) and g(t) using an iterative technique. This procedure does not require a prior knowledge of the functional forms involved. In our modification of Herget's procedure, a first approximation to f(t), $f_1(t)$ is obtained from:

$$f_1(t) = 2\, r(t) - r(t) * g(t) \tag{2.33}$$

Subsequent refinements are made by:

$$f_{k+1}(t) = f_k(t) + (r(t) - f_k(t) * g(t)) * g(t) \tag{2.34}$$

It is a general characteristic of this unfolding that statistical fluctuations in the experimental data are accentuated in the predicted f(t). As pointed out by Rautian (1958) the presence of statistics precludes the possibility of obtaining a unique solution for the unfolded function. However, the technique does produce a fair representation of the desired true distribution.

Other techniques that have been applied to the unfolding problem include the method of moments (e.g. Brody, 1957) and the formal inversion of (2.30) via Laplace or Fourier transforms (e.g. Rautian, 1958; Rollett and Higgs, 1962; Stoddart and Berger, 1965).

Another aspect, which has practical importance in this work, is the effect of a SRF on an exponential input function. To assess the nature of this distortion, it is convenient, for the sake of analysis, to assume a Gaussian form for the SRF (in practice it is pseudo - Gaussian). We presume:

$$f(t) = A\, e^{-\alpha t} \quad \text{for } t > 0$$
$$= 0 \quad \text{for } t < 0 \tag{2.35}$$

$$g(t) = (1/\sigma\sqrt{2\pi}) \exp\left[- (t - d)^2/2\sigma^2 \right] \tag{2.36}$$

where: α is the inverse of the exponential time constant τ,

σ is the standard deviation of the Gaussian SRF,

d is a time displacement.

In equation (2.36) the displacement d is presumed sufficiently large so that g(t) is effectively zero for negative times and for times in excess of 2d. Under these conditions, the response of the system, equation (2.30b), becomes:

$$r(t) = \int_0^t A\, e^{-\alpha(t - y)}\, (1/\sigma\sqrt{2\pi}) \exp\left[- (y - d)^2/2\sigma^2 \right] dy. \tag{2.37}$$

After some manipulation this can be put into the form:

$$r(t) = A\, e^{-\alpha t}\, e^{\gamma} \left[\int_{-\infty}^{W} \exp(-x^2)\, dx \right]/\sqrt{\pi} \tag{2.38}$$

where: $W = (t - \beta)/\sigma\sqrt{2}$

$\gamma = [(\alpha\sigma)^2/2] + \alpha d$

$\beta = \alpha\sigma^2 + d$

Equation (2.38) can be expressed in terms of the error function:

(2.39a) for $0 \leqslant t \leqslant \beta$,

$$r(t) = A\, e^{-\alpha t}\, e^{\gamma}\, \frac{1}{2} \operatorname{erfc}\left[(t - \beta)/\sigma\sqrt{2}\right]$$

(2.39b) for $\beta \leqslant t \leqslant \beta + d$,

$$r(t) = A\, e^{-\alpha t}\, e^{\gamma}\, \frac{1}{2}\left\{1 + \operatorname{erf}\left[(t - \beta)/\sigma\sqrt{2}\right]\right\}$$

(2.39c) for $t \geqslant \beta + d$,

$$r(t) = A\, e^{-\alpha t}\, e^{\gamma}$$

The error functions in the above are defined by:

$$\operatorname{erf}(z) = \frac{2}{\sqrt{\pi}} \int_0^z e^{-x^2}\, dx$$

$$\operatorname{erfc}(z) = 1 - \operatorname{erf}(z)$$

These equations require some minor modifications because they are not based on a time zero chosen at the position of the peak of $g(t)$. A new time scale can be defined by:

$$t' = t - d.$$

If this substitution is made (and the prime dropped), the form of equations (2.39) is not altered. It is only required to redefine:

$$\beta = \alpha\sigma^2$$

(2.40)

$$\gamma = \alpha^2\sigma^2/2$$

As well, the ranges of validity of the three equations become:

(a) $-d \leqslant t \leqslant \beta$ (b) $\beta \leqslant t \leqslant \beta + d$ (c) $t \geqslant \beta + d$

The folding of an exponential with a Gaussian was examined by Halling et al (1967). Equation (2.39) does not agree with their result

although it is similar. It would seem that the earlier work did not formulate the problem correctly and is thus in error.

Equation (2.39c) has a practical application since it shows that the exponential time behaviour of the input function is reproduced faithfully in the output at times larger than $\beta + d$ (d is about 4σ). There will be an error in the projected amplitude due to e^{γ}, but this will be less than 1% if $\alpha\sigma < 0.1$.

CHAPTER III

THE EXPERIMENTAL SYSTEM

3.1 Description

The course of this work has seen the development and construction of three experimental systems. Experience gained with the earlier two systems provided the background required to build the third apparatus which is shown in the block diagram of fig. 3.1.

In this figure, the crystal under investigation, X, is in good optical contact with a 56AVP photomultiplier, P1. A conventional avalanche trigger circuit, T1 (see Appendix A-1), working off the last dynode of P1 produces a relatively jitter-free time zero signal whenever a gamma ray is absorbed or partially absorbed in the crystal.

Photomultiplier P2, also a 56AVP, observes the attenuated photon flux, i.e. detects single photons in occasional gamma ray events. P2 is shown in the 90° configuration in this block diagram. In this orientation P2 is able to detect photons scattered out of the edge of the front window of P1. The sample crystal X need then only have one exit window. This unique arrangement thus permits the non-destructive testing of commercially mounted crystals. The apparatus has been designed to allow the mounting of P2 in the 180° configuration with P1 and P2 collinear. In this case the crystal must have a second window to allow a small amount of light to escape to P2. An iris diaphragm, D, permits fine adjustment of the photon attenuation. A second avalanche circuit, T2, produces a trigger signal marking the detection of a single photon by P2. Both photomultipliers were wired with what is essentially the Philips voltage divider type A (Appendix A-2). The voltage of the focussing electrode was set to optimize the single photoelectron pulse height.

Figure 3.1

Block Diagram of the Photon Sampling Apparatus

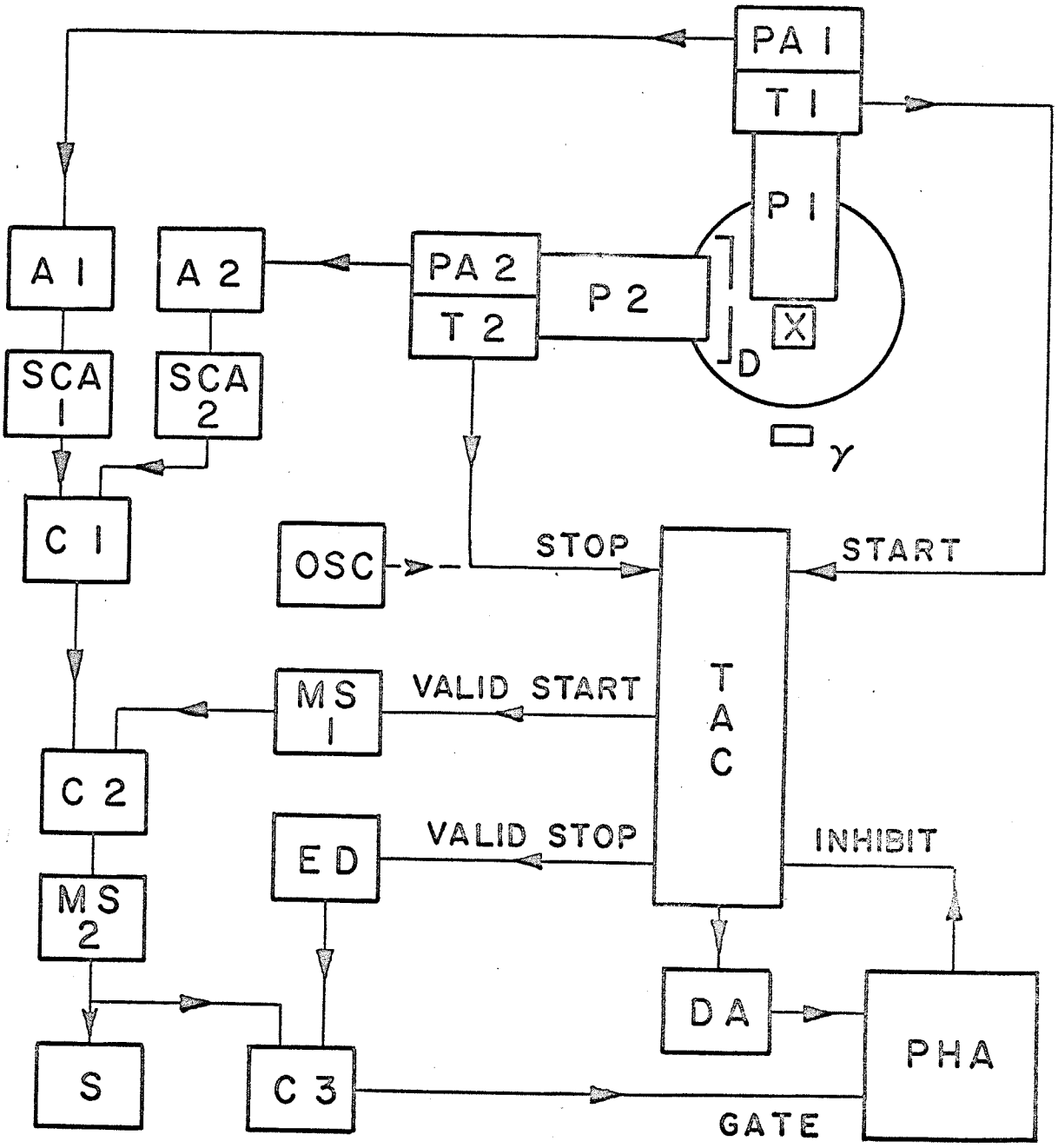
PA 1
T 1
P 1
A 1
A 2
PA 2
T 2
P 2
X
D
γ
SCA 1
SCA 2
C 1
OSC
STOP
START
MS 1
VALID START
TAC
C 2
ED
VALID STOP
INHIBIT
MS 2
DA
PHA
S
C 3
GATE

The time interval between the signals from T1 and T2 is converted into an analogue voltage pulse by the time-to-amplitude converter (TAC). This pulse is transmitted via a two microsecond delayed amplifier (DA) to a pulse height analyser (PHA) for possible storage.

The TAC used in this system is the TH200A manufactured by Edgerton, Germeshausen and Grier. This unit, which is the heart of the system, has several features which experience has shown to be indispensable in experiments of this type (the earlier systems constructed did not use this TAC). The converter is of the "start/stop" type in which the stop cannot be activated unless a preceding start has appeared. An important feature is that TAC overflow (caused by a start signal that is not followed by a timely stop signal) is not read out by the converter but results in quick TAC reset. Both start and stop inputs are disabled if the TAC is in the process of readout or if the unit has been supplied with an inhibit signal. As well the unit provides output logic signals when it has received a valid start (i.e. a start signal which arrives when the TAC is not busy or inhibited) or a valid stop signal. The converter analogue output is a positive or negative square pulse whose width is adjustable. The TAC also has an adjustable dead time. The only feature lacking is a variable delayed readout of valid data (this delay is fixed at 500 ns which is too small).

Both photomultipliers generate linear signals which are taken from dynode nine by preamplifiers, PA1 and PA2, to linear double delay line amplifiers, A1 and A2, for pulse height selection by single channel analysers, SCA1 and SCA2. Channel one is normally set to accept only photopeak pulses from the crystal while channel two is set to reject undersized pulses from P2. If the requirements of both

channels are met, the slow coincidence circuit C1 operates. If the TAC has had a valid start, slow coincidence circuit C2 will trigger the monostable circuit, MS2, and the scaler, S, will count one. If the TAC has received a timely stop from T2, a valid stop will be generated, delayed electronically by ED and slow coincidence circuit C3 will produce a gate to permit storage of the analogue time pulse. The busy signal from the PHA is used to inhibit the TAC while a storage is in process.

The elimination of cross-talk between start and stop channels of this experiment has been a most vexing and time-consuming problem. This cross-talk appears as a short period oscillation on the time spectra and is most serious on converter time ranges under one microsecond. The elimination of this effect was finally achieved by:

(a) using completely separate power supplies for each of T1, T2 and the TAC,

(b) using coaxial cable for the avalanche voltage power lines and filtering these lines at the PM header,

(c) enclosing the photomultipliers in 1/16 inch brass housings as well as the usual magnetic foil shields.

(d) using 1/16 inch steel welded enclosures for the header boxes.

The earlier systems that were built did not have the construction of (c) and (d) above and were not free from cross-talk. The first system, which was worst in this respect, did not have the separate power supplies. Fig. 3.2 shows a photograph of the header/photomultiplier enclosure and crystal chamber.

The entire crystal chamber unit, comprising the two photomultipliers, their trigger and preamplifier circuits and the crystal

Figure 3.2

Photograph of the Crystal Chamber Unit

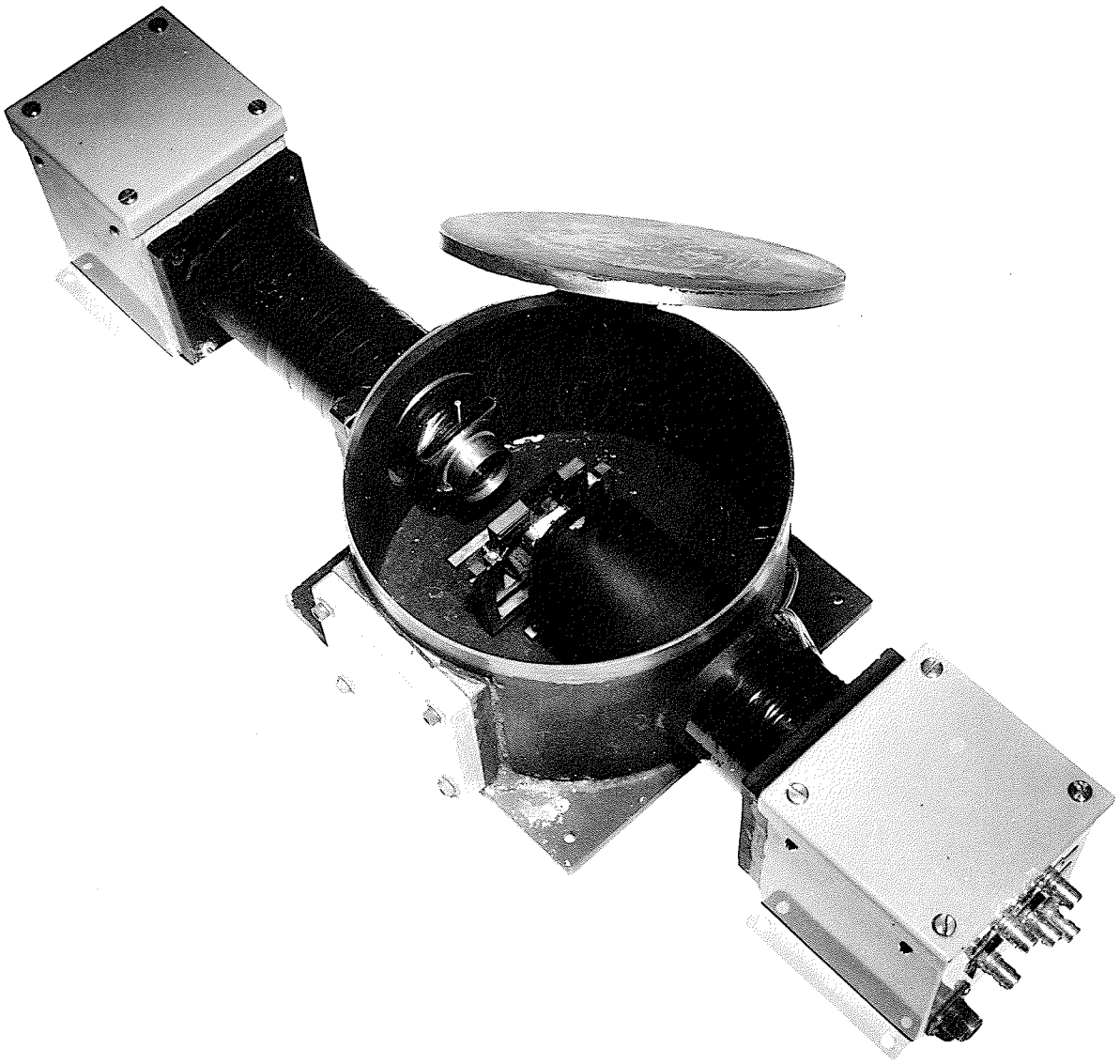

chamber itself, is enclosed in a box, insulated with four inches of polyurethane foam. A control system was designed to maintain the temperature of the box interior constant to within ± 0.5°C for temperature other than ambient room.

The basic unit of this temperature control system is a Bayley Model 116 Precision Temperature Controller. This consists of a thermistor probe in an A.C. bridge which operates a mercury pool relay whenever the probe temperature drops below a preset value. Under optimum conditions the unit is capable of maintaining the temperature of a fluid to considerably better than ± 0.01°C.

For temperatures above ambient room (to 70°C) this unit controlled the temperature of the box interior using a 40 watt lamp as a heater. A copper-constantan thermocouple, mounted near the crystal, monitors crystal temperature. A large tray of ice and water is used to obtain a temperature near 0°C. For temperatures below 0°C (to - 100°C) a controlled flow of liquid nitrogen is used as a coolant. The liquid nitrogen temperature controller is described in Appendix A-3.

3.2 System Calibration

The ultimate utility of the TAC system described above depends upon the care taken in calibration. The system characteristics which must be determined are the time scale, the nonlinearity, the position of time zero, and the system response function. These can be obtained from two subsidiary experiments.

In the first of these the apparatus is called upon to measure random time. Three modifications are made to the system shown in fig. 3.1. The stop input of the TAC is driven by a 100 kHz crystal controlled avalanche pulse generator. The scaler (S) is switched to count the number of valid starts and the gate requirement on the PHA is removed.

The system is allowed to run until a statistically acceptable number of counts N_i, has been recorded in each channel of the PHA. If N_s represents the number of valid starts that have been accumulated by the scaler S during the run, the width of channel i in microseconds is given by $10\ N_i/N_s$.

This random time technique is applicable to any TAC system provided that the TAC unit itself produces a valid start signal which indicates that the entire system is capable of measuring a time interval following the start. It is thus required that the TAC be "slaved" to the PHA so that the TAC cannot operate if the latter is busy. The technique not only produces the required time calibration (with virtually any precision required) in terms of the width of any channel, but as well inherently produces the differential nonlinearity of the system.

Fig. 3.3 shows the results of a typical time calibration of the system. The region between channels 80 and 380 is seen to be fairly linear, having an average time per channel of 6.010 ± 0.002 ns. The system has proven to be remarkably stable since deviations from the above calibration over the space of ten months were less than ± 0.01 ns. The fairly severe nonlinearity visible in the early channels is predominantly due to the PHA. An almost identical nonlinearity display was exhibited by the PHA alone when it was tested in an auxiliary experiment using a Berkeley Model GL - 3 sliding pulse generator. This test also showed that the small rise in the last few channels is also due to the PHA. When the TAC system is used, sufficient cable delay is inserted in the stop input line to step over the initial nonlinear region. As well the last twenty channels are ignored.

Figure 3.3

System Nonlinearity and Calibration

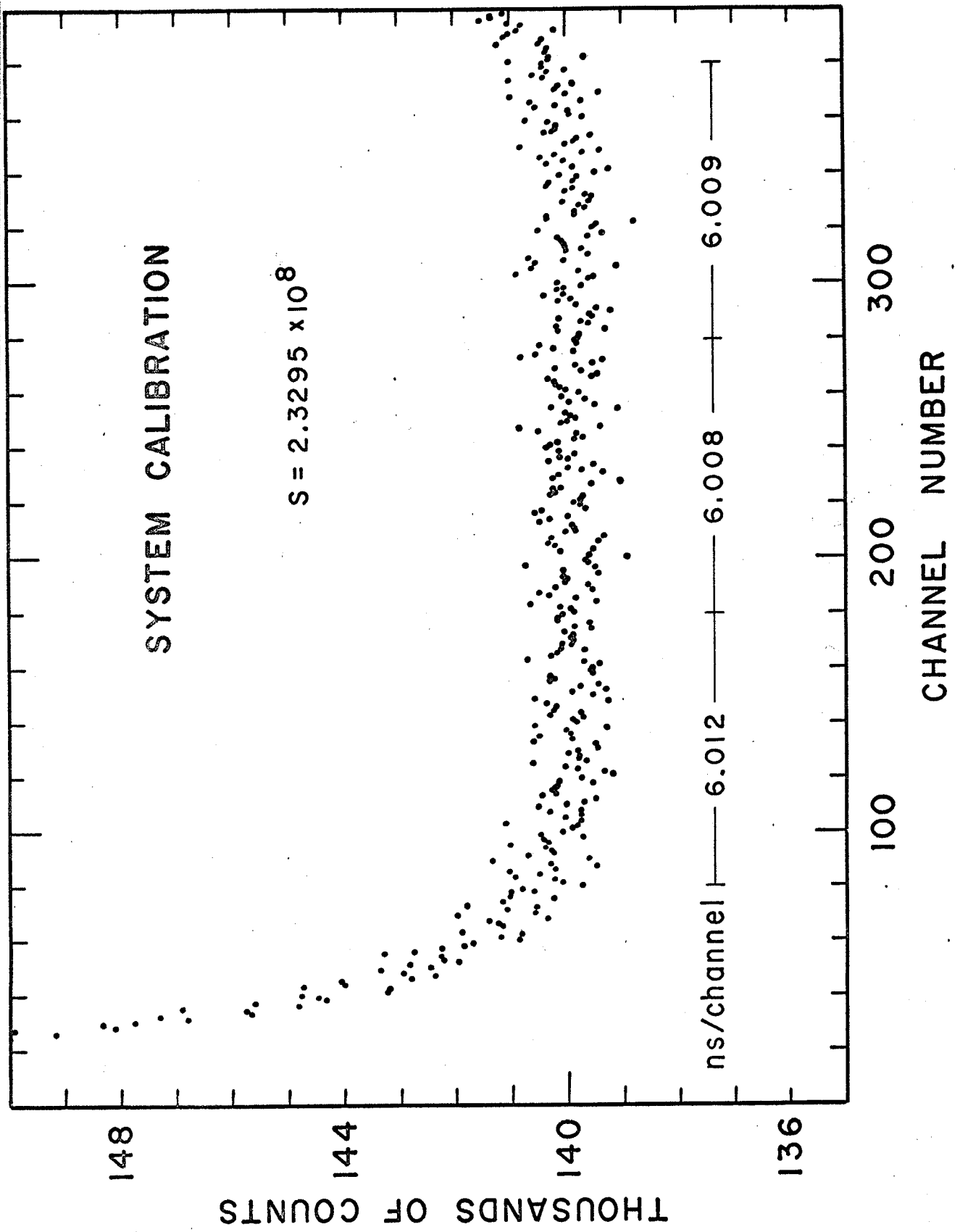
SYSTEM CALIBRATION
S = 2.3295 x10^8
ns/channel
6.012
6.008
6.009
THOUSANDS OF COUNTS
148
144
140
136
100
200
300
CHANNEL NUMBER

Another less precise calibration technique has been used. This was designed for the earlier systems since they could not be calibrated using the random time technique above. A simple tunnel diode oscillator was constructed in which the frequency is determined by reflections from an open-circuited cable (see Appendix A-4). This device was used to measure the delays of a set of coaxial cables. The pulse from T1, fig. 3.1, was power divided and one side was delayed relative to the other. This produced a random double pulse generator to activate start and stop inputs of the TAC. The time separation between start and stop was changed using the previously measured delay cables. This permits a rough measurement of the time scale in the display. Within the limits of experimental error (one to two percent) the cable measurements of the average time per channel agreed with those made using the random time method.

The second calibration, a prompt coincidence experiment, determines the position of time zero and the shape of the system response function. In the system of fig. 3.1, the diaphragm, D, is closed so that no light from the crystal, X, can reach P2. A small plastic scintillator is mounted on P2 and a prompt coincidence spectrum is run using the time correlated gamma rays from a ^{60}Co source placed between the two scintillators. Actually the plastic scintillator is not a necessity as P2 itself is a fair detector of gamma rays.

A typical prompt coincidence time spectrum (i.e. system response function) is shown in fig. 3.4. In this trial the crystal, X, was a standard NaI(Tl) scintillator. The full width of this peak at half maximum height is about 1.4 ns which, if the peak were represented as a Gaussian, would correspond to a standard deviation of

Figure 3.4

Prompt Coincidence Time Spectrum, NaI(Tl): NE102

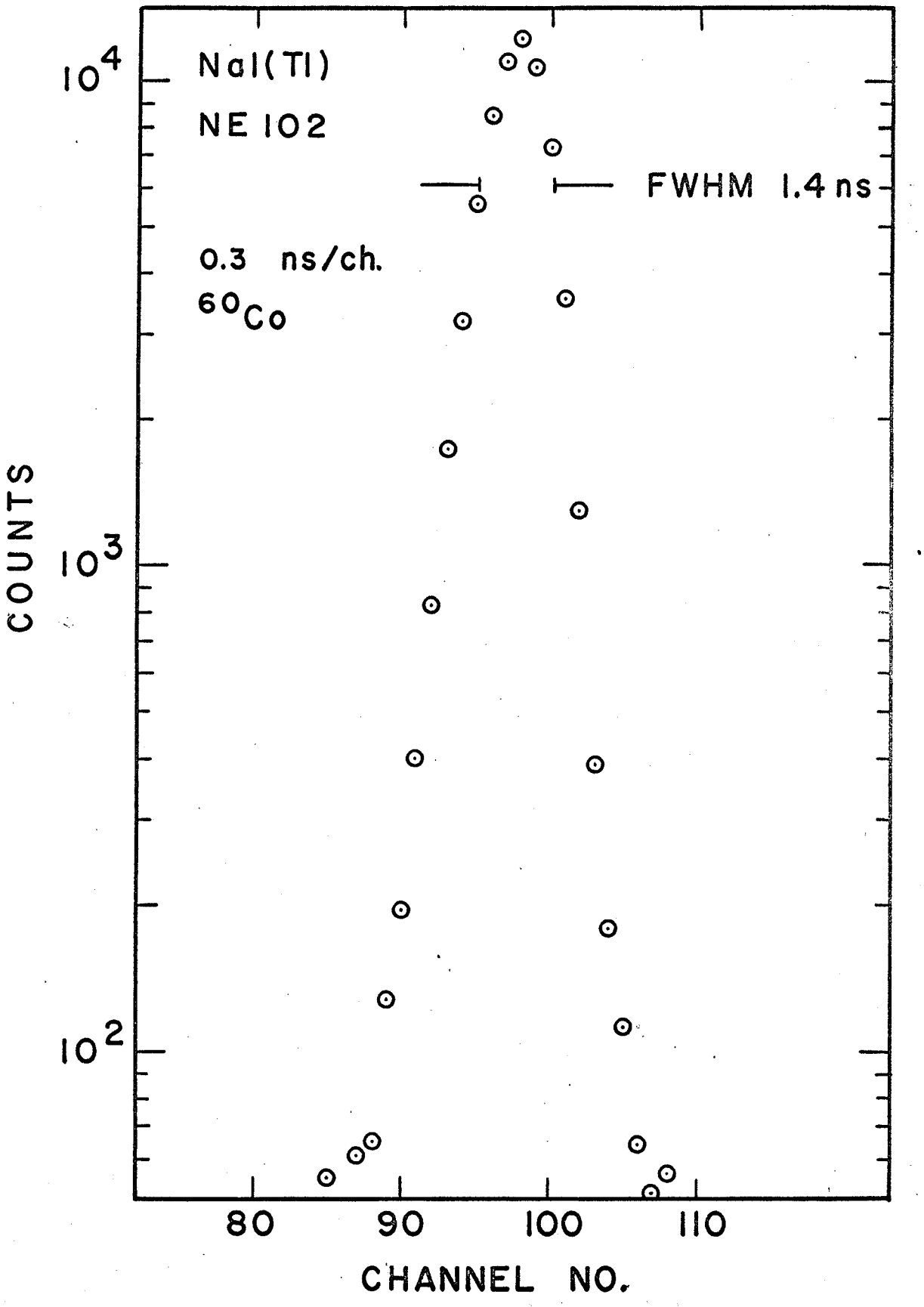
NaI(Tl)
NE 102
FWHM 1.4 ns
0.3 ns/ch.
60Co
COUNTS
10^4
10^3
10^2
80
90
100
110
CHANNEL NO.

roughly 0.6 ns. The parameter d which appears in section 2.7 would be about 2.7 ns. Fig. 3.5 shows the improvement in timing that is obtained when the crystal, X, is replaced by another plastic scintillator.

3.3 Crystal Preparation and Mounting

In the case of commercially mounted Na(Tl) crystals no additional preparation is necessary if the 90° configuration of the crystal chamber is employed. However one such crystal was studied in the 180° orientation in which case a small window was cut in the back of the crystal can. The MgO powder was brushed aside to expose the crystal and a microscope cover glass was sealed over the opening with epoxy glue. Due to the hygroscopic nature of NaI all work with exposed crystals was performed in a "dry box".

Several small unmounted crystals, having various concentrations of thallium, were provided by the Harshaw Chemical Co. These were sealed into cylindrical glass cells using first epoxy and then followed by an overcoating of Dow-Corning Silastic RTV 732. Several of the mounted crystals are shown in fig. 3.6.

The crystals were clamped in a double gimbal frame which is spring loaded to press the crystal firmly against the face of P1 in the crystal chamber, optical contact being made with Dow-Corning C-20057 jelly. The copper-constantan thermocouple is then attached to the side of the crystal case.

3.4 Experimental Procedure

In the measurement of scintillation pulse shape it has been found necessary to use a mono-energetic gamma source with the SCA1 window set on the photopeak. If this is not done the presence of time correlated

Figure 3.5

Prompt Coincidence Time Spectrum, NE102: NE102

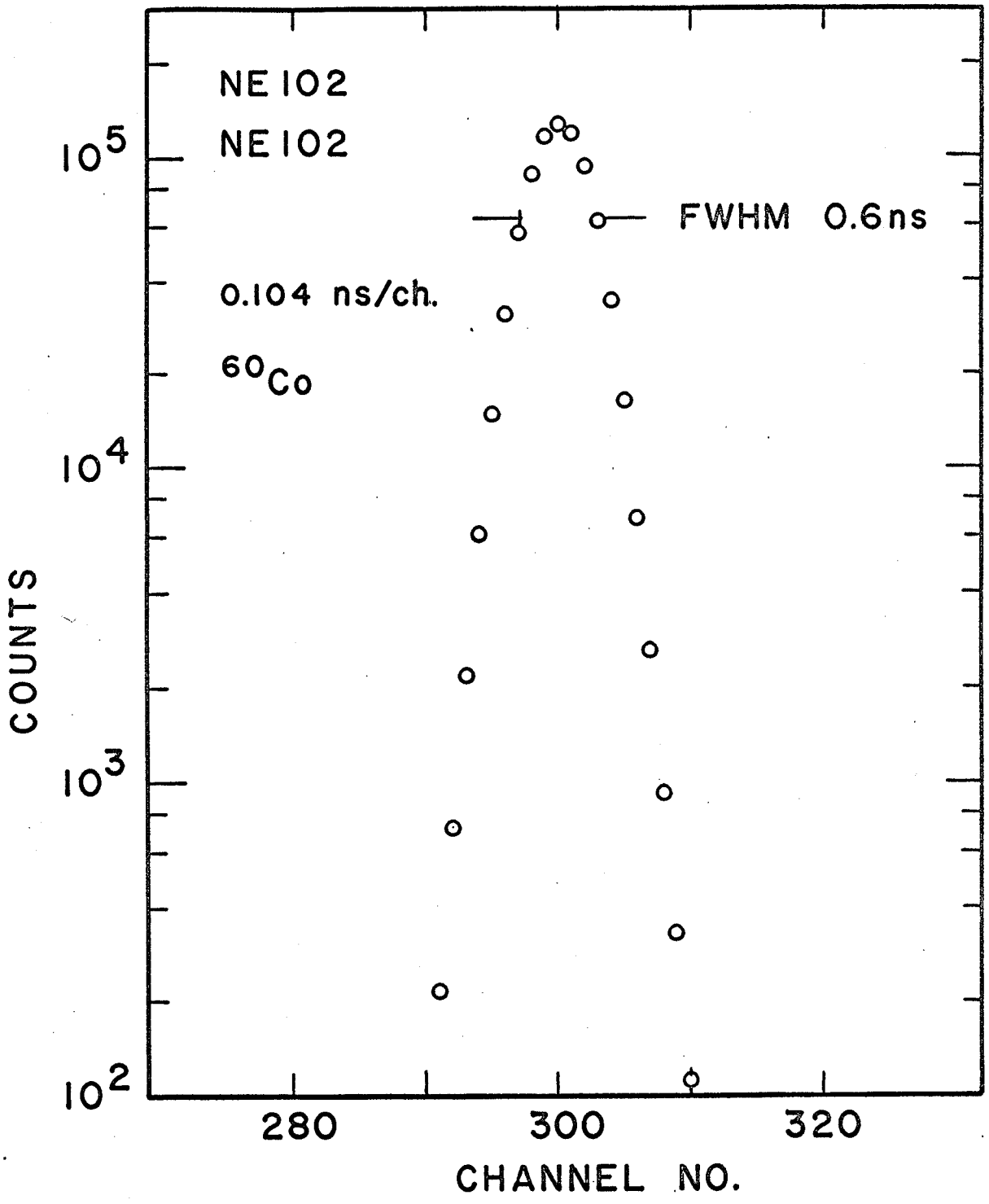
NE102
NE102
FWHM 0.6ns
0.104 ns/ch.
60Co
10^5
10^4
10^3
10^2
COUNTS
280
300
320
CHANNEL NO.

Figure 3.6

Photograph of Several Mounted Crystals

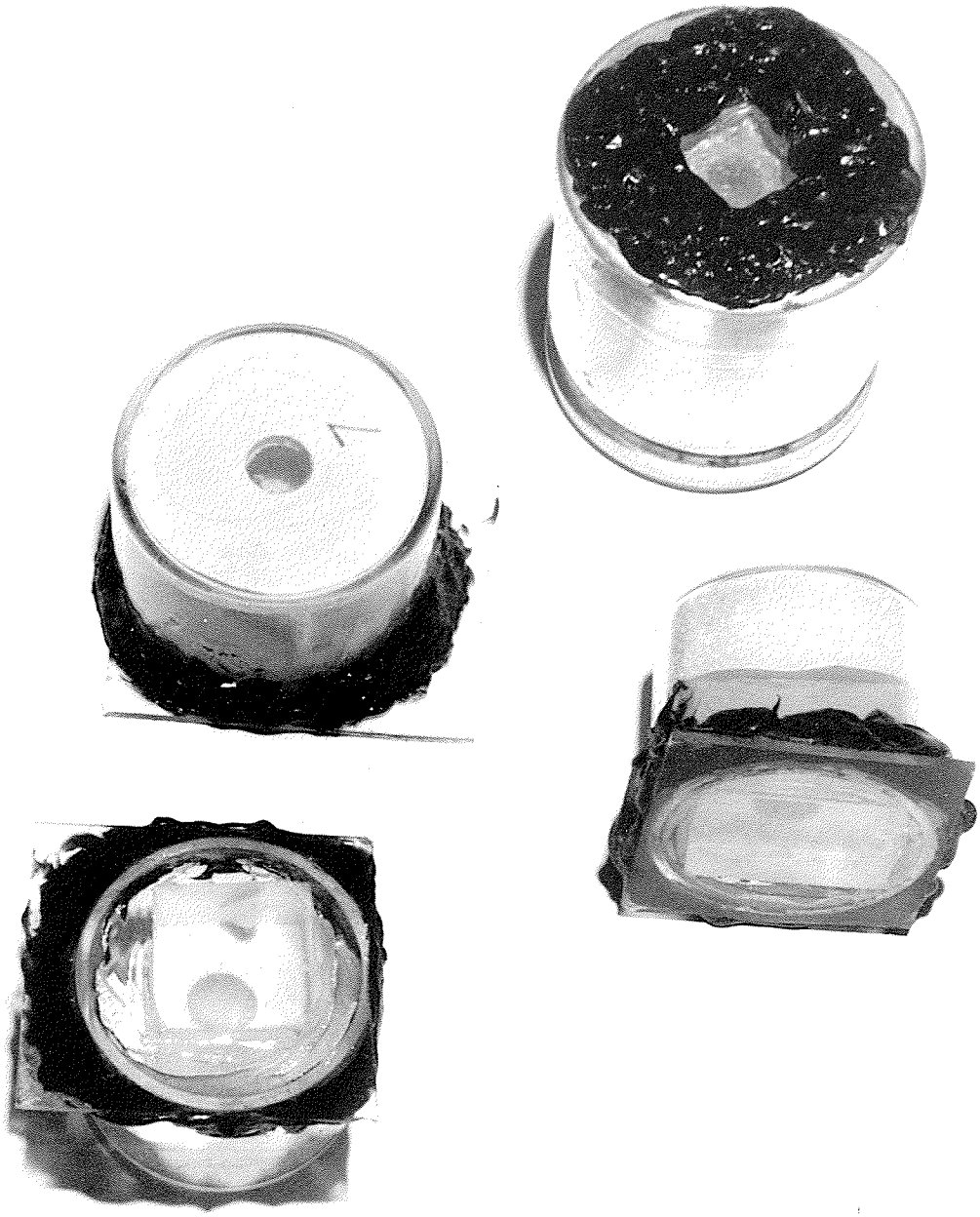

or scattered gamma quanta will be detected by P2 resulting in extra counts near time zero. Most of the scintillation pulse shape determinations in this work used the 0.835 MeV gamma rays from a ^{54}Mn source. Since the energy of this gamma ray is above the threshold for Cherenkov radiation in NaI, there will be a small amount of such radiation added to the luminescence of the crystal. Rough calculations indicate that at most ten to twenty Cherenkov photons are involved. This contribution can be safely ignored on the longer time bases of this work. The directional properties of the emission were used to reduce the probability of the detection by P2 of Cherenkov photons, by means of a suitable location for the gamma ray source.

After mounting the crystal, bags of silica gel desiccant were packed in the chamber and the chamber was sealed. The diaphragm, D, is adjusted so that the gate counting rate is about 10% of the counting rate of the scaler, S, in fig. 3.1. The duration of the accumulation for a single pulse shape determination is dependent on the statistical precision required. As will be seen later the precision required is a function of the shape of the pulse, i.e. the time components present. The accumulation of 10^4 to 10^5 counts in the peak of the time distribution (at 6 ns per channel) usually requires running times of from one to three days. If the temperature of the crystal chamber is changed, an equilibration time of from four to six hours is allowed between runs. The system is recalibrated at the beginning and conclusion of a cycle of measurements.

In the course of the experimental investigations the following aspects were studied:

(a) the reproducibility of results,

(b) the dependence of the pulse shape on:

(i) gamma ray energy,

(ii) emission wavelength,

(iii) crystal size,

(iv) crystal temperature,

(v) thallium concentration.

As well some preliminary work was done on the scintillation pulse shape under alpha particle stimulation.

3.5 Data Processing

Much of the utility of the photon sampling method rests on the data reduction made possible by the availability of high speed digital computers. Equally important is the fact that the experiment produces data in digital form, which is directly compatible with computer analysis. In this functional analysis it is assumed that the experimental data points over the greater portion of the time spectrum can be represented by a sum of exponential terms:

$$f_i = \Sigma A_k \exp(-t_i/\tau_k), \quad k = 1, n; \quad i = 1, N. \tag{3.1}$$
$$= f(i; q_j), \quad j = 1, 2n.$$

where n is the assumed number of components and N is the number of data points.

A least - squares approach is adopted, in which the parameters q_j are chosen to minimize the sum of the weighted squares of the deviations of the data from the assumed function, i.e. a minimum value is sought for:

$$R = \Sigma w_i (r_i - f_i)^2, \quad i = 1, N \tag{3.2}$$

where r_i is the i^{th} data point and the w_i are the weights to be associated with the r_i. Since the assumed function $f(i;q_j)$ is not linear in all of the parameters, the Gauss method of linearization is employed. In this approach, initial guesses of the parameters, q_j^o, are made and equation (3.1) is expanded in a truncated Taylor's series:

$$f_i \approx f(i;q_j^o) + \Sigma \left(\frac{\partial f}{\partial q_j}\right)_o \delta q_j, \quad j = 1, 2n. \tag{3.3}$$

Since equation (3.3) is now linear in the parameter, changes, δq_j standard multiple regression techniques can be applied to determine the changes. These can then be used to form better initial guesses for (3.3) and the process iterated until some convergence criterion on the parameters is satisfied (in this work, all parameter changes less than 0.1%). One constraint is placed on the iterations, other than a maximum number of 20. This is that parameters are not allowed to change by more than 50% between iterations. This insures that parameters cannot change sign. Detailed discussions of the method may be found in the works of Orear (1958), Cziffra and Moravcsik (1959), Moore and Zeigler (1960) and Helmer and Heath (1967).

The data analysis programme incorporates the dead time correction of equation (2.11) and the finite channel width correction of equation (2.18). Nonlinearity corrections were not included since

the differential time nonlinearity of the system was less than ± 0.5% over the region used for analysis. Since the effect of the SRF on the data, as shown in equation (2.39c), does not distort life - times for times in excess of four or five standard deviations of the SRF, the programme was designed to ignore the first L channels (L = 1, 20) and fit parameters to the remaining data points. Thus the effects of the SRF and the presence of leading edge spikes are excluded from the computer analysis. To assist in the comparison of data and the insertion of initial parameter estimates, the computer programme normalizes the experimental data. This is done after the dead time correction has been applied and background has been subtracted.

It is recognized that practical difficulties arise in multiple-exponential analysis due to the extremely non-orthogonal behaviour of exponential functions. Since any monotonically decreasing curve can be expressed as a superposition of exponentials, the results of such analyses can be misleading. This point is pursued by Lanczos (1956) and by Emigh and Megill (1954). Meaningful results are generally obtainable provided that the initial data have sufficient statistical precision. What constitutes sufficient precision depends strongly on the number of components present and their relative time constants and intensities. The fitting of exponentials in this work is made somewhat easier when a negative term appears in equation (3.1), i.e. the data are not representable by a monotonic function.

The choice of the number of components in (3.1) and the initial guesses of the parameter values is made from preliminary graphical analysis. It is found that a fit with too few exponential components, i.e. less than the number actually present in the pulse, produces a

high variance on the basis of a Chi-square analysis. The choice of too many components (or components having the wrong sign), on the other hand, produces non-convergent solutions or parameters whose standard deviations are so large as to render them non-significant.

The above data analysis programme has as input: the data points, the number of valid starts, the background, the initial parameter estimates, the time per channel and the position of time zero. The output includes the corrected and normalized spectra and for each of the accepted ranges of data points: the details of the convergence, the final parameters and their standard deviations, the variance of the fit, the sum of the amplitudes, the intensities of each component and the sum of the intensities. Fig. 3.7 shows a sample data summary sheet giving the results of the fit as a function of initial channel used for analysis. The programme is written in Fortran IV, requires 9000 bytes of storage and has an average execution time on the IBM 360/65 of two minutes.

Three auxiliary programmes were written to assist with the analysis. The first of these is used for a visual verification of the goodness of fit. The programme has as input the experimental data and the parameters returned by the data analysis programme above. Output options include:

(a) a table showing the r_i, f_i and the corresponding residuals $(r_i - f_i)$,

(b) a graph (linear or semilogarithmic) of r_i and f_i versus channel number i,

(c) a graph of r_i or f_i together with $(r_i - f_i)$ versus channel number i.

This verification programme has been used to verify that the residuals are randomly positive and negative. It has also been useful in spectrum stripping.

Figure 3.7

Photograph of Sample Data Summary Sheet

```
H5 D03 208 G.84        307      65.  7072439.    0.0010    6.0100    6.0000

          7.        8.        9.       10.       11.       12.       13.       14.       15.       16.
          6.        6.        6.        6.        6.        6.        6.        6.        6.        6.
       2.277     1.141     1.012     0.988     0.987     0.986     0.982     0.984     0.980     0.982

INTERCEPT, TIME CONSTANT, SIGMAS FOR COMPONENT NO.    1
      317503.   339660.   346273.   349306.   350427.   351466.   353012.   353370.   351893.   351665.
        1386.     1610.     2042.     2437.     2712.     3016.     3461.     3722.     3488.     3603.
     187.489   176.766   174.352   173.384   173.050   172.755   172.341   172.251   172.625   172.684
       1.084     0.845     0.894     0.967     1.024     1.084     1.167     1.218     1.178     1.204

INTERCEPT, TIME CONSTANT, SIGMAS FOR COMPONENT NO.    2
     -287597.  -147205.  -132739.  -126766.  -124294.  -121570.  -117006.  -115776.  -122768.  -124254.
        6034.     2338.     2413.     2740.     3222.     3813.     4351.     5288.     7708.    10084.
       12.346    32.226    39.092    42.434    43.756    45.077    47.194    47.727    45.304    44.893
        0.404     0.964     1.338     1.705     2.036     2.419     2.929     3.361     3.459     3.864

INTERCEPT, TIME CONSTANT, SIGMAS FOR COMPONENT NO.    3
        4727.     8313.     9169.     9500.     9610.     9704.     9830.     9857.     9748.     9731.
         565.      475.      480.      499.      513.      528.      546.      557.      546.      551.
      1096.334   788.719   751.726   739.246   735.294   731.983   727.637   726.742   730.435   731.020
        97.158    24.809    20.522    19.826    19.893    20.021    20.138    20.382    20.419    20.634

CORRECTED INTERCEPT, SIGMA AND   ERROR FOR COMPONENT NO.    1
        51987.    55561.    56629.    57119.    57300.    57469.    57719.    57777.    57539.    57500.
          227.      263.      334.      399.      443.      493.      566.      609.      570.      589.
        0.437     0.474     0.590     0.698     0.774     0.858     0.980     1.053     0.991     1.024

CORRECTED INTERCEPT, SIGMA AND % ERROR FOR COMPONENT NO.    2
       -37147.   -22280.   -20432.   -19634.   -19293.   -18909.   -18255.   -18076.   -19102.   -19321.
          779.      354.      371.      424.      500.      593.      679.      826.     1199.     1568.
       -2.098    -1.589    -1.818    -2.162    -2.592    -3.137    -3.719    -4.567    -6.279    -8.116

CORRECTED INTERCEPT, SIGMA AND % ERROR FOR COMPONENT NO.    3
          784.     1378.     1520.     1574.     1592.     1608.     1629.     1633.     1615.     1613.
           92.       79.       80.       83.       85.       87.       90.       92.       90.       91.
       11.742     5.719     5.235     5.249     5.338     5.437     5.555     5.651     5.597     5.658

INTENSITIES OF EACH COMPONENT
      9946303.  9820934.  9873077.  9903273.  9915493.  9927761.  9947056.  9951782.  9932322.  9929094.
      -458596.  -719004.  -798721.  -833146.  -844203.  -852386.  -861537.  -862725.  -865403.  -867398.
       694770.   977049.  1039357.  1062987.  1070845.  1077566.  1086576.  1088565.  1080764.  1079547.
       -17525.    79975.   113712.   133114.   142136.   152940.   172094.   177622.   147683.   141242.

PREDICTED EAST COMPONENT
        15624.    34659.    37716.    39060.    39589.    40167.    41092.    41334.    40052.    39791.
       -1.122     2.308     3.015     3.408     3.589     3.808     4.188     4.297     3.687     3.550

   ANALYSIS STARTING FROM CHANNEL NO.    17

ESTIMATE NUMBER  1    0.35117E 06 -0.12886E 06  0.10016E 05  0.28725E 02  0.72860E 01  0.11896E 03
ESTIMATE NUMBER  2    0.35191E 06 -0.12318E 06  0.97549E 04  0.28720E 02  0.75211E 01  0.12143E 03
ESTIMATE NUMBER  3    0.35162E 06 -0.12439E 06  0.97274E 04  0.28735E 02  0.74594E 01  0.12165E 03
ESTIMATE NUMBER  4    0.35168E 06 -0.12417E 06  0.97324E 04  0.28732E 02  0.74741E 01  0.12163E 03
COMPLETE CONVERGENCE: % CHANGE LESS THAN 0.00100
FINAL PARAMETERS      0.35167E 06 -0.12423E 06  0.97311E 04  0.28733E 02  0.74706E 01  0.12163E 03
PARAMETER VARIANCE    0.37825E 04  0.12783E 05  0.55812E 03  0.20648E 00  0.72933E 00  0.34734E 01
PERCENTAGE ERROR      0.10756E 01 -0.10290E 02  0.57354E 01  0.71862E 00  0.97627E 01  0.28556E 01

TABLE OF VARIANCE AND COVARIANCE. VARIANCE IS:  0.983670E 00

                      0.378250 04  0.52193D 04  0.12105D 04  0.269540 02  0.497070 02  0.918580 02
                      0.521930 04  0.12783D 05  0.133090 04  0.332180 02  0.995080 02  0.999470 02
                      0.121050 04  0.13309D 04  0.55812D 03  0.101410 02  0.150320 02  0.437050 02
```

The two other programmes were designed to assess the effects of the SRF. The first of these is essentially the "cut and try" procedure outlined in section 2.7. This programme folds the components returned by the data analysis programme with a Gaussian whose standard deviation is varied over the range expected from the experimental SRF. The results of this folding are integrated over channel widths to produce a histogram which is then compared with the initial data points. The second programme implements the iterative unfolding of equations 2.33 and 2.34. The unfolded curve that results may be fed into the data analysis programme.

CHAPTER IV

RESULTS

4.1 Introduction

With the experimental system described in the preceding chapter it has been possible to measure strong components in the scintillation pulses with an accuracy of from 2% to 3% for both time and amplitude when the circumstances are favourable. For weak components and fast components (less than 15 ns) the precision attainable is somewhat less. Unfavourable circumstances do, however, occur at certain temperatures due to changes in the scintillation mechanism, and large errors are possible. Trends over a temperature range must then be carefully considered.

The various crystal samples that have been investigated are listed in table 4.1. The cylindrical samples are commercial scintillation counter crystals whose precise thallium doping is not known but is expected to be in the range from 0.1 to 0.15% Tl. All of the H crystals were manufactured by the Harshaw Chemical Company. The thallium concentrations listed for the rectangular samples are those supplied by Harshaw. The crystal J1 was produced by the Kyoto Electronics Manufacturing Company.

All crystals, with the exception of J1, were studied in the 180° configuration of the crystal chamber. Crystal, H1, was removed from a defective Integral Line Assembly and was mounted in the crystal chamber without any protective casing or glass windows (other than the PM's themselves). The loading of this crystal was, of course, done in a "dry box".

4.2 Reproducibility of Results

The first problem to be considered is that of reproducibility. The results of two sets of measurements on crystal H2 at ambient room

Table 4.1

Crystals Investigated

NUMBER	SHAPE	DIMENSIONS (inches)	VOLUME (cc)	Tl CONC. (%)
J1	Cylindrical	2 x 2	103	$\sim$ 0.1
H1	Cylindrical	$1\frac{7}{16} \times \frac{15}{16}$	35	$\sim$ 0.1
H2	Cylindrical	$\frac{15}{16} \times \frac{15}{16}$	23	$\sim$ 0.1
H4	Rectangular	$\frac{1}{2} \times \frac{1}{2} \times \frac{1}{2}$	2	< 0.01
H5	Rectangular	$\frac{5}{8} \times \frac{1}{2} \times \frac{1}{2}$	3	0.11
H6	Rectangular	$\frac{1}{2} \times \frac{1}{2} \times \frac{1}{2}$	2	0.71
H7	Rectangular	$\frac{3}{4} \times \frac{5}{8} \times \frac{5}{8}$	5	zero
H8	Rectangular	$\frac{3}{4} \times \frac{1}{2} \times \frac{1}{2}$	3	0.094

temperature are shown in table 4.2. These measurements were performed over the space of three weeks. The first set (D02 through D05) used a gamma ray energy of 1.33 MeV ^{60}Co, while the second employed the 0.84 MeV gamma from ^{54}Mn. The break in numbers between D09 and D19 represents an intervening set of measurements above ambient room temperature while the interval between D19 and D32 is for a set below room temperature.

In these curves the first channel of data used for the curve fitting is chosen as close as possible to the front edge of the pulse, consistent with a good fit. For the runs for table 4.2 this was usually 3.5 channels from time zero. Thus the fitted curve represents the experimental pulse shape for times in excess of approximately 21 ns (up to about 2 microseconds).

The detection of the time-correlated 1.17 MeV gamma (see section 3.4) in the ^{60}Co set produced extra counts in the time zero channel of about 1% of the spectrum peak (ten times background). The omitting of the first few data points in the curve fitting program allowed the ignoring of these extra counts.

The goodness-of-fit criterion is concerned with the statistic R^2 of equation 3.2.

(3.2) $$R^2 = \Sigma w_i (r_i - f_i)^2, \quad i = 1,N.$$

The r_i are assumed to be Gaussian distributed with standard deviation σ_i. The weights are taken to be $w_i = 1/\sigma_i^2$. Under these conditions, it can be shown (Orear, page 29) that R^2 is expected to have a Chi-squared distribution centered on the number of degrees of freedom, Q:

(4.1) $$Q = N - 2n$$

where N is the number of data points and 2n is the number of parameters.

Table 4.2

Room Temperature Parameters for Crystal H2

RUN NUMBER	PEAK COUNTS	A_7	τ_7 (ns)	A_6	τ_6 (ns)	A_8	τ_8 (ns)	VARIANCE
D02	55 000	57 038 ± 635	183.99 ± 1.3	−25 370 ± 553	63.21 ± 1.6	1466 ± 82	859.5 ± 28	1.080
D03	71 000	57 636 ± 561	182.85 ± 1.1	−26 037 ± 515	64.79 ± 1.3	1553 ± 71	838.5 ± 22	0.994
D04	108 000	58 231 ± 509	181.84 ± 0.9	−26 349 ± 455	66.11 ± 1.2	1619 ± 61	812.4 ± 17	0.960
D05	41 000	57 090 ± 689	182.32 ± 1.4	−25 475 ± 628	62.54 ± 1.7	1588 ± 96	816.7 ± 27	1.030
Average		57 499 ± 560	182.75 ± 0.9	−25 808 ± 460	64.16 ± 1.6	1556 ± 66	831.8 ± 22	1.016
D06	34 000	59 667 ± 833	178.02 ± 1.4	−27 607 ± 765	65.56 ± 1.7	1689 ± 95	774.0 ± 22	0.889
D07	39 000	59 702 ± 803	179.22 ± 1.4	−27 953 ± 728	64.77 ± 1.7	1543 ± 87	821.0 ± 26	1.067
D08	37 000	58 064 ± 653	180.91 ± 1.3	−26 496 ± 609	61.65 ± 1.5	1523 ± 86	821.2 ± 26	1.002
D09	36 000	59 589 ± 826	178.92 ± 1.4	−27 228 ± 749	65.20 ± 1.8	1518 ± 87	824.3 ± 26	0.992
D19	56 000	58 656 ± 680	180.89 ± 1.2	−26 392 ± 620	66.33 ± 1.5	1531 ± 72	831.3 ± 21	1.036
D32	87 000	58 908 ± 499	180.28 ± 0.9	−27 010 ± 451	64.68 ± 1.1	1486 ± 53	836.6 ± 17	0.982
Average		59 098 ± 670	179.71 ± 1.2	−27 114 ± 610	64.70 ± 1.6	1548 ± 72	818.1 ± 22	0.995

Thus the variance of the fit

$$(4.2) \qquad V = \frac{R^2}{Q}$$

is expected to be near unity.

For large Q (Q > 100) an approximate form for the Chi-square distribution is given by Abramovitz and Stegun (1965):

$$(4.3) \qquad \chi^2 = \frac{1}{2}\left(X + \sqrt{2Q - 1}\right)^2$$

For the case of H2, Q is about 276 and for a probability, p, of 10%, $\chi^2 = 306.3$). Then the maximum acceptable variance, V_m, would be

$$V_m = \chi^2/Q = 1.110$$

An upper limit suggested by Orear is

$$V_m = \frac{Q + \sqrt{2Q}}{Q} = 1.085$$

In general, experiments having variances in excess of 1.15 were rejected completely while those having variances in excess of about 1.1 were considered as poor fits. The variances shown in table 4.2 are typical of the curve fits obtained at room temperature. As can be seen the reproducibility is fairly good.

4.3 NaI (0.1% Tl)

An example of the room temperature scintillation pulse shape that is typical of large standard commercial scintillation counter crystals is shown in fig. 4.1. The time scale is 8.08 + 0.02 ns/channel and the data have been corrected for background and dead time losses. Fig. 4.2(a) shows the pulse shape from a small crystal (0.11% Tl) at room temperature while fig. 4.3 is the first 40 ns of 4.2(a) on an expanded time scale (uncorrected for system response).

Figure 4.1

Scintillation Pulse Shape for a Commercial Scintillation Counter Crystal

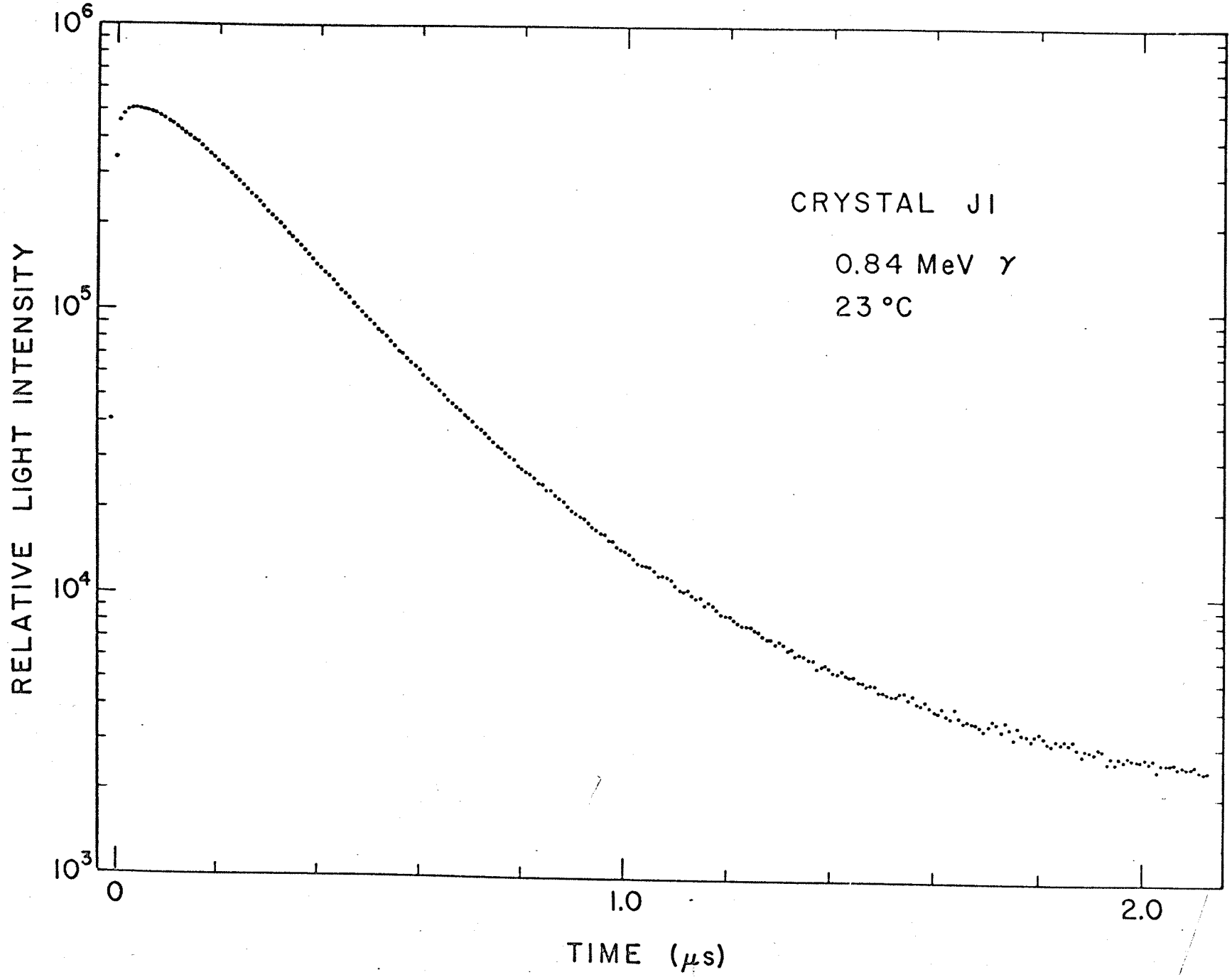
CRYSTAL JI
0.84 MeV γ
23 °C
RELATIVE LIGHT INTENSITY
TIME (μs)
10^6
10^5
10^4
10^3
0
1.0
2.0

Figure 4.2

Scintillation Pulse Shapes for NaI(0.11% Tl)
(a) at 25°C, (b) at -15°C, (c) at -90°C.

Time scale is 6.01 ns per channel. Corrected and normalized data.

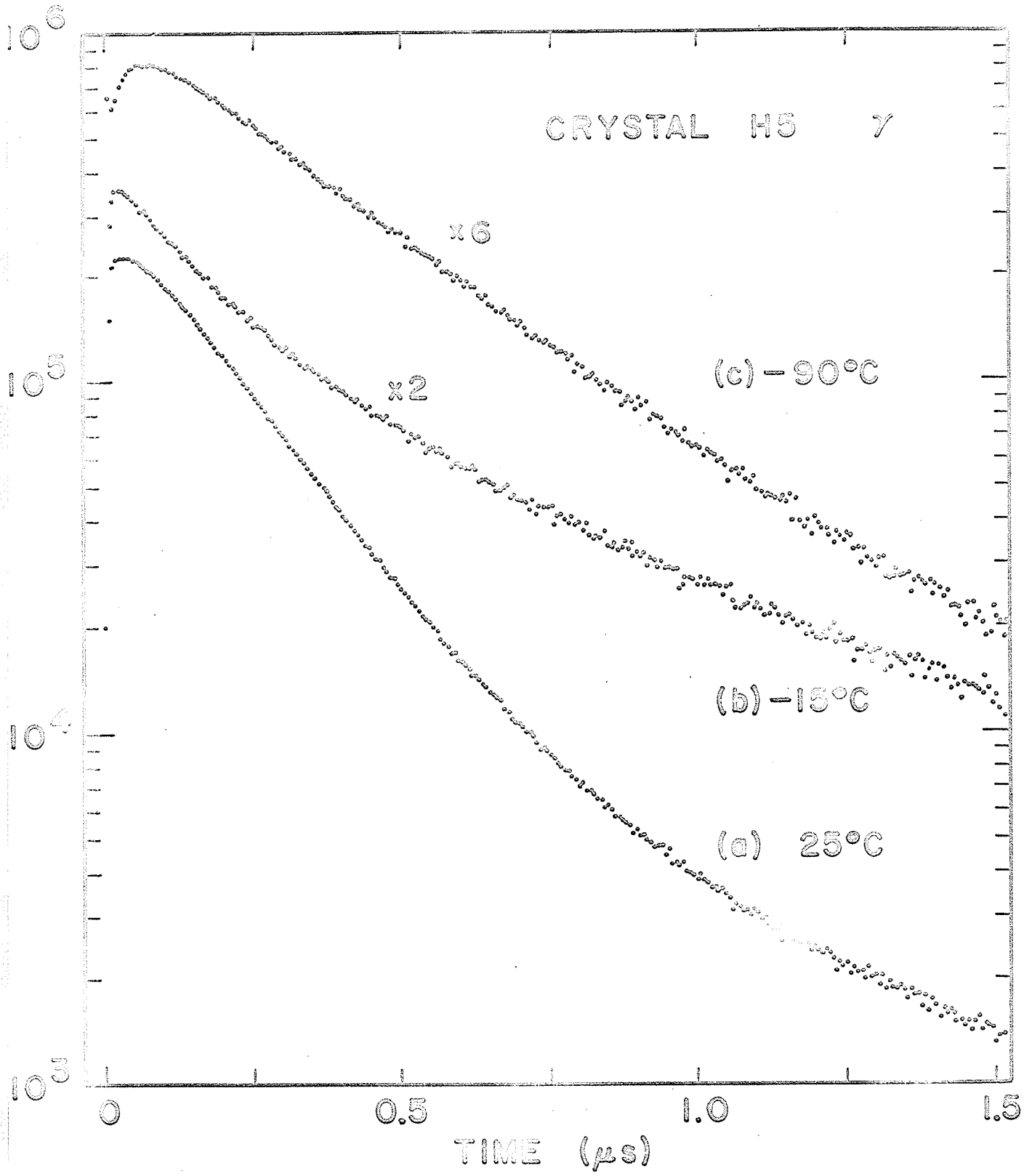
CRYSTAL H5 γ
x6
x2
(c) −90°C
(b) −15°C
(a) 25°C
10^6
10^5
10^4
10^3
0
0.5
1.0
1.5
TIME (μs)

Figure 4.3

The Leading Edge of the Scintillation of NaI(0.11% Tl) at 25°C

Time scale is 0.607 ns per channel.

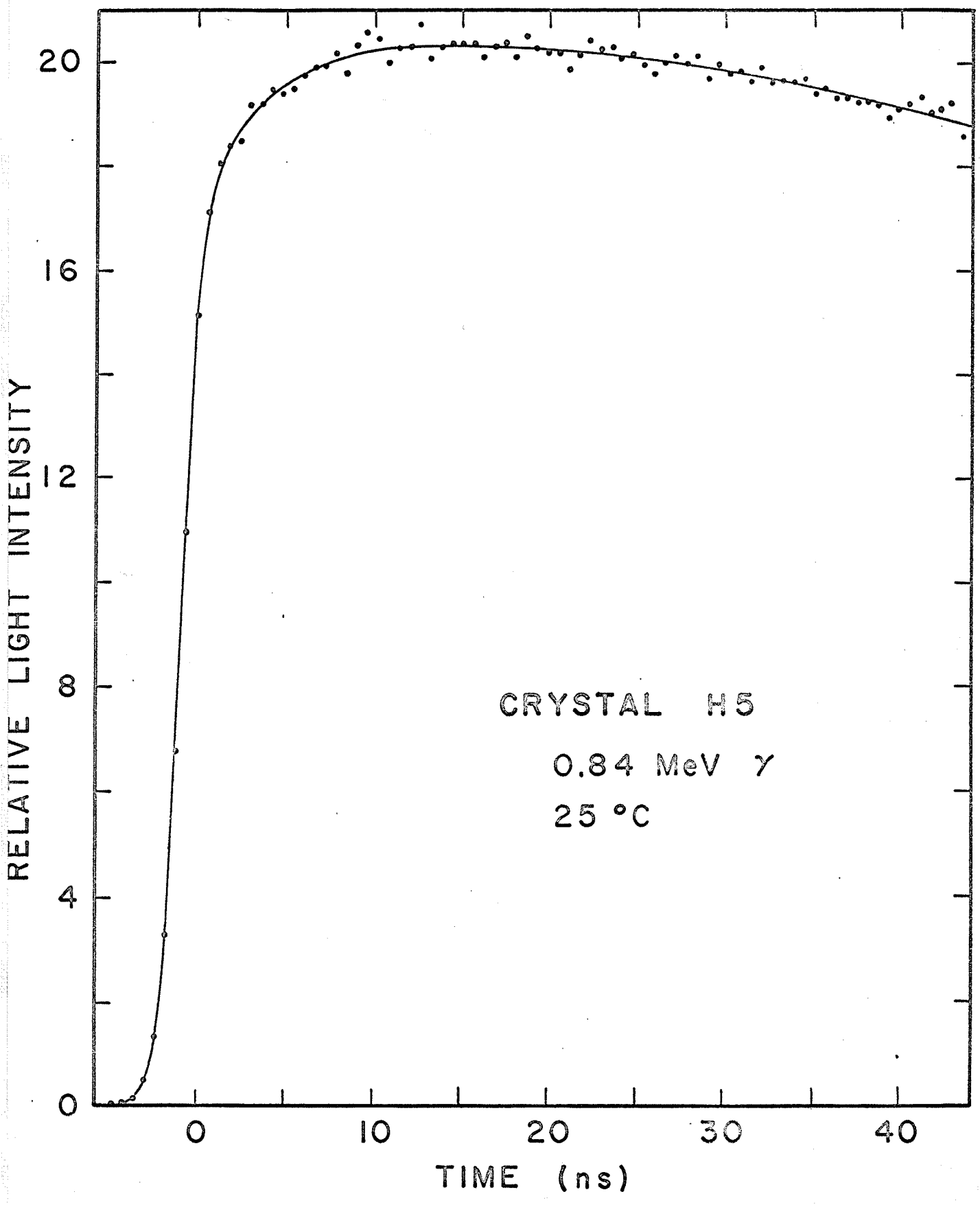
RELATIVE LIGHT INTENSITY
0
4
8
12
16
20
0
10
20
30
40
TIME (ns)
CRYSTAL H5
0.84 MeV γ
25 °C

At room temperature the pulse shape consists of at least five components. Three of these are apparent from a visual inspection of figs. 4.1 and 4.2(a), viz.

(i) the negative amplitude component responsible for the slow rise of the pulse,

(ii) the main decay component,

(iii) a longer time constant delay, somewhat weaker than (ii).

The fourth is apparent in fig. 4.3 where it is seen that

(iv) the front edge has an initial fast rise which is then followed by (i).

The remaining component appears when the computer is used to obtain the parameters for the above four components. It is found that the data points for the last 120 ns (approximately) of the pulse in fig. 4.1 consistently fall above the computer fitted curves. This indicates the presence of at least one other weaker decay component whose life time is longer than (iii). No attempt was made in this work to determine the parameters of the one or more components present in this long lived phosphorescence. Descriptions of these components appear in the works of Bonanomi and Rossel (1952), Emigh and Megill (1954) and Cameron et al (1962).

If the data curves such as figs. 4.1 and 4.2 (a) are subjected to multiple exponential analysis, the parameters for four exponential terms (equation 3.1) can be obtained. Average values for the parameters of these components are shown in table 4.3 for four of the sodium iodide crystals containing the normal (0.1%) doping of thallium. Components six, seven and eight are determined by the nonlinear least squares programme of section 3.5. Component number zero is then inferred from the two conditions:

Table 4.3

Parameters for Crystals Containing Normal Thallium Concentrations

CRYSTAL	VOLUME (cc)	TEMP. (°K)	A_8	τ_8 (ns)	A_7	τ_7 (ns)	A_6	τ_6 (ns)	A_0	τ_0 (ns)
J1	103	296 ± 1	83 ± 3	1104 ± 30	5340±50	205 ± 2	−2880±50	65 ± 1	−2543	~ 3
H1	35	296 ± 1	170 ± 4	714 ± 10	5160±100	188 ± 2	−1720±160	53 ± 2	−3610	≲ 1
H2	23	298 ± 1	155 ± 7	818 ± 22	5910±70	180 ± 1	−2710±60	62 ± 2	−3355	≲ 1
H5	3	298 ± 1	159 ± 5	723 ± 20	5600±300	173 ± 1	−1946±40	43 ± 2	−3813	≲ 1

(4.4) $\Sigma A_k = 0, \quad k = 1, n.$

(4.5) $\Sigma A_k \quad \tau_k \left[1 - \exp\left(-N\lambda/\tau_k\right)\right] = \Sigma r_i, \; k = 1, n$

$i = 1, N.$

The first of these conditions requires that the intensity of the photon emission be zero at time zero. This is evident since the excitation of the crystal is virtually a delta function in time ($\lesssim$ 10 ps) and the light emission system cannot respond before it has been excited. The second condition simply states that the areas of the experimental and fitted curves must be the same. Note that the smearing effect of the SRF does not alter areas provided that N is sufficiently large to include the bulk of the emission.

Table 1.1 summarizes some of the measurements made by previous experimenters on standard thallium concentration crystals. Room temperature decay times for the scintillation pulse range from 130 ns to 330 ns with the majority reporting values from 230 to 250 ns. The results of the present work (table 4.3) indicate values of the main component, τ_7, ranging from 205 ns for the largest crystal down to 173 ns for the smallest.

It should be noted that the strict multiple exponential analysis used in this work will yield rather shorter decay times for the major component than the earlier analyses based on the time required to collect 63% of the light or on the slope of a single straight line fitted to the semilog plot of the emission intensity versus time. For example, in the case of the crystal, J1, life times computed by the latter two methods would be approximately 300 ns and 230 ns respectively.

The apparent dependence of the main component, τ_7 on crystal size is probably not attributable to small variations in thallium con-

centration of crystals J1, H1 and H2 since the work of Eby and Jentschke (1954) indicates a broad minimum in the dependence of decay time on concentration in the range from 0.1% to 0.4% Tl. Some confirmation of this size dependence is found in the work of Bonanomi and Rossel (1951) although they do not make a point of it. An approximate four-fold reduction in decay time can be inferred at room temperature when a monocrystal is compared with a microcrystalline powder.

Turning to the longest component in the emission, number eight, the room temperature decay times measured range from 714 ns to 1104 ns with no regular dependence on crystal size. These values are somewhat shorter than the 1500 $\pm$ 80 ns reported by Robertson and Lynch (1961) but do lie in the range quoted by Startsev et al (1960), that is, 700 to 1200 ns. We find the component to be weak and of about the same relative contribution quoted by Startsev et al (5 to 10%), considerably less than the 43% contribution reported by Robertson and Lynch. The present results are also in qualitative agreement with the NaI(Tl) curve published by Bollinger and Thomas (1961).

The leading edge of the scintillation pulse shape at room temperature exhibits an initial sharp rise followed by a more gradual increase (due to component six) to the peak (fig. 4.3). The characteristic rise time component of NaI(Tl) has been measured by Eby and Jentschke (1954) who found a value of 59 ns which was independent of thallium concentration. The present work yields values from 43 to 65 ns with no regular dependence on crystal size.

The scintillation emission spectrum of the standard NaI(Tl) scintillation crystal consists of two broad bands (Van Sciver, 1964; Eby and Jentschke, 1954) at room temperature. The stronger of these is

centred at about 420 nm with a full width at half maximum of about 100 nm. The second band has a maximum intensity some 35% to 40% of the first and is centred at about 340 nm with a full width at half maximum of 40 nm. This band is estimated by Van Sciver (1964) to account for some 25% of the emission at room temperature. The band is very temperature sensitive, shifting to 325 nm at 80°K. In an attempt to separate the possible different emission time components for these two bands, a Kodak Wratten No. 48A optical filter was inserted in the light path to P2 (fig. 3.1). This filter has a peak transmittance at 450 nm with a full width at half maximum of about 60 nm. Components six and seven showed no statistical difference with, or without, the filter. The insertion of the filter was found to reduce the value of τ_8 by about 80 ns. Crystal J1 was used in this set of experiments.

The scintillation pulse shape was found to have a slight dependence on the energy of the incident gamma ray. This can be seen in the two sets of data of table 4.2. For a 1.33 MeV gamma excitation τ_7 is about three nanoseconds longer than for the 0.84 MeV excitation. A Chi-square analysis shows that the probability of this difference being due to statistical fluctuations is only about 4%. This behaviour was looked for in two crystals, J1 and H2, and was found to be consistently present. The other components (six and eight) do not seem to show anything more than statistical differences. There does not seem to be any dependence on gamma ray energies below 0.84 MeV.

The scintillation pulse shape has a temperature dependence which is shown in the progression of curves of fig. 4.2. At room temperature the luminescence pulse shape exhibits a characteristic "flat top". As the temperature is lowered this is replaced by a form more nearly like

an initial simple exponential decay. A further lowering of the temperature sees the shape returning gradually to its room temperature form with the addition of a leading edge spike.

Concentrating first on the main portion of the emission and ignoring, for the moment, the low temperature spike, table 4.4 shows the results of the multiple exponential analysis in the case of crystals H1 and H2. The temperature dependence shown here is typical of the three NaI(~0.1% Tl) crystals studied as a function of temperature. A more detailed temperature investigation for crystal H5 is summarized in figs. 4.4 and 4.5. In fig. 4.4, time constants associated with negative amplitudes have been indicated by filled-in circles.

Of some interest is the observation that the main component at room temperature, number seven, becomes weaker in relative intensity as the temperature is lowered and is not evident at temperatures below about 243°K. This behaviour was probably observed by Plyavin' (1959) since he was not able to measure his room temperature component I (table 1.1) below -35°C. Thus the mechanism through which the bulk of the emission occurs at and near room temperature is apparently not operative at lower temperatures.

Turning to the longest of the components measured in the emission, the behaviour of component eight is seen to be quite complex. There seem to be two discontinuities in the measurements, one in the vicinity of 0°C and the other near -75°C. Part of this complexity may be only apparent since the apparatus used in this work was not adjusted to measure time behaviour much beyond two microseconds, i.e. the longer components in the emission should be measured on a ten or twenty microsecond time base rather than the two microsecond base of this work. In

Table 4.4

Parameter Temperature Dependence for Crystals H1 and H2

CRYSTAL	THALLIUM CONC.(%)	TEMP. (°K)	A_8	τ_8 (ns)	A_7	τ_7 (ns)	A_6	τ_6 (ns)	A_0	τ_0 (ns)
H2	∿ 0.1	341±1	125±7	776±30	7338±70	137±1	−4090±150	25±2	−3373	∿ 5
		322±1	105±5	870±30	6919±50	149±1	−3450±90	36±2	−3574	≲ 1
		311±1	120±7	825±25	6510±150	162±1	−3210±290	48±1	−3420	≲ 1
		298±1	155±7	818±22	5910±70	180±1	−2710±60	65±2	−3355	≲ 1
		277±1	183±8	1030±120	4090±160	237±3	−1200±140	132±10	−3070	≲ 1
		259±1	306±86	1140±160	1490±40	350±30	1128±110	115±10	−2924	≲ 1
H1	∿ 0.1	296±1	170±4	714±10	5160±100	188±2	−1720±160	53±2	−3610	≲ 1
		172±2	70±17	1330±200	§	§	2736±30	346±2	−1636	Δ

Δ — leading edge spike

§ — component seven is not apparent at this temperature

Figure 4.4

The Temperature Variation of the Longer Life Times in the Scintillation of NaI(0.11% Tl)

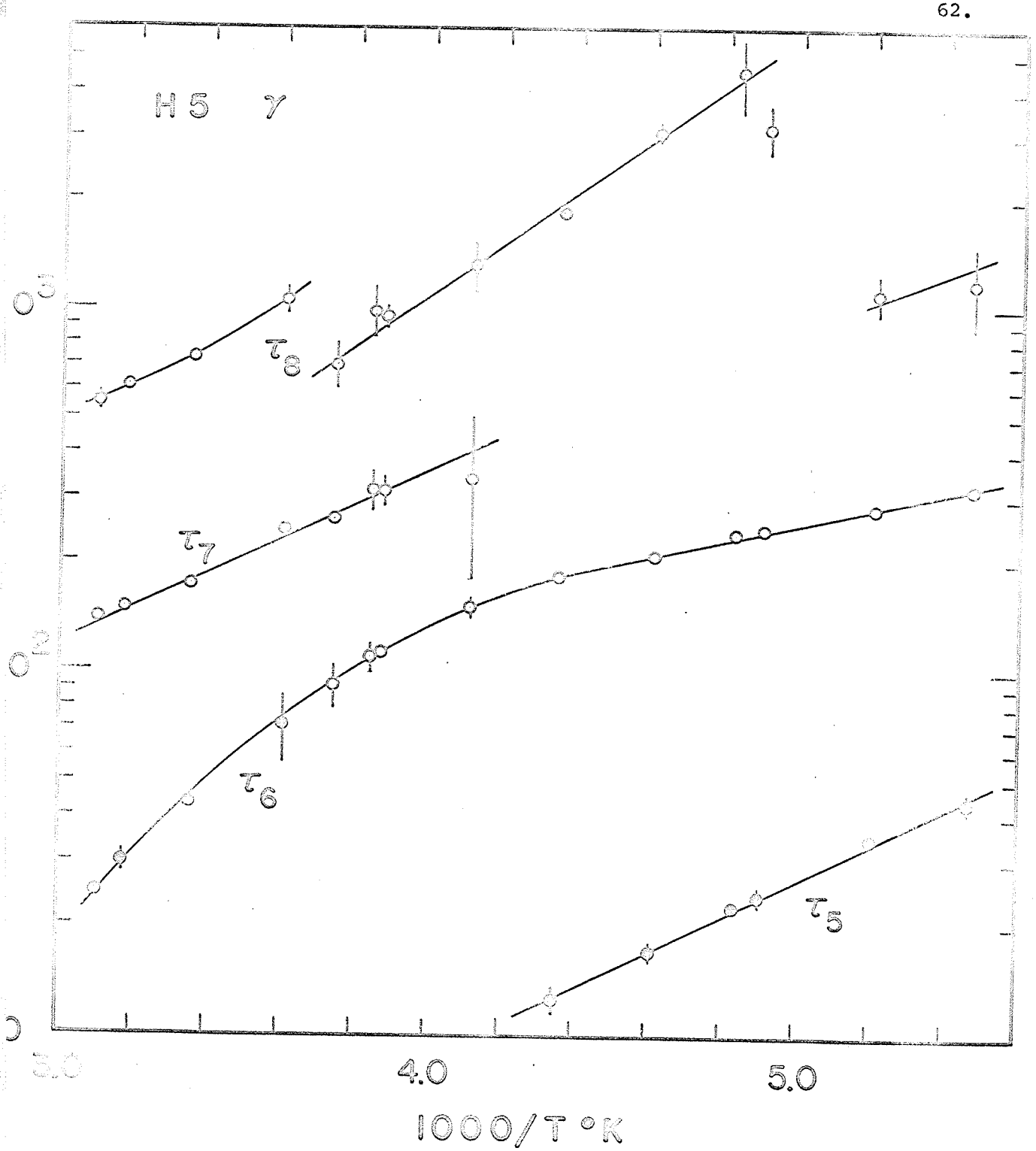
H5 γ
τ_8
τ_7
τ_6
τ_5
4.0
5.0
1000/T °K

Figure 4.5

The Effects of Temperature on the Amplitudes of the Components in the Scintillation of NaI(0.11% Tl)

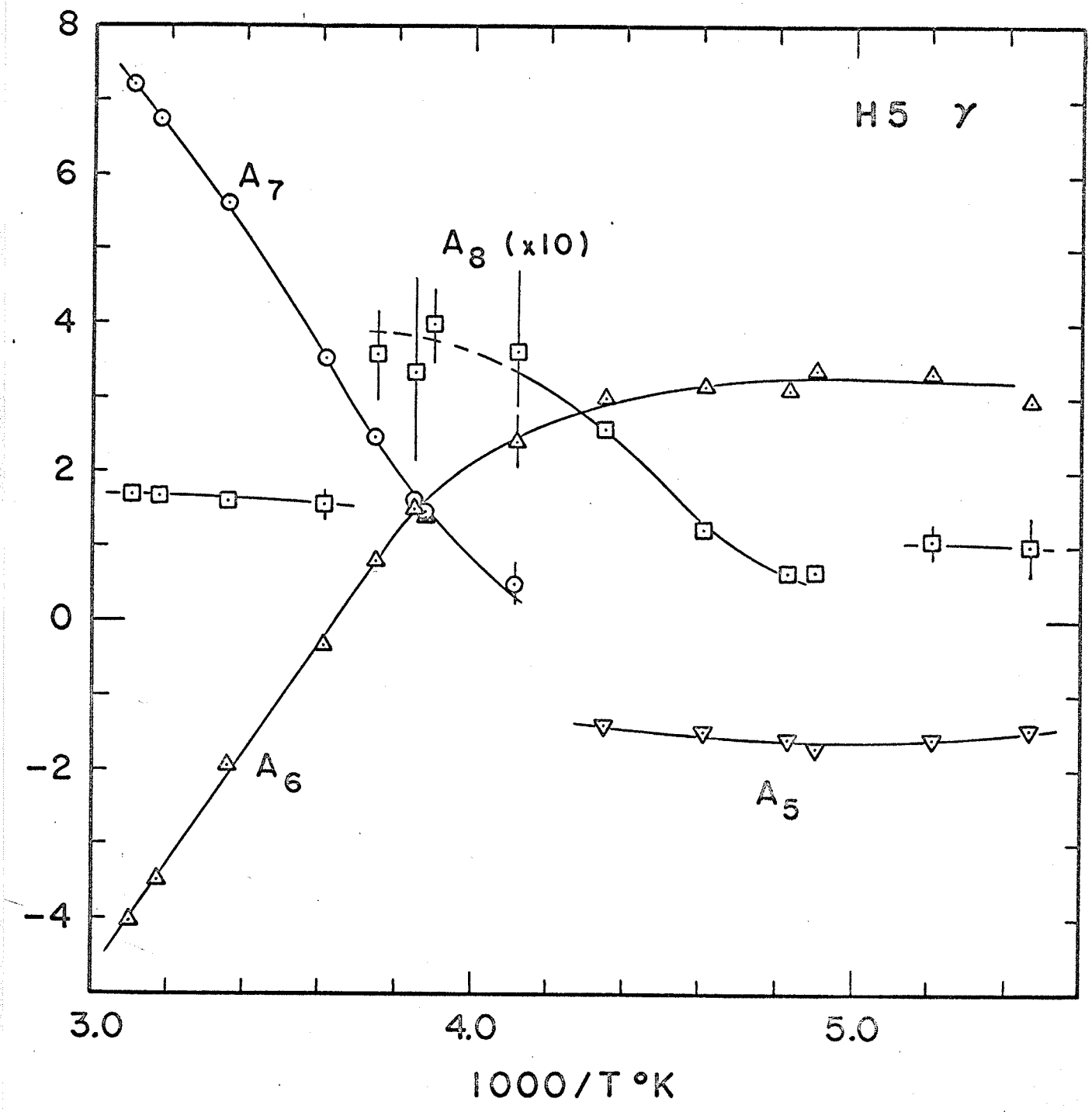
H5 γ
A7
A8 (x10)
A6
A5
8
6
4
2
0
-2
-4
3.0
4.0
5.0
1000/T °K

any event it seems clear the component eight is a mixture of at least two and possibly three long-lived processes.

At and near room temperature component six describes the slowly rising front of the emission pulse and thus contributes a negative term to the expression for the pulse shape (equation 3.1), i.e. the amplitude A_6 is negative. In the vicinity of 0°C this amplitude changes sign and the component does not describe the rise of the pulse at temperatures below 0°C. At temperatures below -30°C component six assumes the role of the main decay component. Below about -40°C the luminescence emission again shows a slower rise due to the growth of a second negative amplitude component, number five.

The leading edge spike becomes discernable as an anomalous front edge at temperatures in the region of -80°C. On the time scale of fig. 4.2(c) the spike is apparent only as a single channel at time zero which lies high. The insertion of a Corning No. 9863 optical filter (transmission band from 235 to 400 nm, see Appendix A-5) in the light path to P2 produces a marked strengthening of this emission spike relative to the longer main components of the emission. This fast component thus lies in an emission band below the main 420 nm band and is probably in the 325 nm band (at 80°K) commented on earlier in this section. A fast, low temperature, 325 nm emission has been reported by Van Sciver (1960, 1964, 1966). Lynch (1966) has measured the decay time of this emission using ultraviolet stimulation at 77°K and found a value of 6.2 ± 1.5 ns. Herb et al (1968), again with ultraviolet stimulation, have determined that the life time lies between the limits of 7 ns and 4 to 5 ns. This life time was found by them not to depend on thallium concentration (from 0.08 to 1.01 mole %) or on temperature

(from 13 to 170°K). Above 170°K this emission, which they attribute to thallium dimers, was too weak to be measured. In the present work, under gamma stimulation, this fast component was too weak at 190°K to permit anything other than qualitative agreement with the earlier measurements.

4.4 NaI (0.71% Tl)

The scintillation pulse shape at room temperature for crystal H6 which contains a higher than normal thallium concentration is shown in fig. 4.6(a). The shape is considerably flatter at the peak than was observed in the case of the normal thallium concentration crystals of the preceding section. In addition the pulse also exhibits, at room temperature, a pronounced leading edge spike. This is visible on the expanded time scale of fig. 4.7. Through the use of the Corning No. 9863 optical filter, it was found that this emission spike does not lie below 380 nm and is thus not to be confused with the fast emission noted at low temperatures in section 4.3. This spike evidently has roughly the same emission band as the main band of NaI(Tl) (∿420 nm). A fast emission with somewhat the same characteristics was observed by Eby and Jentschke (1954) when crystals having thallium concentrations in excess of 0.1% were stimulated by alpha particles. It is possible that considerably more thallium than 0.1% is required for a significant gamma stimulation of this component since the work of Lynch (1966) showed no appreciable change in gamma pulse shape between crystals containing normal and three times normal thallium concentration. From room temperature to about 180°K the scintillation pulse has a rise which is mainly limited by the system response.

Figure 4.6

Scintillation Pulse Shapes for NaI(Tl)

(a) Containing 0.71% Tl at 26°C

(b) Containing less than 0.01% Tl at 25°C

Time scale is 6.01 ns per channel.

Corrected and Normalized Data.

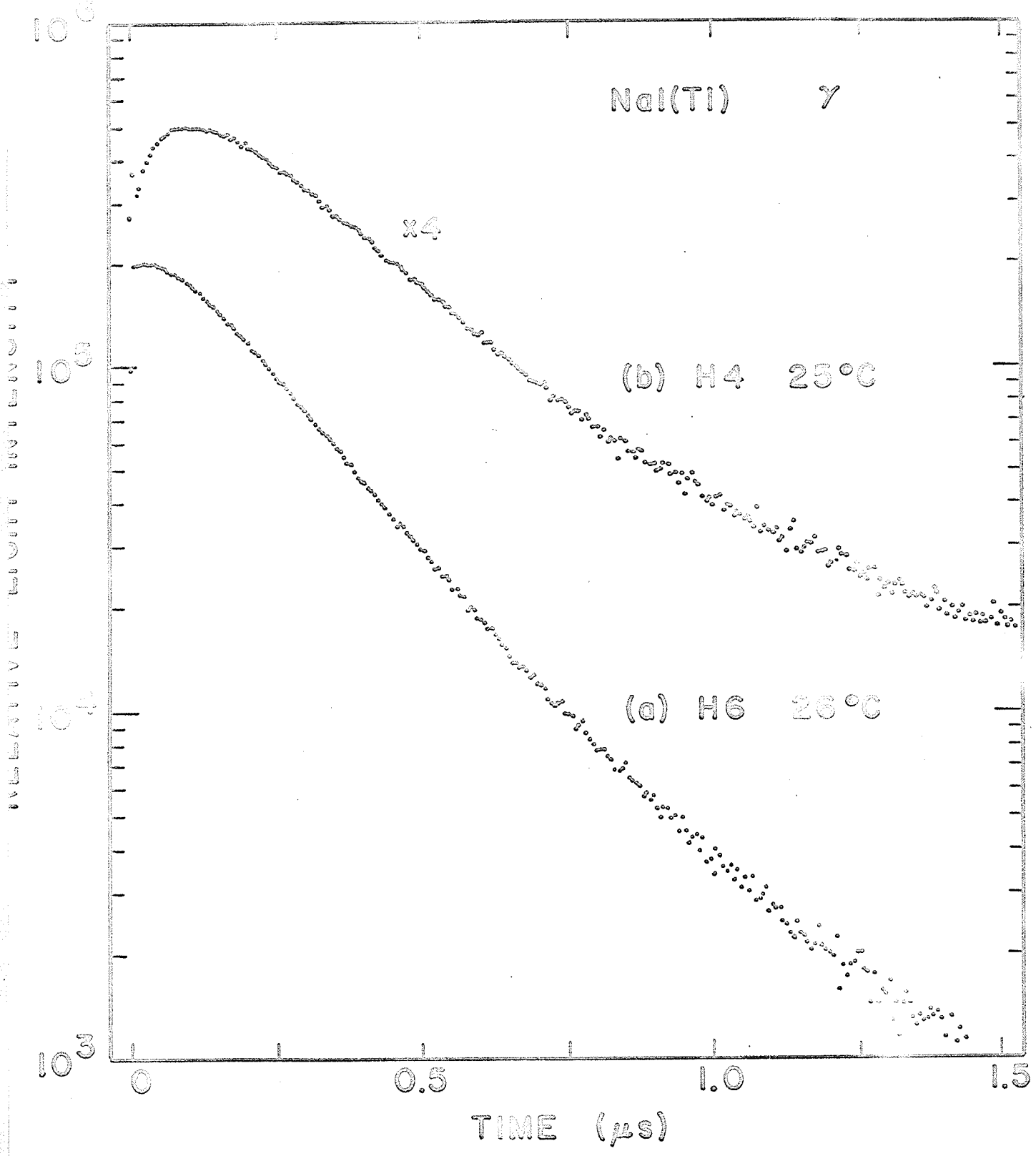
NaI(Tl) γ
x4
(b) H4 25°C
(a) H6 25°C
10^6
10^5
10^4
10^3
0
0.5
1.0
1.5
TIME (μs)

Figure 4.7

The Leading Edge of the Scintillation

of NaI(0.7% Tl) at 26°C

Time scale is 0.607 ns per channel.

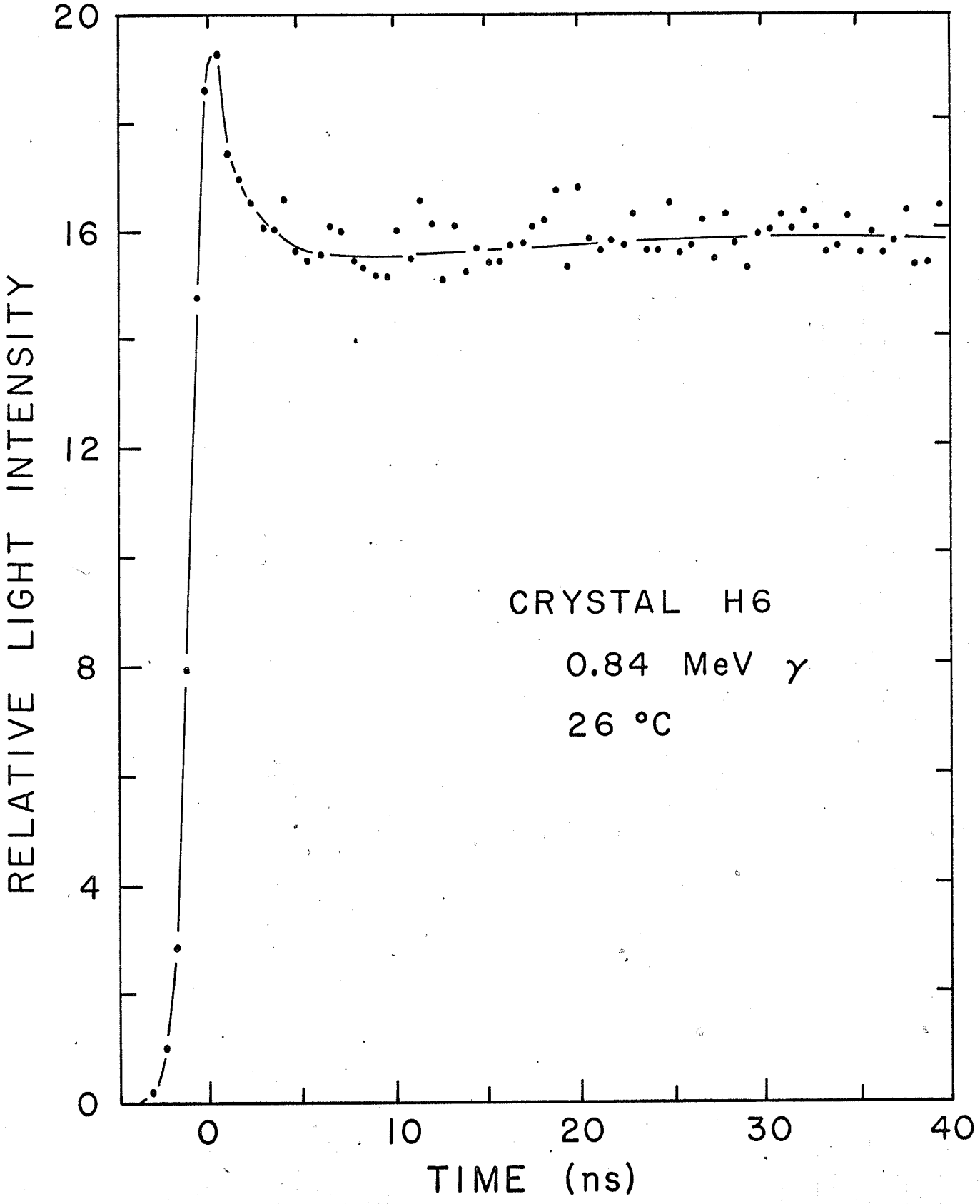
20
16
12
8
4
0
RELATIVE LIGHT INTENSITY
CRYSTAL H6
0.84 MeV γ
26 °C
0
10
20
30
40
TIME (ns)

Turning to the main emission, the last entry of table 4.5 shows the results of the computer analysis for the components present at room temperature. Since crystals H5 and H6 are about the same size, the parameter differences indicated in this table may be attributed to the change in thallium concentration. The life time of the main component, τ_7, shows an increase with increased thallium concentration which agrees qualitatively with the earlier work of Eby and Jentschke (1954). However τ_6 also shows an increase which does not agree with Eby and Jentschke who found this component to be thallium concentration independent. The long component, τ_8, exhibits a marked decrease with increased thallium concentration.

The details of the temperature dependence of the parameters of the main emission for crystal H6 are summarized in figs. 4.8 and 4.9. There are two major differences from the normal crystal, H5. First, component five, which contributes to a rising front at low temperatures in the normal crystal, does not seem to appear until much lower temperatures are reached in the high thallium concentration crystal. It is just measurable below 180°K. Then there is noted the presence of a new positive amplitude component, number four, in the decay of the pulse. The behaviour of the other components, 6, 7 and 8 is similar to that seen in the normal thallium crystal. Note the vanishing of component 7 in the vicinity of -25°C, the discontinuous component 8, and the change in sign of A_6 at a temperature of -5°C.

It is fair to presume that component four and the fast emission spike at room temperature are to be associated with an excess of thallium. The fast component increases in relative intensity as the temperature of the crystal is reduced. Optical filter work shows that

Table 4.3

Room Temperature Parameters for Crystal of Differing Tl Concentration

CRYSTAL	THALLIUM CONC.(%)	TEMP. (°K)	A_8	τ_8 (ns)	A_7	τ_7 (ns)	A_6	τ_6 (ns)	A_0	τ_0 (ns)
H4	< 0.01	298±1	276±30	1000±60	4600±300	227±4	−3560±300	90±8	−1316	Δ
H5	0.11	298±1	159±5	723±20	5600±300	173±1	−1946±40	43±2	−3813	≲ 1
H6	0.71	299±1	289±50	488±20	5330±100	188±3	−2350±70	61±3	−3271	Δ

Δ — leading edge spike

Figure 4.8

The Temperature Variation of the Longer Life Times in the Scintillation of NaI(0.7% Tl)

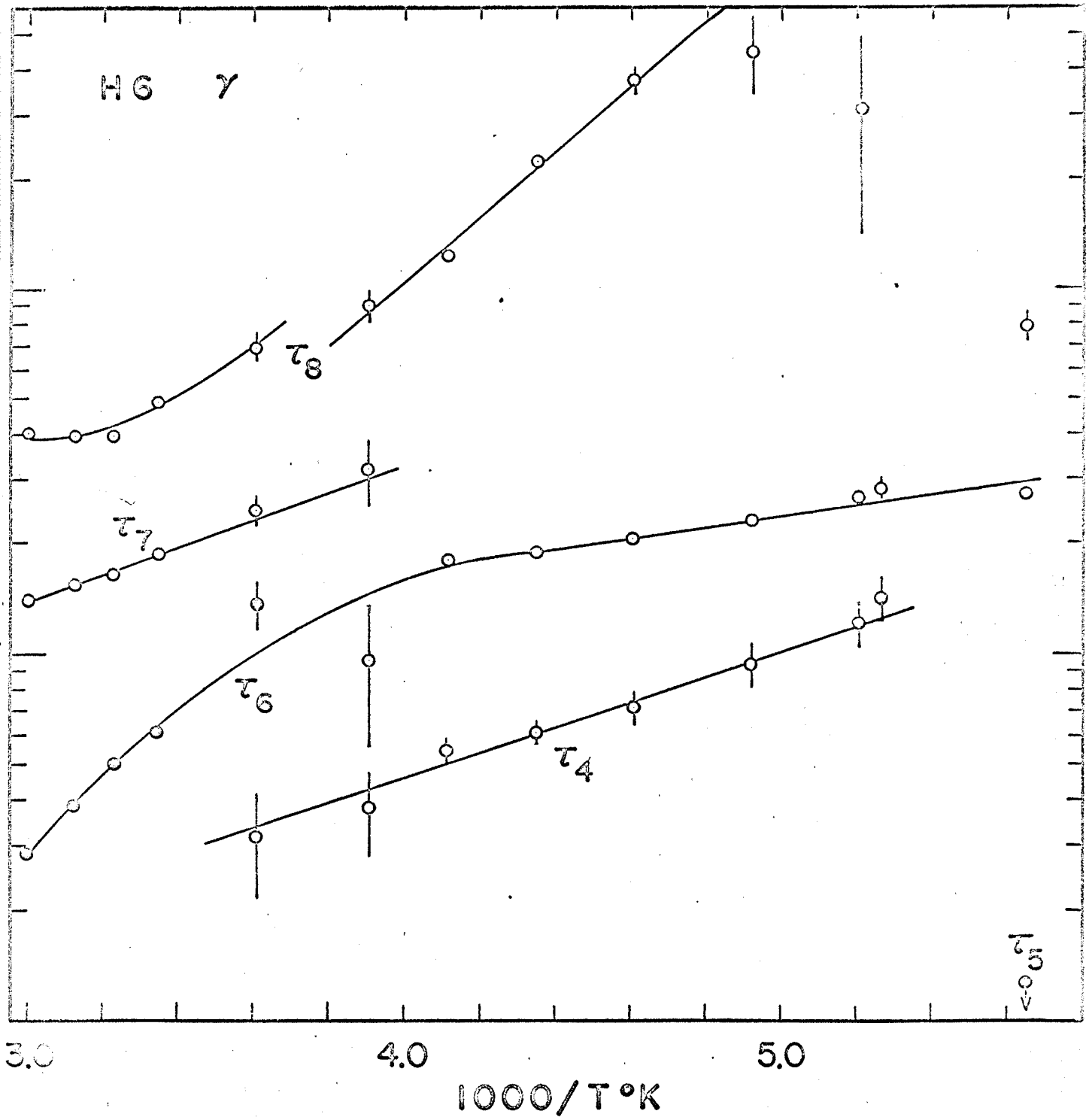
Hg γ
τ8
τ7
τ6
τ4
τ5
3.0
4.0
5.0
1000/T °K

Figure 4.9

The Effects of Temperature on the Amplitudes of the Components in the Scintillation of NaI(0.7% Tl)

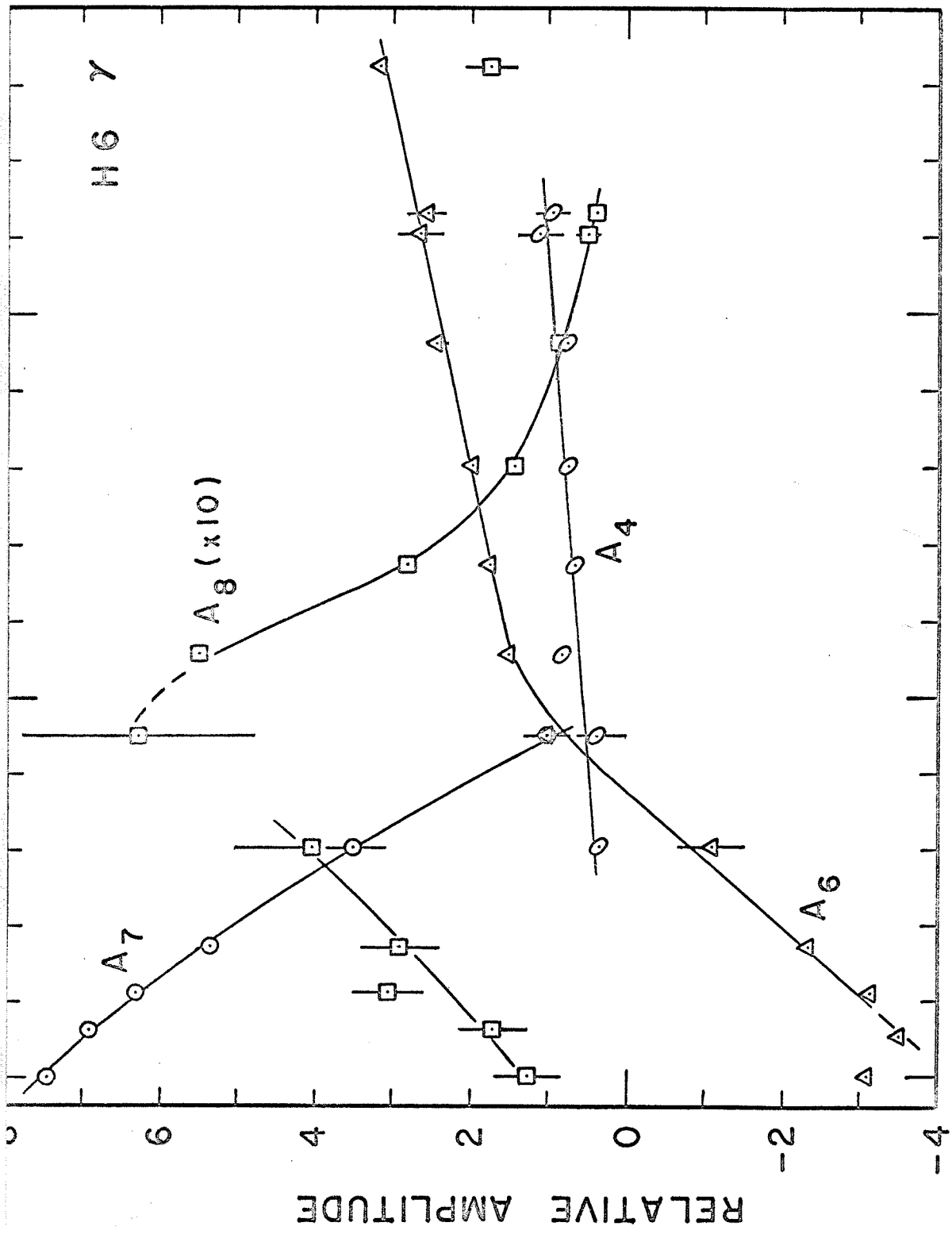
H6 γ
A8 (x10)
A4
A7
A6
RELATIVE AMPLITUDE
6
4
2
0
-2
-4
3.0
4.0
5.0
1000/T°K

at least a part of this increase is due to emission below 380 nm. This indicates the presence of the fast emission seen at reduced temperatures in the normal thallium crystal.

4.5 NaI (<0.01% Tl)

The room temperature pulse shape of the trace thallium crystal, H4, is shown in fig. 4.6(b). The pulse has a considerably more rounded front than any of the higher thallium concentration crystals. In addition there is noted, even on the time scale of fig. 4.6(b) a leading edge spike. The component parameters of the main room temperature emission are given in the first entry of table 4.5. It is observed that the decay time of the main component, τ_7, is substantially longer than those found in crystals H5 or H6. This is in agreement with the behaviour of the main decay component given by Eby and Jentschke (1954). However the rise time component, τ_6 is also much longer which disagrees with the latter mentioned work. From the series H4, H5, H6 there is noted a steady decrease in the decay time τ_8 with increasing thallium concentration.

The temperature behaviour of the parameters of the main emission is presented in figs. 4.10 and 4.11. Although the temperature dependence resembles in some ways that seen in crystals H5 and H6, there are major differences. The main pulse shape has much the same form over the range of temperatures used. Note that component seven does not seem to vanish and that component five is apparently not present. The amplitude of component six is depressed so that it does not go positive. Component eight again shows a discontinuous nature.

The leading edge spike noted at room temperature becomes more prominent as the temperature of the crystal is lowered. This fast

Figure 4.10

The Temperature Variation of the Longer Life Times in the Scintillation of NaI(<0.01% Tl)

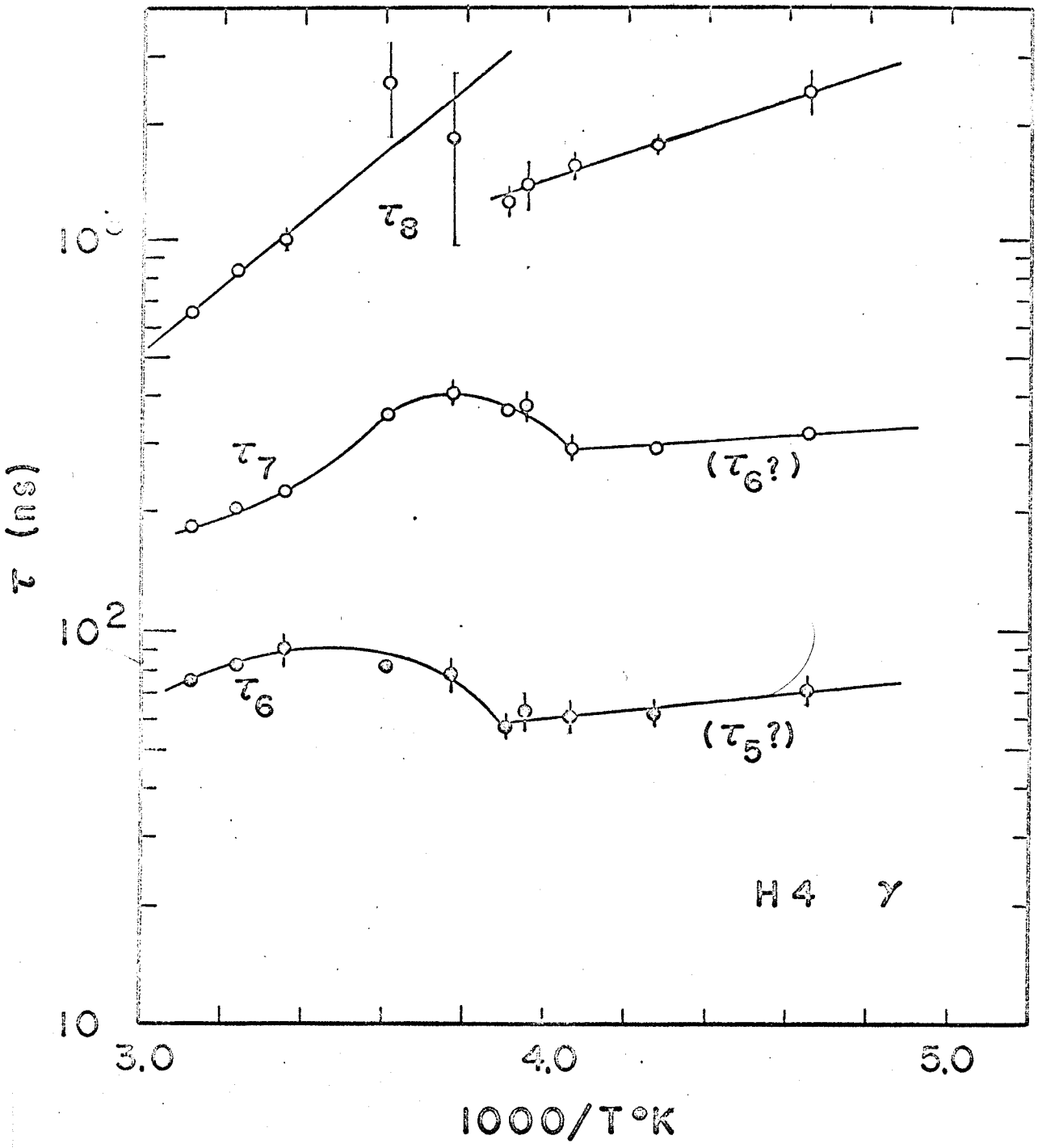
10^3
10^2
10
τ (ns)
τ_8
τ_7
$(\tau_6?)$
τ_6
$(\tau_5?)$
H4 γ
3.0
4.0
5.0
1000/T°K

Figure 4.11

The Effects of Temperature on the Amplitudes of the Components in the Scintillation of NaI(<0.01% Tl)

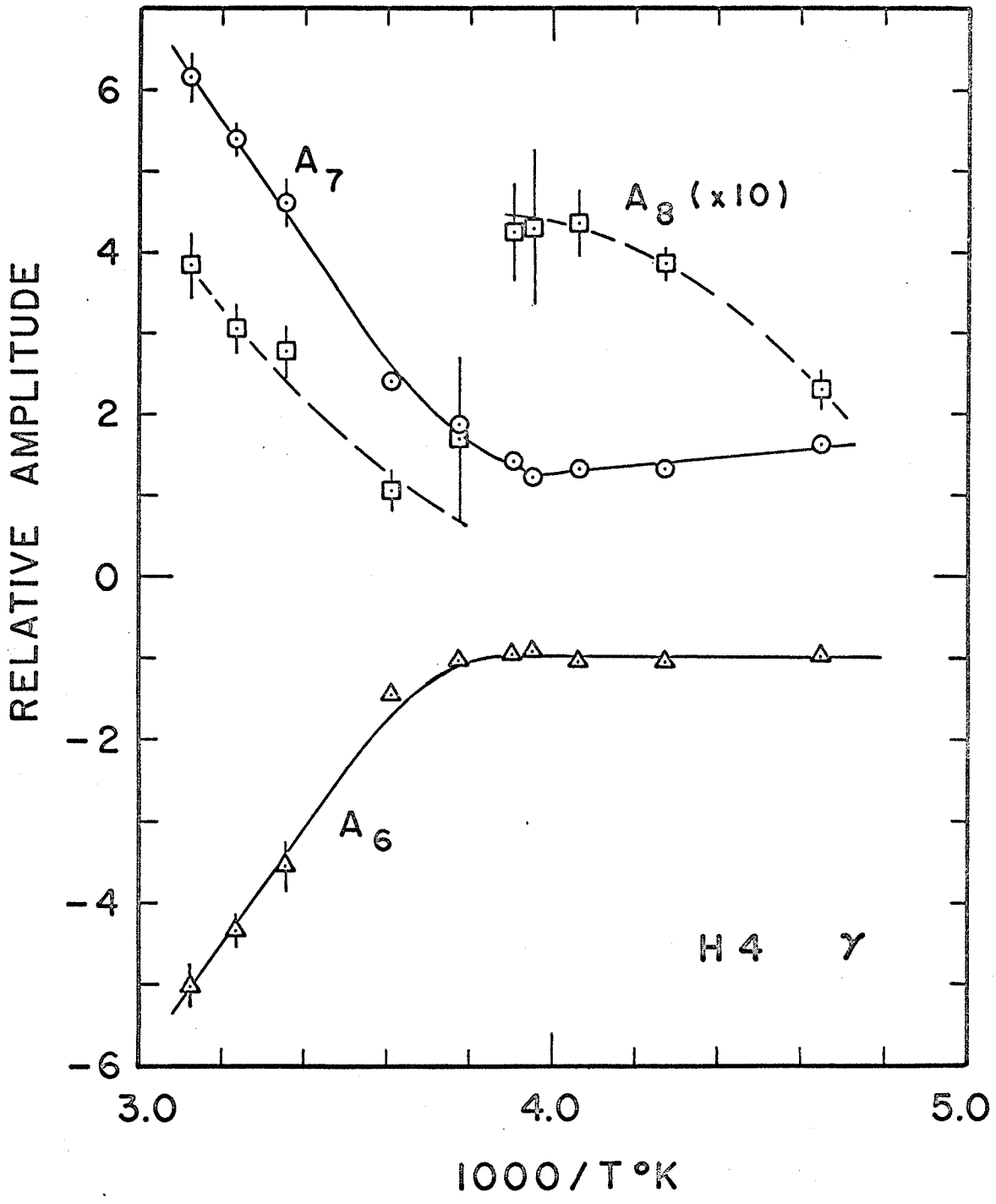
RELATIVE AMPLITUDE
6
4
2
0
-2
-4
-6
3.0
4.0
5.0
1000/T°K
A7
A8 (x10)
A6
H4 γ

emission was found to be in a band below 380 nm and is probably to be associated with the 300 nm emission that is characteristic of pure sodium iodide (Van Sciver and Bogart, 1958). Using a short wavelength pass optical filter (Corning No. 9863) to reduce the longer wavelength main emission, this spike can be resolved sufficiently well at lower temperatures to permit a rough measurement of the time components present. Fig. 4.12 shows the leading edge of the emission at a temperature of -58°C as seen through the 320 nm filter. At least two components are present, the first of decay time 13.2 ± 1 ns and the second 2.8 ± 1 ns. The faster component has about half the intensity of the first.

4.6 Pure NaI

A brief study was made of the scintillations in pure NaI to ascertain whether the fast emission seen in the trace thallium crystal was characteristic of pure NaI. The scintillation pulse shape at room temperature from a nominally pure NaI crystal, H7, is shown in fig. 4.13, uncorrected for system response. The luminescence was found to contain at least three components under gamma excitation. These are given in table 4.6. The parameters for components one and two are much the same as those reported above for the fast emissions in the trace thallium crystal H4.

Through the use of a set of optical filters (Corning Nos. 9863, 7380, 3850; Appendix A-5) it was determined that the fast components one and two, are in an emission band below approximately 380 nm while the longer component, number three, probably has an emission band in the vicinity of 380 nm. Since the time constant for the third component increased with reduction of the relative amount of short

Figure 4.12

The Leading Edge of the Scintillation

of NaI(<0.01% Tl) at -58°C

Time scale is 0.607 ns per channel.

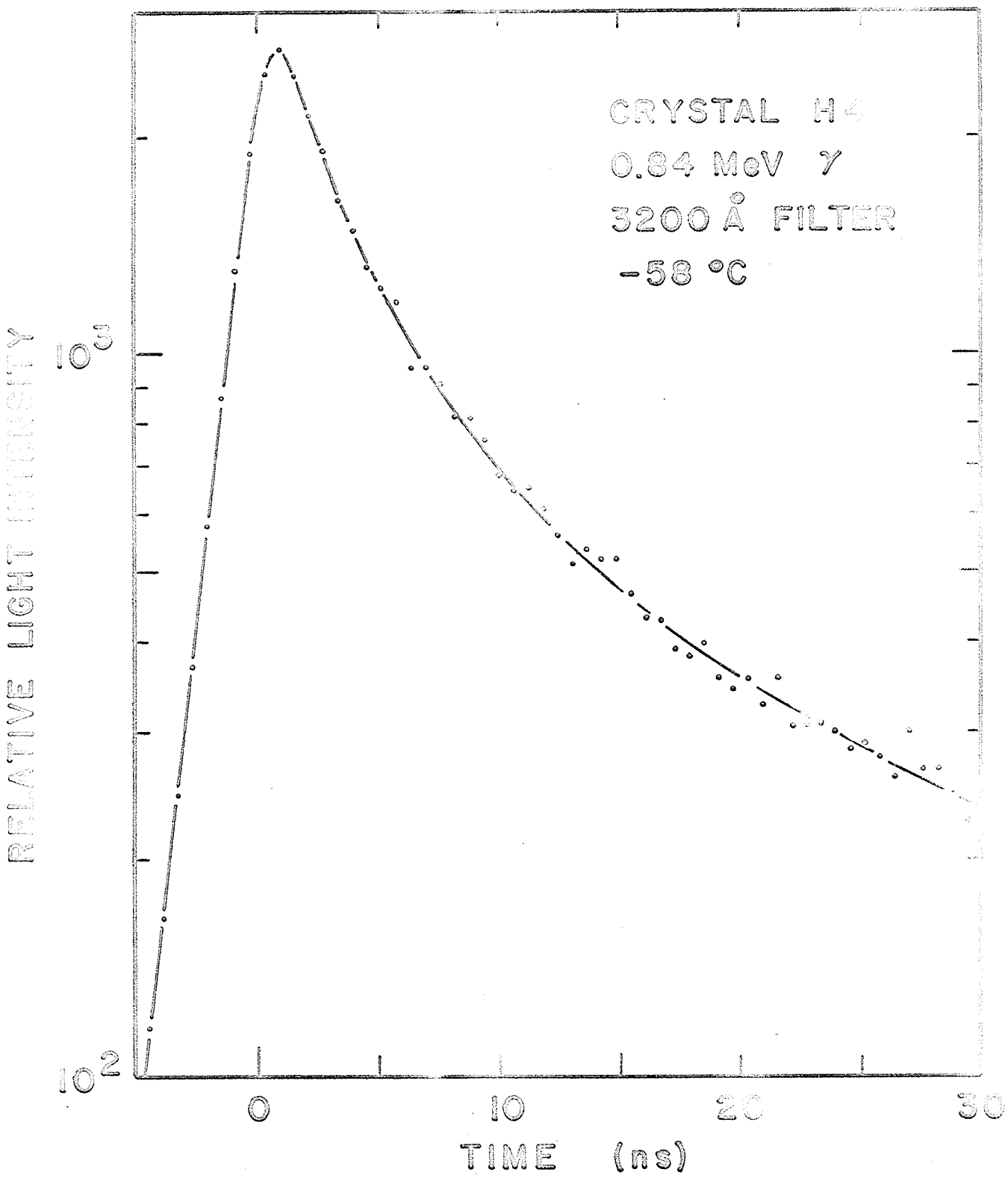
CRYSTAL H4
0.84 MeV γ
3200 Å FILTER
-58 °C
RELATIVE LIGHT INTENSITY
10³
10²
0
10
20
30
TIME (ns)

Figure 4.13

Scintillation Pulse Shape for Pure NaI at 25°C

Time scale is 0.607 ns per channel.

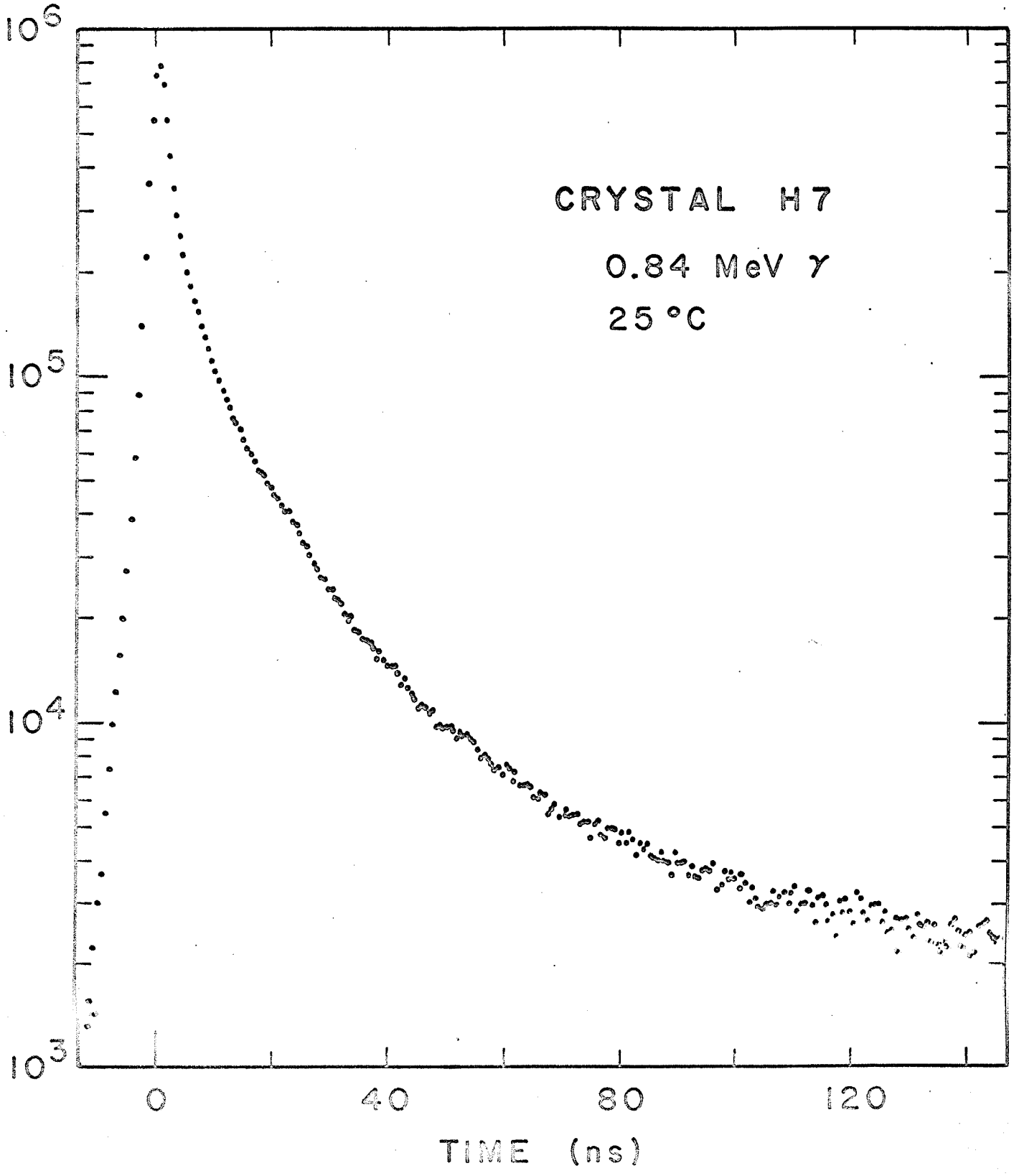
CRYSTAL H7
0.84 MeV γ
25 °C
10^6
10^5
10^4
10^3
0
40
80
120
TIME (ns)

Table 4.6

Room Temperature Parameters for Pure NaI

COMPONENT	AMPLITUDE	DECAY TIME (ns)
1	1200 ± 400	2 ± 1
2	400 ± 150	13.5 ± 2
3	22 ± 15	100 ± 10

wavelength emission accepted by P2, this component is in fact multiple. A portion is due to a longer life time (>100 ns) having a wavelength in excess of 380 nm. The major part is due to the 380 nm emission whose decay time is more like 70 ns.

There has been little work done on pure NaI at room temperature where its efficiency is poor. Van Sciver and Hofstadter (1955) reported a life time at 20°C of 10 ± 2 ns and later Van Sciver and Bogart (1958) indicated in a graph a value of 13 ± 3 ns. The intermediate lifetime reported in this work agrees well with the earlier values.

There has been some evidence that the emission from pure NaI has multiple components at low temperatures, e.g. Bonanomi and Rossel (1951, 1952) and Van Sciver and Bogart (1958). In particular Watts et al (1961) have reported a component of approximately 1500 ns whose emission wavelength they determined to be between 360 and 530 nm.

The major portion of the 100 ns emission in this work may be associated with a stoichiometric excess of iodine present in the sample studied. The emission spectrum under gamma excitation for a crystal cut from the same boule has been measured by another group in this department (C. Watson, private communication). At room temperature the emission spectrum shows a band in the vicinity of 300 nm, a second at about 380 nm and a weak third at 420 nm. The work of Van Sciver (1960) has associated an emission at 375 nm with a stoichiometric excess of iodine.

CHAPTER V

DISCUSSION

5.1 Introduction

Luminescence is the phenomenon of the emission of electromagnetic radiation in excess of thermal radiation and involves optical transitions between electronic states which are characteristic of the radiating substance. Although excitation of the luminescent material is required for subsequent luminescent emission, the emission spectrum is usually independent of the nature of the excitation. Probably the first observation in this vein was made by Zecchi in the year 1652. In most inorganic solids, luminescence involves activators in the form of impurities or structural defects. In the case of luminescence due to impurities, the electronic states involved can be approximated, in some cases, by the energy levels of the impurity ion as perturbed by the crystal field. In general, these impurity electronic states give rise to optical absorption bands on the long-wavelength side of the fundamental absorption edge of the perfect crystal. It is usual to find the luminescent emission in the form of bands or a broad bell-shaped spectrum at even longer wavelengths, i.e. the crystal is fairly transparent to its own luminescent emission (observed by Stokes, 1852).

In addition to the electronic states actually involved in the emission transition, other electronic states (belonging to the activator or to other impurities, etc.) may require consideration when questions concerning luminescence efficiency or time constants are considered. Nonradiative de-excitations can compete with radiative processes. With increasing temperature these competing nonradiative processes become more probable and the luminescent emission intensity decreases. If both

radiative and nonradiative transitions are possible from the same excited state, the time constant for fluorescence decreases with increasing temperature. The luminescence emission can be delayed by the presence of metastable states, either of the activator itself or of defects (electron/hole traps) spatially separated from the activator. Since thermal activation of such metastable states is required prior to emission, this process is strongly temperature dependent and may as well depend on the intensity of excitation.

Prior to the development of the quantum theory, only an empirical knowledge of luminescence was possible (e.g. the Stokes' law). The basis of a fundamental understanding of luminescence in solids was provided by the growth of the quantum mechanics. The concepts required include:

(i) the existence of stationary electronic states between which radiative transitions occur,

(ii) the adiabatic approximation, i.e. the separation of electronic and nuclear parts of the wave function,

(iii) the band theory model for electrons in a periodic potential,

(iv) the theoretical basis for excitons, i.e. excited nonconducting states.

The first of the models for luminescence was an energy level scheme proposed by Jablonski (1933) for fluorescence in organic dyes. This included emitting, metastable and ground states between which states, radiative and nonradiative transitions were possible. The superposition of such discrete energy levels on a simple energy band structure for the solid is a model that has found favour in phenomenological descriptions of luminescence associated with photoconductivity (e.g. Johnson, 1939; Nyberg and Colbow, 1967).

An attempt to explain the optical properties of single crystals of the alkali halides doped with small concentrations of thallium was made by Seitz (1938) and is today the simplest satisfactory model for the interpretation of the absorption and emission spectra in such crystals. Two possible models were suggested by Seitz, both based on the assumption that the thallous ion replaces the alkali ion substitutionally. The impurity plus all of the neighbouring ions whose equilibrium positions are altered by its presence constitute the luminescent centre. It is usually assumed that the centre is a highly localized one and that the nearest neighbour halide ions are the most influential components of the host lattice. The first of Seitz' models was based on the excited states of a free thallous ion in a cubic crystal field. The effect on spectra of changes in the nuclear coordinates of all the atoms constituting the centre resulted in the configuration coordinate model of luminescence. A qualitative understanding of the Stokes' shift and the widths of absorption and emission bands follows from the configuration coordinate model. Edgerton (1965) and Illingworth (1964) have interpreted the emission spectra of KI(Tl) on the basis of an extension of the Seitz model. The second model proposed by Seitz considered the transitions of the electrons from the neighbouring halides to the thallous ion. Although Seitz rejected this model, Knox (1959) reopened the possibility that such electron transfer states may be important in interpreting absorption phenomena.

A quantitative treatment of the Seitz model for the KCl(Tl) luminescent system was made by Williams (1951). Using the proposals of Seitz on the energy level structure of the thallium substitutional

impurity and on the use of the adiabatic approximation to obtain a configurational coordinate model, Williams approximated the symbolic configuration coordinate with a single real coordinate of the activator centre (the distance between the Tl^+ ion and the nearest neighbour Cl^- ions). He was able to calculate semiempirically, the energies of the $^3P_1$ and $^1S_0$ free thallous ion states as functions of the configuration coordinate. Using these calculated configuration coordinate curves, predictions of the spectral locations and temperature dependence of the widths of the 247.5 nm absorption and 305 nm emission bands were made (Williams and Hebb, 1951). This Seitz-Williams model was later shown by Knox and Dexter (1956) to be inadequate and the agreement with experiment to be, to some extent, fortuitous. Improvements and refinements in the theory have been suggested by different workers, e.g. Johnson and Williams (1960), Kristofel (1960), Potekhina (1960), Kristofel and Zavt (1966).

Although the bulk of the luminescence in thallium activated alkali halides has generally been attributed to internal electronic states of the thallous ion, there has been some controversy as to the nature of the centre responsible for the emission. On the basis of a comparative study of doped and undoped samples of several alkali halides as a function of temperature, Bonanomi and Rossel (1952) found it difficult to attribute to the thallous ion a direct role in the fast decay scintillations. They associated the luminescent centre with a defect to be found in the pure crystal, presumably a vacancy site. The function of the thallium additive was then to increase the number of vacancy centres. In their studies of the optical properties of KI, KBr, KCl, and NaCl, Hersh and Hadley (1963) investigated annealed, plastically

deformed, thallium doped and undoped crystals. They conclude that internal metastable states of the thallous impurity play only a minor role and that structural defects of the host crystal are most important. The effect of plasic deformation was subsequently investigated by Cooke and Palser (1964) and the importance of surface states in NaI was noted.

Although it is generally agreed that transitions between electronic states of the thallous centre are responsible for luminescence, the phenomenon is sufficiently complex that disagreement persists in the literature on the nature of some of these states and on the intracentre kinetics involved. Studies of the luminescence in KI(Tl), KCl(Tl) and KBr(Tl) have produced two rather different schools of thought. The works of Illingworth (1964) and Edgerton and Teegarden (1963, 1964) are typical of what has been called the American concept. The American work is criticized at some length by Trinkler and Plyavin' (1965) who represent the Russian point of view.

Excitation of KI(Tl) in the A band (4.38 eV, Yuster and Delbecq, 1953) results in a strong emission at 336 nm and a weaker emission at 430 nm. Illingworth (1964) found that the 336 nm emission was fast (decay time < 50 ns) and that the 430 nm band had two components, one fast (< 50 ns), the other being slow ($\sim$ 200 ns at room temperature) and temperature dependent. On the basis of the temperature dependence of the lifetimes involved, a qualitative configuration coordinate model, fig. 5.1(a), was suggested by Illingworth in which the upper two excited states are associated with the thallous ion ($^3P_1$ and $^3P_0$ using the notations for atomic symmetries). The lower state is linked with an excited state of the I^- ions surrounding the Tl^+ impurity. The radiative and nonradiative transitions that are possible are shown in the energy level diagram of fig. 5.1(b).

Figure 5.1

Models for the A Band Luminescence of KI(Tl)

(a) Qualitative configuration coordinate diagram for the luminescence decay of KI(Tl) excited in the "A" band (after Illingworth, 1964).

(b) Energy level diagram for (a). Nonequilibrium model.

(c) Equilibrium energy level diagram suggested by the work of Trinkler and Plyavin' (1965).

(a)

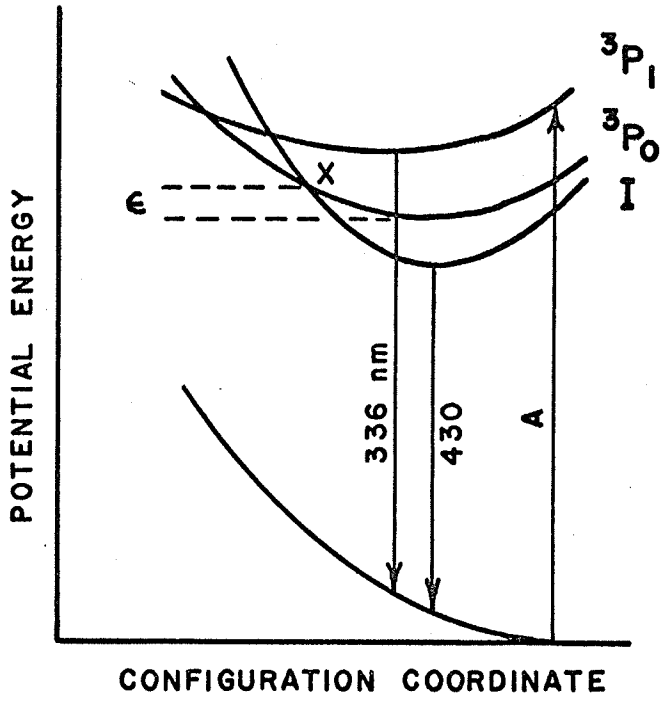
$^3P_1$
$^3P_0$
I
X
ϵ
336 nm
430
A
POTENTIAL ENERGY
CONFIGURATION COORDINATE

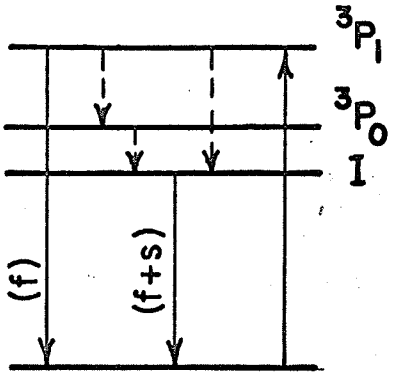
$^3P_1$
$^3P_0$
I
(f)
(f+s)

(b)

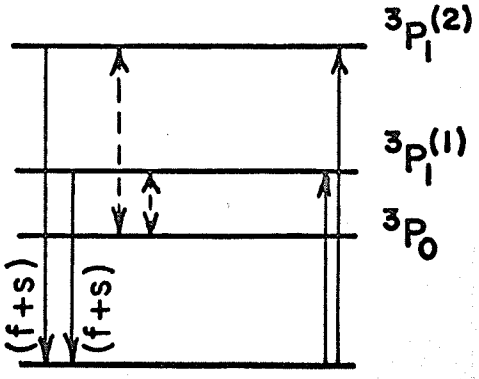
$^3P_1^{(2)}$
$^3P_1^{(1)}$
$^3P_0$
(f+s)
(f+s)

(c)

The experimental work of Trinkler and Plyavin' (1965) differs in that the A absorption band was not found to be elementary and the short wavelenth emission was determined to be complex, having both fast and slow components. Both the slow components (345 nm and 425 nm) were found to have the same decay times (190 ns at 293°K). The two radiative states were associated by Trinkler and Plyavin' with the Jahn-Teller split $^3P_1$ thallous ion level. The associated energy level diagram is shown in fig. 5.1(c). Fowler (1968) questions whether the Jahn-Teller effect can reasonably account for the large energy difference between the suggested split $^3P_1$ levels.

In addition to the differences in experimental data and their interpretation in terms of the nature of the electronic states involved, there is a disagreement concerning the kinetics of the luminescence. The point at issue here is whether, or not, there arises, shortly after the stimulation of the crystal, an equilibrium distribution of electrons over all three excited levels of the centre, i.e. a Boltzmann distribution. Trinkler and Plyavin' suggest that upward and downward nonradiative transitions among the three excited electronic states (fig. 5.1(c)) are highly probable and that once this equilibrium has been established the emission in both bands must decay with the same time constant. Illingworth considers that only downward nonradiative transitions are of import and it follows that an equilibrium distribution cannot ever be achieved. This question will be pursued in section 5.5 with reference to the kinetics of NaI(Tl).

In addition to the thallous ion related luminescence, all of the nonactivated alkali iodides exhibit luminescence in the near ultraviolet under excitation by charged particles or sufficiently energetic photons. In the case of NaI, Van Sciver (1956) attributed the 295 nm emission at

liquid nitrogen temperature to the radiative decay of a localized exciton. The works of Kabler (1964) and Murray and Keller (1965) have shown that the corresponding luminescence in KI, and KBr and NaCl is due to the radiative decay of excited states produced by the recombination of an electron with a self-trapped hole. The self-trapped hole, or V_k centre, (see Delbecq et al, 1961) is a molecular ion of the form X_2^-, and consists of a localized charge deficiency (a hole) together with a lattice distortion in which two neighbouring halide ions are pulled together along a <110> direction of the crystal (in a face centred cubic lattice). In their study of CsI(Tl), Gwin and Murray (1963) consider that the V_k centres are capable of motion through the lattice. The thermal activation for V_k motion in the case of NaI was found by Murray and Keller (1967) to be 0.15 eV.

The recombination of an electron with a V_k centre produces an excited state, referred to in this work as a V_{ke} centre, which, according to the studies of Murray and Keller (1967), retains the <110> symmetry axis characteristic of I_2^-. Such states are not to be confused with the exciton states produced in fundamental band absorption, but correspond instead to "self-trapped" excitons. Thus there are two methods of arriving at a V_{ke} state of the pure crystal, either via ($V_k + e^-$) or by (exciton + $2I^-$). Murray and Keller (1967) note that although the two methods evidently produce the same luminescence in NaI, this is not true in general. There is not a one-to-one correspondence in the states arrived at by the two processes in such crystals as KI, KBr and RbI. Configuration coordinate diagrams for the V_{ke} centre have been calculated by Wood (1966) and give a possible interpretation for the observed emission bands of NaI, KI, and RbI and their temperature dependence.

5.2 Energy Transport

Associated with questions concerning the nature of the electronic states responsible for luminescence are the details of energy transfer in the crystal. In the case of thallium centre luminescence, the direct excitation of $Tl^{\pm}$ sites by an incident charged particle cannot account for the observed emission intensity because the thallium concentration in such crystals is normally orders of magnitude too low. Thus some method of energy transport in the crystal must exist in order that the Tl^{+} sites be excited.

The detection of a gamma ray in an alkali crystal is understood to proceed through several steps. The hard radiation produces Compton electrons and photoelectrons which in turn give rise to cascades of secondary electrons, or delta rays (Meyer and Murray, 1962). These primary and secondary electrons will quickly (~10 ps) lose their excess energy in the production of electron-hole pairs (i.e. electrons in the conduction band and holes in the valence band) as well as excitons. These fundamental excitations are indicated in the process block diagram of fig. 5.2.

Of concern are the two major mechanisms by which the thallous centre can be excited to allow subsequent radiation. The first of these involves the migration of excitons to the thallous ion sites (Van Sciver, 1965: Murray and Meyer, 1961):

$$Tl^{+} + \text{exciton} \longrightarrow Tl^{+*} \qquad (5.1)$$

$$Tl^{+*} \longrightarrow Tl^{+} + \text{photon}$$

Secondly it is possible to excite the thallous centre by independent binary diffusion of electrons and holes (Van Sciver, 1956; Gwin and

Figure 5.2

Block Diagram of the Scintillation Process

in Na(Tl) under Gamma Excitation

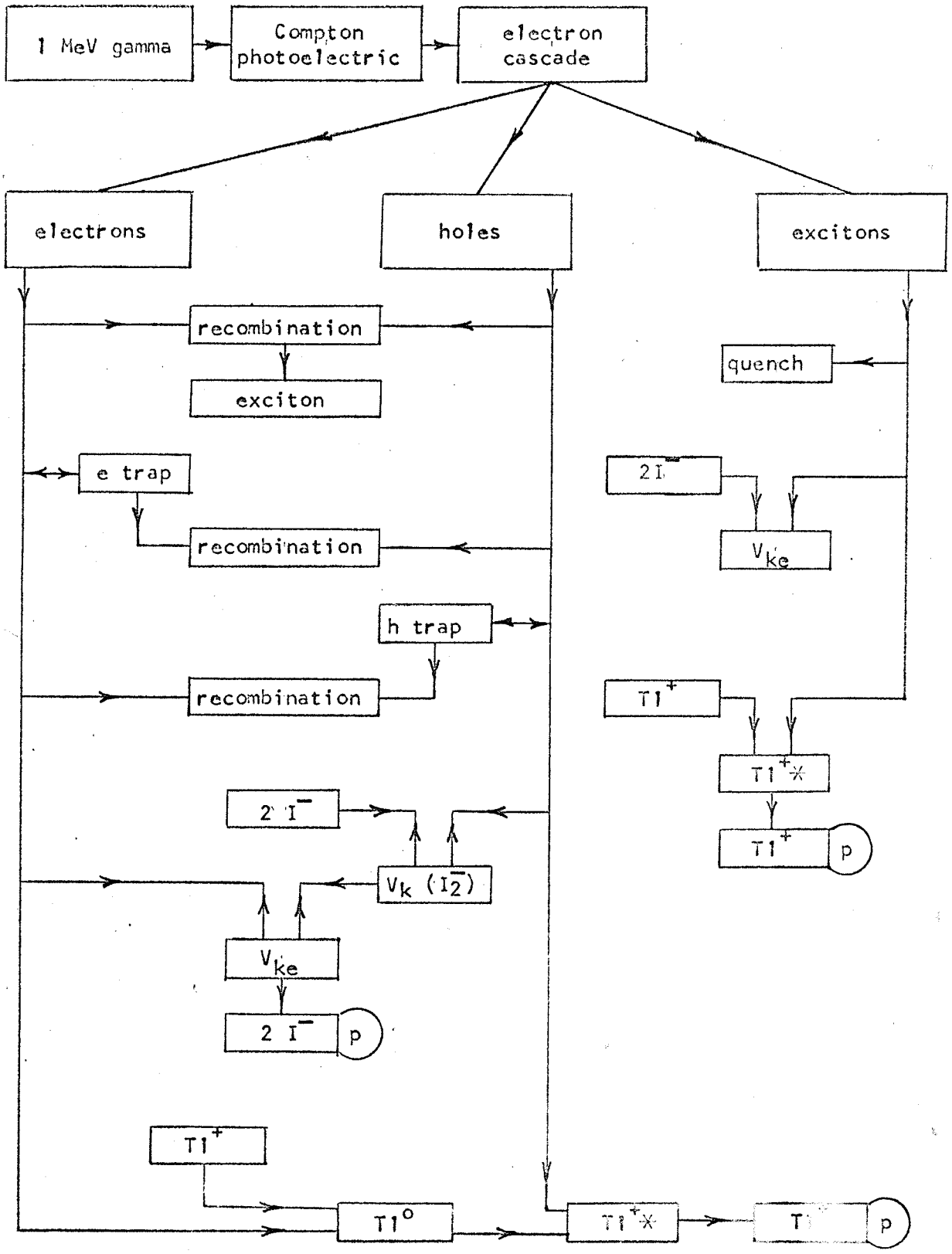
1 MeV gamma
Compton photoelectric
electron cascade
electrons
holes
excitons
recombination
exciton
quench
e trap
2 I⁻
recombination
Vke
h trap
recombination
Tl⁺
Tl⁺*
2 I⁻
Tl⁺
p
Vk (I2⁻)
Vke
2 I⁻
p
Tl⁺
Tl⁰
Tl⁺*
T
p

Murray, 1963; Chornii and Lyskovich, 1965).

$$Tl^{+} + e^{-} \longrightarrow Tl^{\circ}$$

$$Tl^{\circ} + h^{+} \longrightarrow Tl^{+*} \qquad (5.2)$$

$$Tl^{+*} \longrightarrow Tl^{+} + \text{photon}$$

Since the V_k centre itself is mobile at temperatures above 58°K in NaI (Murray and Keller, 1967), the hole diffusion to the Tl° centre indicated in fig. 5.2 and in equation (5.2) may be by means of V_k motion.

A third possible method of energy transfer resulting in thallous centre emission is one in which the pure crystal scintillates (at approximately 300 nm in NaI) only to have the emission absorbed and re-emitted at a longer wavelength by the thallium centres. In this suggested mechanism, the Tl^{+} acts as a wavelength shifter. Van Sciver (1958), on the basis of an efficiency argument, concluded that this photon emission and reabsorption can at most be a minor contributor to energy transfer.

The block diagram of fig. 5.2 also shows the two processes mentioned in section 5.1 through which V_{ke} centres may be excited to produce the intrinsic luminescence observed in the alkali halides.

5.3 Scintillation Kinetics: Empirical Development

It is clear from the experimental data that have been presented in Chapter IV and from the discussions in the preceding two sections, that the scintillation process in NaI(Tl) under gamma excitation is quite complex. Limitation of scintillation equipment time-measuring capabilities restricts measurements of time components to those greater than about 0.2 ns. Thus processes taking less time than this may be considered to be

essentially instantaneous, e.g. all steps in fig. 5.2 prior to the formation of the fundamental crystal excitations (electrons, holes, excitons). The subsequent steps in the production of the luminescence may be expected to proceed more slowly and to follow exponential decay laws. Mean life times in the microsecond and submicrosecond region are typical and have been measured. The scintillation pulse shape can be expected to yield information not only on these characteristic mean lives but also to indicate the presence of competitive paths, the number of steps in each path and the branching ratios.

In general, a luminescence process consisting of n consecutive steps each having a life time τ_j, or transition probability $\alpha_j=1/\tau_j$, produces a scintillation response of the form:

$$I = \Sigma a_j \, e^{-(\alpha_j t)} \quad \text{photons/sec}, \quad j = 1, n. \tag{5.3}$$

Such a process is shown diagrammatically in fig. 5.3(a). This figure represents an energy source, S, which through various intermediate processes excites a radiative state D. The observed luminescence results from the radiative transition from D to the ground state E. If the initial populations of the intermediate states A through D are taken to be essentially zero, then the amplitudes a_j are given by

$$a_j = \frac{\tau_j^{(n-2)}}{\Pi(\tau_j - \tau_k)} \quad , \quad k = 1, n; \neq j. \tag{5.4}$$

The amplitudes are dependent on the life times and sum to zero. If the terms of equation (5.3) are arranged in descending order of the τ's, then the odd numbered terms have positive amplitudes and the even terms

Figure 5.3

Block Diagram for Luminescence Kinetics

(a) Involving n steps.

(b) Involving a parallel path.

(a)

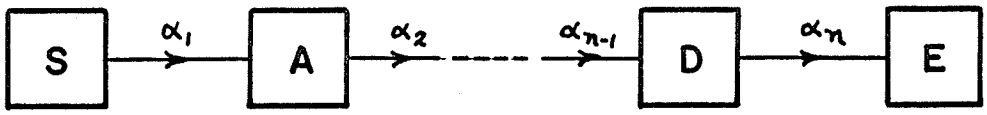
S
α_1
A
α_2
α_{n-1}
D
α_n
E

(b)

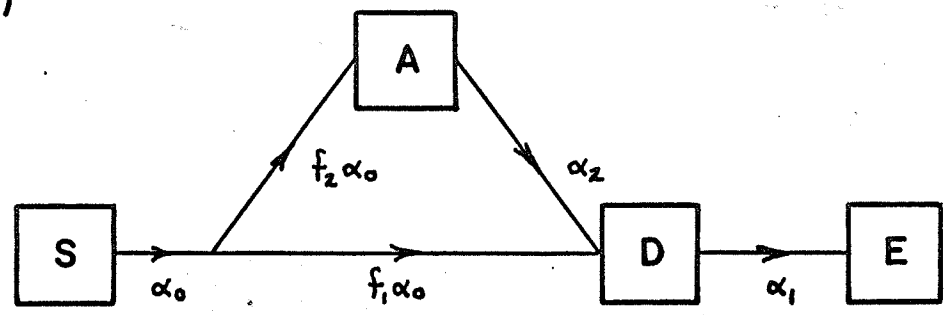
A
$f_2\alpha_0$
α_2
S
D
E
α_0
$f_1\alpha_0$
α_1

have negative amplitudes.

To synthesize a pulse shape for a system containing parallel paths, the responses for the individual paths must be multiplied by their relative probabilities and then added. Experimentally we are presented with this composite response and are concerned with the inverse problem of deducing the underlying processes.

If one considers the response to be expected from the luminescence model of fig. 5.3(b), the scintillation pulse will be the sum of two branch path contributions, a three step process via A and a two step directly through D. The time dependence to be expected is:

$$I = f_2\left[\frac{\tau_2\, e^{-\alpha_2 t}}{(\tau_2-\tau_o)(\tau_2-\tau_1)} - \frac{\tau_1\, e^{-\alpha_1 t}}{(\tau_1-\tau_o)(\tau_2-\tau_1)} + \frac{\tau_o\, e^{-\alpha_o t}}{(\tau_2-\tau_0)(\tau_1-\tau_o)}\right]$$

$$+ f_1\left[\frac{e^{-\alpha_1 t}}{\tau_1-\tau_o} - \frac{e^{-\alpha_o t}}{\tau_1-\tau_o}\right] \qquad (5.5)$$

$$= \Sigma A_j\, e^{-\alpha_j t}, \qquad j = 0, 2.$$

In this equation the appropriate branching ratios have been denoted by the probabilities f_1 and f_2 where: $f_1 + f_2 = 1$. The algebraic signs of the various terms have been anticipated assuming that $\tau_o < \tau_1 < \tau_2$. Under these circumstances it is noted that the amplitude A_2 will be positive while the signs of the resultant amplitudes A_0 and A_1 may be positive or negative:

$$A_o = \frac{\tau_o - f_1 \tau_2}{(\tau_1 - \tau_o)(\tau_2 - \tau_o)} \tag{5.6}$$

$$A_1 = \frac{f_1 \tau_2 - \tau_1}{(\tau_1 - \tau_o)(\tau_2 - \tau_1)} \tag{5.7}$$

In particular: $A_1 > 0$ if $f_1 > \tau_1/\tau_2$

$= 0$ if $f_1 = \tau_1/\tau_2$

< 0 if $f_1 < \tau_1/\tau_2$.

A model for the scintillation kinetics follows from the form of the pulse shape which has been experimentally measured. Considering the room temperature pulse shape for crystal H5, the fitted parameters are reproduced in the upper portion of table 5.1(a). Amplitudes A_8 and A_7 are both positive and belong to long time constants with no other term having a life time intermediate to these. From the kinetics features outlined above, these facts indicate that components seven and eight must be the longest lived members of different paths. The negative value of A_0 for the shortest time component implies the existence of a two or a four step process. The four step process cannot produce a large A_0 with these particular parameter values since A_8 is too small. Thus there must be at least one two step process involving component zero with either component six, seven, or eight. Component eight can be ignored because A_8 is too small and τ_8 too large. Since the amplitude A_6 changes sign with decreasing temperature, A_6 must be the result of a sum of terms of competing signs. For a positive contribution component six must be the longest lived member of a path. Thus component six is selected as the member of the two step process in conjunction with component zero. Since component six has as well a negative portion, it must also be the intermediate life time member of a three step process which can only be the trio: seven, six

Table 5.1

Kinetics Analysis for Crystal H5

(a)	H5 298°K				
COMPONENT	8	7	6	0	
T (ns)	723	173	43	1	
AMPLITUDE	+ 159	+ 5600	− 1946	− 3813	
DECOMPOSITION:					f (%)
to A		+ 5600	− 5699	+ 99	72
to B	+ 159		− 162	+ 3	11
to D			+ 3915	− 3915	17

(b)	H5 260°K				
COMPONENT	8	7	6	0	
T (ns)	990	316	109	1	
AMPLITUDE	+ 332	+ 1608	+ 1500	− 3440	
DECOMPOSITION:					f (%)
to A		+ 1608	− 1618	+ 10	33
to B	+ 332		− 335	+ 3	29
to D			+ 3453	− 3453	37

(c)	H5 217°K				
COMPONENT	8	6	5	0	
T (ns)	3080	208	17	1	
AMPLITUDE	+ 121	+ 3142	− 1490	− 1773	
DECOMPOSITION:					f (%)
to B	+ 121	− 121		∿ 0	35
to C		+ 1409	− 1490	+ 81	27
to D		+ 1854		− 1854	38

and zero.

It must be remembered that the mathematics of kinetics does not distinguish between the different possible genetic sequences. For example the process (6 $\longrightarrow$ 0) is mathematically equivalent to (0 $\longrightarrow$ 6). Physical insight must be used in the selection of viable processes to form an empirical model such as fig. 5.3(b).

The first term in any sequence should be representative of energy transport in the crystal from the region in which the incident gamma is absorbed to the location of the thallous ion luminescent centre. This is expected to be a very fast process since the energy carriers (electrons, holes, excitons) are short-lived. The exciton life time is estimated by Seitz (1954) to be of the order of 10^{-9} sec and it may be as short as 10^{-13} sec (Knox and Teegarden, 1968). Taylor and Hartman (1959) suggest that the lack of appreciable photoconductivity in the alkali halides is due to an exceedingly short life time for the free carriers. Swank and Brown (1963), in their work on F centre life times and associated photoconductivity, quote a free conduction electron life time of less than 10 ns. Thus component zero, whose life time is only inferred in this work, is selected as the first member of the three sequences. This choice then requires that component six be a radiative state. Components seven and eight are chosen as intermediate members in their respective sequences since some population of the associated electronic states is expected in the energy transport to the centre (Van Sciver, 1956).

The kinetics of the room temperature scintillation is thus interpreted on the basis of two metastable states feeding a common main radiative state. An empirical block diagram of the above

scintillation processes was suggested by Wall and Roulston (1966, 1968), a slightly modified version of which is shown in fig. 5.4. The central portion of this figure, involving the energy source and blocks A through E, is to be associated with the main thallous ion emission components of figs. 4.4 and 4.5. For simplicity component eight is treated as a single block (B) although as pointed out earlier (section 4.3) it is probably multiple in nature. The three room temperature processes discussed above are represented by the paths:

$$\text{Source } (\tau_o) \longrightarrow A\ (\tau_7) \longrightarrow D\ (\tau_6) \longrightarrow E, \text{ (3 step, } f_7)$$

$$\text{Source } (\tau_o) \longrightarrow B\ (\tau_8) \longrightarrow D\ (\tau_6) \longrightarrow E, \text{ (3 step, } f_8) \tag{5.8}$$

$$\text{Source } (\tau_o) \longrightarrow D\ (\tau_6) \longrightarrow E,$$

The bottom half of table 5.1(a) shows the decomposition of the room temperature pulse into the above three parallel processes. The decomposition is accomplished through the use of the relative sizes of the amplitudes as computed from the insertion of the measured time constants in equation (5.4). The last column indicates the fraction, f, of the total emission involved in the particular process.

$$f_j = \frac{\Sigma a_k \tau_k}{\Sigma A_r \tau_r} \quad , \quad k = 1, n; \ r = 1, m, \tag{5.9}$$

where the number n includes the components of the j^{th} path and m is the total number of components in the entire pulse.

At room temperature approximately 72% of the light is emitted by a process involving the main NaI(Tl) decay component while about 17% arises through the direct population of the radiative state. This is in rough agreement with the work of Eby and Jentschke (1954) who

Figure 5.4

Block Diagram Representation of the Processes

Present in the Scintillation of NaI(Tl)

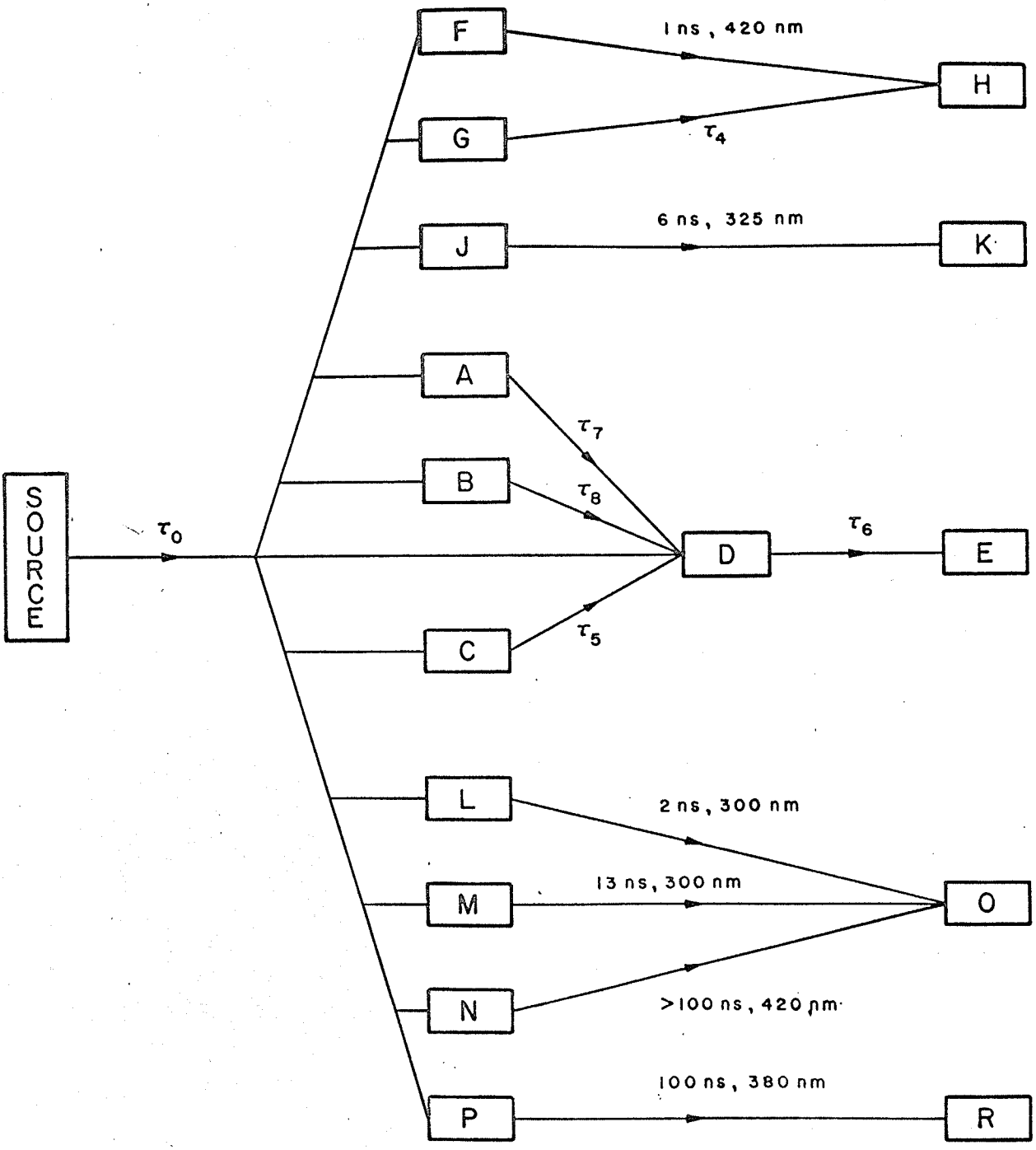
SOURCE
τ_0
F
G
J
A
B
C
L
M
N
P
D
H
K
E
O
R
1 ns, 420 nm
τ_4
6 ns, 325 nm
τ_7
τ_8
τ_5
τ_6
2 ns, 300 nm
13 ns, 300 nm
>100 ns, 420 nm
100 ns, 380 nm

attributed 20% of the emission to the initial population of the radiative state on the basis of a pulse containing only two time components. The long time component path, involving component eight, accounts for 11% of the emission.

Part (b) of table 5.1 repeats the computations of part (a) at a temperature of 260°K. Note that the sign reversal of A_6 appears to be due to a relative strengthening of the two step process, i.e. an increase in f_6. In this temperature region the fractional contributions from each of the three processes are very roughly equal.

A further lowering of the temperature results in the vanishing of component seven and the appearance of a new negative amplitude, short time constant term, number five. The upper portion of table 5.1(c) indicates the relevant parameters at a temperature of 217°K. This component must be the intermediate life time member of a three step process involving components six, five and zero. This new path appears in fig. 5.4 as:

(5.10) Source $(\tau_o) \longrightarrow C\ (\tau_5) \longrightarrow D\ (\tau_6) \longrightarrow E,\quad (f_5)$.

At 217°K this path accounts for some 27% of the emission.

A summary of the behaviour of the fractions of the total emission involved in each of the four processes is given in the curves of fig. 5.5. The probability of emission via the main decay component, number seven, is seen to drop rather quickly with lowering of the crystal temperature. The fraction proceeding through component eight goes through a relative maximum in the vicinity of 240°K. The branching ratio for the direct population of the radiative state generally increases with decreasing temperature. The discontinuity in the f_6 curve may be

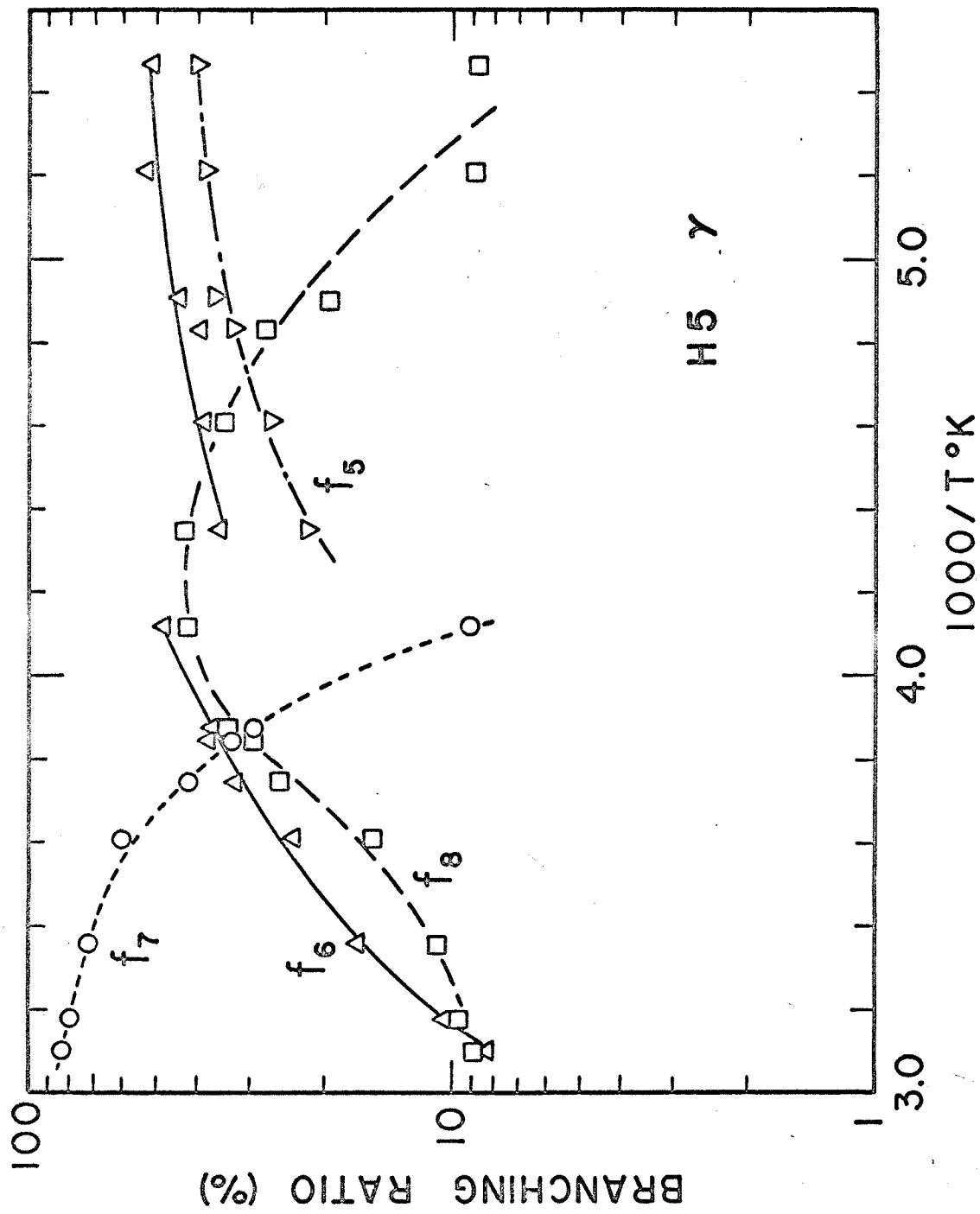
H5 γ
f5
f6
f7
f8
100
10
1
3.0
4.0
5.0
1000/T°K
BRANCHING RATIO (%)

due to the abrupt inclusion of component five in the scintillation process. If extrapolated values for A_5 and τ_5 are included at the higher temperatures, the discontinuity does not appear.

The results of a similar kinetics analysis for the 0.71% thallium crystal are shown in fig. 5.6 (crystal H6). The behaviour of the ratios f_6, f_7 and f_8 in this excess thallium crystal is seen to be much the same as that of the previous normal crystal. A discontinuity again appears in the f_6 curve but its explanation is less certain in this case since f_5 is not present and f_4 is too weak to account for much of an effect. It can only be noted that τ_6 at a temperature of 277°K seems to be anomalously high (fig. 4.8). Curve fitting in this temperature region is rather more difficult than at lower or higher temperatures because A_6 is close to zero. The appearance of a new positive amplitude short time constant term, number four, has been accommodated in the block diagram of fig. 5.4 by the path:

(5.11) Source (τ_o) $\longrightarrow$ G (τ_4) $\longrightarrow$ H, (f_4).

The room temperature spike which is observed in fig. 4.7 to have a life time of the order of 1 ns is represented by the path:

(5.12) Source $\longrightarrow$ F $\longrightarrow$ H

Blocks F through K indicate processes which are thought to be associated with multiple thallous ion centres. The thallium dimer spike which is prominent at low temperatures in the crystals having at least normal thallium concentrations is represented by:

(5.13) Source $\longrightarrow$ J $\longrightarrow$ K.

The blocks L through R represent the processes found in the scintillation of the pure crystal with the processes involving blocks L and M also being apparent in the trace thallium crystal.

Figure 5.6

The Temperature Variation of the

Branching Ratios in NaI(0.7l% Tl)

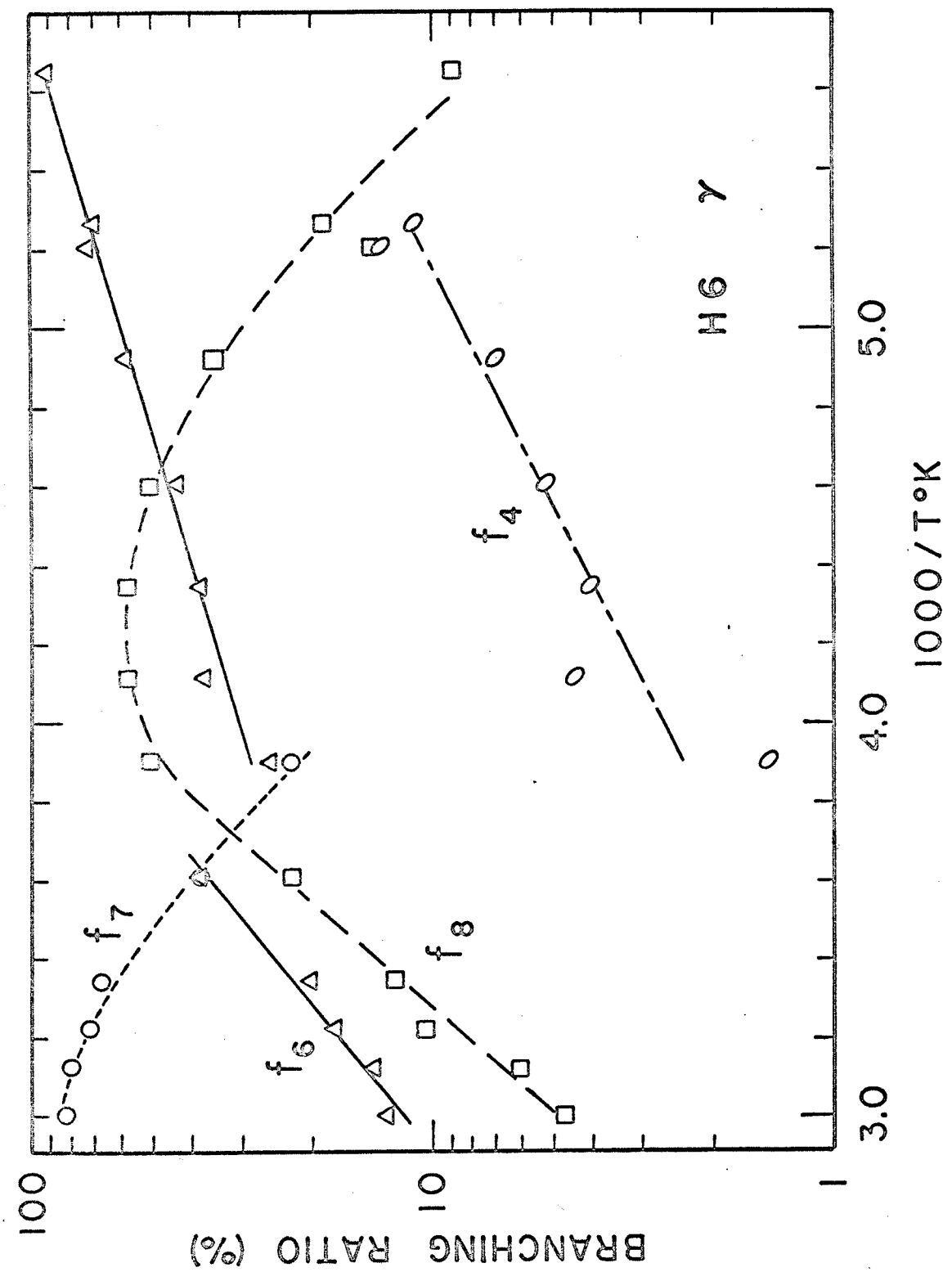
BRANCHING RATIO (%)
100
10
1
3.0
4.0
5.0
1000/T°K
H6 γ
f4
f6
f7
f8

The results of the kinetics analysis for the main emission in the case of the trace thallium crystal (H4) are shown in fig. 5.7. The behaviour here bears little resemblance to that seen in the preceding two figures for the higher thallium concentration crystals. The fraction of the emission by the direct excitation of the radiative state is only 12% at room temperature. This is in rough agreement with the work of Eby and Jentschke (1954) who estimated something like 10% for this figure (but on the basis of a two component pulse). This fraction generally decreases with decreasing temperature which is opposite to the behaviour of f_6 in the other two crystals.

The temperature dependence of components six and seven for this trace thallium crystal may possibly be explained by the apparent absence of component five. The effect of decreasing thallium concentration seems, from figs. 4.4 and 4.8, to shift the temperature at which component five is measurable towards higher temperatures. A further reduction in thallium concentration could cause another such shift of the T_5 component. This would then result in the mixing of the effects of components five and six. Since component seven presumably fades out as temperature is lowered, and component six changes sign, it is possible that a computer fit on the basis of three exponentials would be misleading. The experimental data acquired in this work were not of sufficient statistical precision to attempt a curve fit with four components. It is suggested that the low temperature portions of the curves for parameters six and seven in figs. 4.10, 4.11 and 5.7 are in fact to be associated with components five and six respectively.

5.4 Scintillation Efficiency and Energy Transport

The relative scintillation efficiency of NaI(Tl) has a

Figure 5.7

The Temperature Variation of the

Branching Ration in NaI(<0.01% Tl)

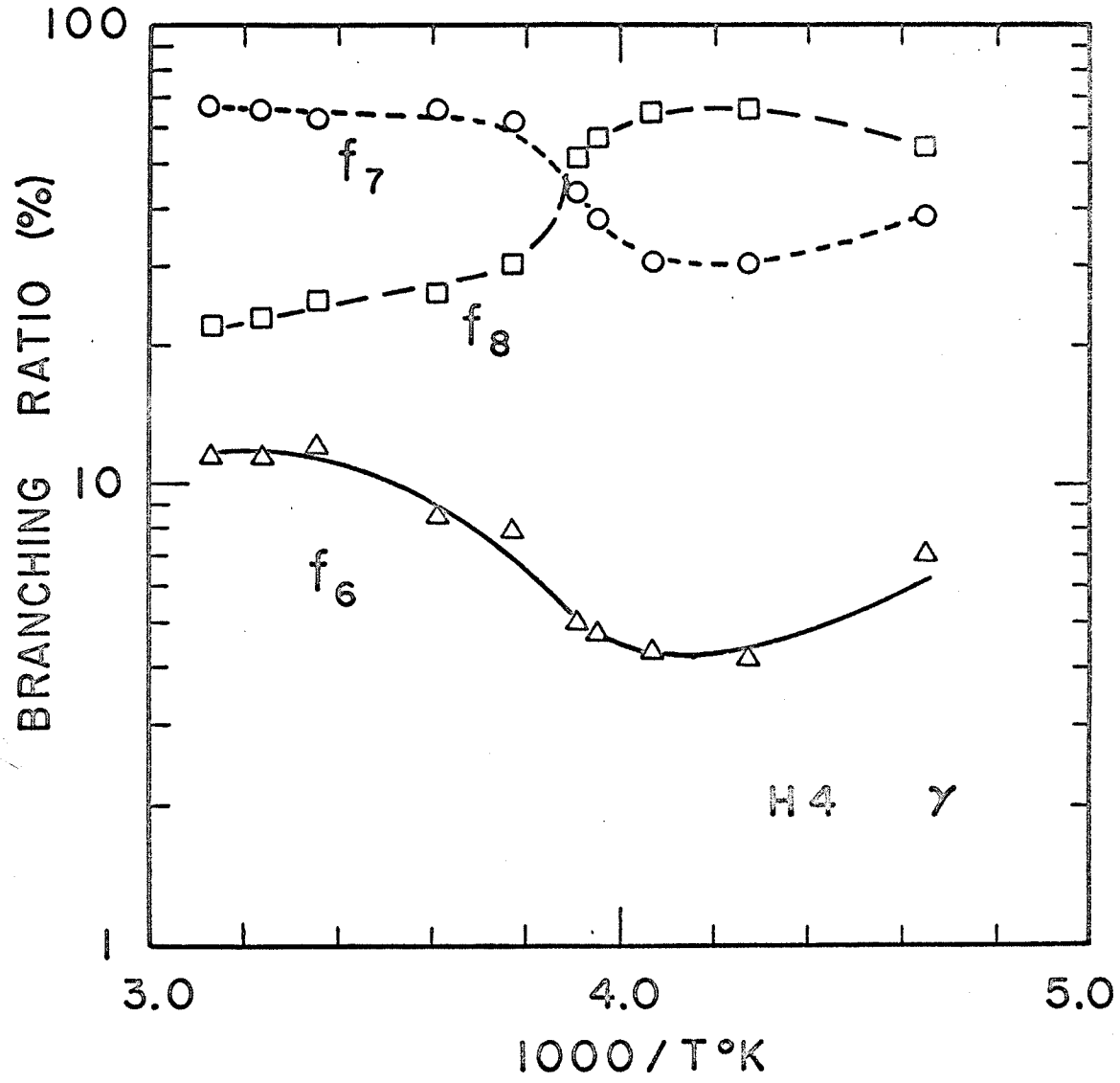
100
10
1
BRANCHING RATIO (%)
f_7
f_8
f_6
H4 γ
3.0
4.0
5.0
1000/T°K

maximum value in the room temperature region and falls off for temperatures above and below room. Although this behaviour is generally agreed to, the amount of the temperature variation that has been reported is variable. Der Mateosian et al (1956) observed a decrease of the ^{137}Cs photopeak height of about 20% when the temperature of a NaI(Tl) crystal grown by the Bridgman method was reduced from room temperature to -40°C. A 45% decrease was observed under the same temperature shift for a crystal grown by the Kyropoulos method. They attributed the variability of the temperature effect to the increased density of electron traps present in the Kyropoulos pulled crystals. Meesen (1958) collates much of the previous work in this field and reports an approximately 55% decrease in the ^{137}Cs photopeak from room temperature to -30°C. In the present work the photopeak for ^{54}Mn was observed in crystal H5 to drop some 20% from 25°C to -60°C. This, however, includes the effects of temperature on the photomultiplier and its associated preamplifier.

The work of Cameron et al (1961) also indicates a decrease in the scintillation efficiency with decreasing temperature with a 50% drop from 20°C to -40°C. However, the total fluorescence efficiency, which includes the long-lived phosphorescent components, was found to increase with decreasing temperature (10% rise from 20°C to -40°C). They suggest that electron trapping sites become effective as the crystal temperature is lowered from room to -60°C. At the lower temperatures some electrons, arising from the absorption of the incident gamma ray, are likely to be held back in traps to be thermally freed at a later time. This diminishes the amplitude of the observed photopeak since the pulse amplifying system is usually constructed with a relatively short integrating time constant, typically 1 microsecond. Phosphorescence at room temperature was shown

by them to involve three levels of metastable states having mean lives of approximately 1, 5 and 40 minutes.

Much the same suggestion was made by Eby and Jentschke (1954) to explain the different scintillation efficiencies of alpha particles and deuterons. They concluded that differences in relative efficiency "must be explained entirely on the basis of the probability of exciting the radiative and various nonradiative states during the initial energy transfer process". Der Mateosian et al (1956) point out that this is the only mechanism which would allow the alpha particle to become more efficient than the electron.

Gwin and Murray (1963) suggested a model in which the main thallium excitation process was the successive capture of first an electron and then a hole. They interpreted the decrease in the Tl^+ scintillation with decreasing temperature on the basis of a reduced probability for thermal excitation of self-trapped holes. They did not exclude the possibility of thallous centre excitation by means of excitons.

It follows then that the room temperature scintillation pulse probably arises predominantly from the migration of independent electrons and holes to the Tl^+ centre (bottom process in fig. 5.2). The suppression of this mechanism with lowering temperature will result in a relative enhancement of the exciton transfer process. If this suggested interpretation of the temperature dependence of the scintillation efficiency is associated with the proposal of Van Sciver (1956) that the consecutive capture of an electron and a hole at the Tl^+ centre can result in the excitation of electronic states not normally accessible to the exciton, there results a possible explanation of the behaviour of the branching ratios observed in fig. 5.5.

Van Sciver (1956) uses the Wannier model for the exciton which pictures an electron and hole bound together by electrostatic force in a hydrogen-like structure (see for example Dexter and Knox, 1965). He suggests that exciton capture at a thallous ion site can only populate those excited states from which subsequent radiative transitions to ground are allowed, i.e. exciton stimulation is similar to ultraviolet excitation insofar as transition probabilities are concerned. In the case of the independent migration of electrons and holes, since the spins of the particles are uncoupled, the nature of the excited states which are populated will depend on the spins of the captured electron and hole. He argues that metastable states of the thallous ion centre will be accessible to the binary diffusion process which are not probable in the exciton case. The differences observed by Murray and Keller (1967) for the two methods of exciting the "intrinsic" luminescence in the pure alkali halides (section 5.1) may perhaps be explained on the same basis.

In fig. 5.5, the probability, f_7, of exciting the main decay component seven is seen to decrease with decreasing temperature while the probability of directly exciting what has been interpreted as the radiative state six becomes stronger. This is interpreted on the basis of a shift in energy transfer processes from predominatly electron/hole at room temperature to mainly exciton at reduced temperatures.

5.5 Scintillation Kinetics: Interpretation

It is tempting to associate the blocks of fig. 5.4 directly with electronic states in the crystal. If this is done $1/\tau_j$ becomes the transition probability from the $j^{\underline{th}}$ electronic state. In particular blocks A and C would represent metastable states of the thallous ion centre ($^3P_0$ and $^3P_2$) from which radiative transitions to ground are

forbidden. Block B may also be in this category but its multiple nature may require extracentre interpretation. The temperature dependence of the metastable time constants provides some insight into the configuration coordinate model of fig. 5.1(a). With reference to this figure, the life time τ of an electron in, say, the metastable state $^3P_0$ is proportional to the reciprocal of the probability of the electron acquiring sufficient energy through phonon interaction with the crystal to reach the transition point X. In the simplest form of the theory of thermal activation, the probability of freeing a trapped electron is given by

$$\alpha = \frac{1}{\tau} = S \exp(-\varepsilon/kT) \tag{5.14}$$

where: ε is the energy difference between the minimum of the $^3P_0$ curve and point X (the activation energy).

k is Boltzmann's constant,

T is the absolute temperature of the crystal,

S is a constant generally referred to as the frequency factor.

The details of a semiclassical approach to this problem involving successive absorption of phonons and, as well, a strict quantum mechanical treatment in terms of multiphonon transitions may be found in the text by Curie (1963, pp 144, 191, 208).

A semilogarithmic graph of decay time as a function of the reciprocal absolute temperature should indicate a linear relationship whenever the description of equation (5.14) is valid. In this work the figures indicating the temperature dependence of the various parameters have been plotted in this fashion. The frequency factors and activation energies obtained from an analysis of figs. 4.4 and 4.8 are given in table 5.2.

Table 5.2

Thermal Activation Parameters for Crystals H5 and H6

CRYSTAL	COMPONENT	FREQUENCY FACTOR (sec^{-1})	ACTIVATION ENERGY (eV)
H5	5	13×10^{9}	0.10
	6 (I)	13×10^{6}	0.02
	(II)	2×10^{12}	0.3
	7	2×10^{8}	0.09
	8	4×10^{8}	0.13
H6	4	5×10^{8}	0.07
	6 (I)	9×10^{6}	0.014
	(II)	8×10^{10}	0.2
	7	1×10^{8}	0.08
	8	3×10^{9}	0.17

These constants for the decay of the main room temperature component, number seven, agree fairly well with the work of Plyavin' (1959). An estimate, taken from the graph of the temperature dependence of the gamma stimulation of his component I, yields rough values of 1.1×10^{8} sec^{-1} and 0.1 eV for the frequency factor and activation energy. These results do not agree with those of Bonanomi and Rossel (1951, 1952) (see table 1.1). The disagreement of the work of Plyavin' (1958) using ultraviolet stimulation and that of Bonanomi and Rossel (1952) for alpha particle stimulation has been the cause of some concern to Birks (1964, p. 455). The difference is probably resolvable on the basis of the fairly complex character of the scintillation phenomenon and the general inadequacies of the early research apparatus.

The radiative component number six may be associated with the $^{3}P_{1}$ thallous ion state. The behaviour of the life time τ_6 may be interpreted on the basis of the superposition of radiative and nonradiative transitions to ground (thermal quenching). The theory of such a process is described by Payen de la Garanderie and Curie (1962) in which both transition probabilities are temperature dependent. In this work the temperature behaviour was simulated by the expression:

$$\alpha_6 = \frac{1}{\tau_6} = \alpha_I + \alpha_{II} \qquad (5.15)$$

in which each of the terms on the right hand side depends on the temperature through the form of equation (5.14). Rough values of the four parameters involved are given in table 5.2.

The interpretation of the scintillation kinetics is considerably more complicated if feedback paths are present in the block diagram of fig. 5.4. In particular, if block D has a transition pro-

bability not only to ground, but, as well, back to A, B, and C, the α_j that are observed will not in general be the transition probabilities between the indicated states. Under such circumstances the life times observed will be complex combinations of the actual life times present.

As a simple example of such a process, fig. 5.8 represents a metastable state A and a radiative state D, between which nonradiative transitions are possible in either direction. The rate constants are the α_k with $0 \leqslant f \leqslant 1$ representing the branching ratio for energy transmission to the two excited states of the centre. Presuming zero initial population of the two states A and D, the emission intensity as a function of time will be given by:

$$I(t) = N\alpha_0\alpha_1 \left[A_0 e^{-\alpha_0 t} + A_1 e^{-\beta_1 t} + A_2 e^{-\beta_2 t}\right] \tag{5.16}$$

where:

$$A_0 = \frac{\alpha_3 - f\alpha_0}{(\alpha_0 - \beta_1)(\alpha_0 - \beta_2)}$$

$$A_1 = \frac{\alpha_3 - f\beta_1}{(\beta_1 - \alpha_0)(\beta_1 - \beta_2)} \tag{5.17}$$

$$A_2 = \frac{\alpha_3 - f\beta_2}{(\beta_2 - \alpha_0)(\beta_2 - \beta_1)}$$

and:

$$\beta_1 = (\alpha + \sqrt{\alpha^2 - 4\alpha_1\alpha_3})/2$$

$$\beta_2 = (\alpha - \sqrt{\alpha^2 - 4\alpha_1\alpha_3})/2 \tag{5.18}$$

$$\alpha = \alpha_1 + \alpha_2 + \alpha_3 \tag{5.19}$$

Figure 5.8

Block Diagram for Luminescence Kinetics Involving Feedback

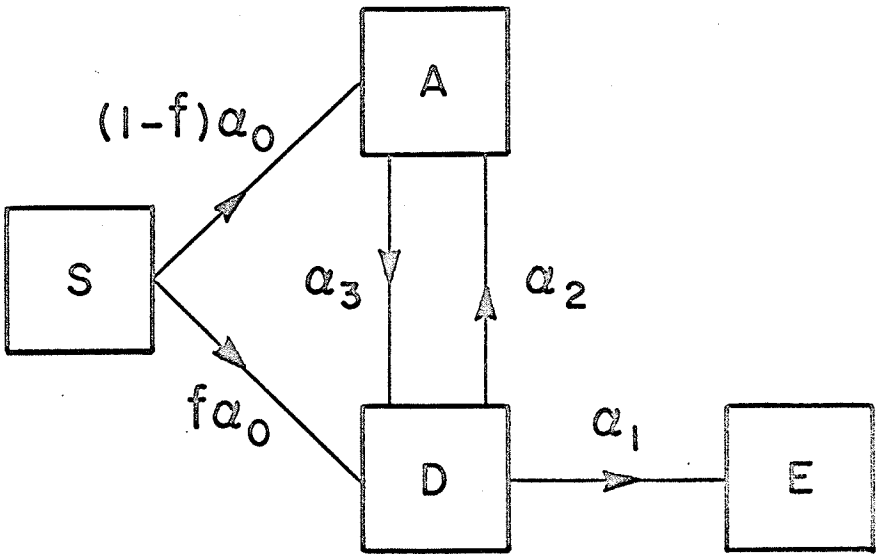

SIMPLE FEEDBACK SYSTEM

In equation (5.16), N is the number of photons in the resultant scintillation.

Experimentally one would observe in the luminescence pulse the time components: $1/\alpha_0$, $1/\beta_1$, $1/\beta_2$. In general, the effect of the feedback, α_2, is to shorten the apparent life time of the radiative state and to lengthen the apparent life time of the metastable state. The feedback mixes the effects of the paths through A and D so that it is no longer possible to decompose the pulse into branch contributions as was done in table 5.1. The inclusion of the extra parameter, α_2, renders indeterminate the branching ratio f and the rate constants α_1, α_2 and α_3. Interrelations between these parameters can be specified as well as upper and lower limits. For example, if the room temperature pulse shape of H5 is considered, and the long component eight is ignored, the limits on f are 0.18 and 0.89, $\alpha_3/f = 3.26 \times 10^7$ sec^{-1}, $\alpha_1 + \alpha_2 + \alpha_3 = 2.90 \times 10^7$ sec^{-1} and $\alpha_1\alpha_3 = 1.35 \times 10^{14}$ sec^{-2}.

A form of analysis which is an extreme case of the above feedback problem has been proposed by several authors, Plyavin' (1959), Vitol and Plyavin' (1960), Trinkler and Plyavin' (1965) in studies of the luminescence of KCl(Tl), KBr(Tl) and KI(Tl). In their arguments, the magnitude of the interaction of the thallous ion centre with lattice vibrations is considered to be sufficiently strong to produce a Boltzmann distribution among the various excited states of the centre, i.e. neighbouring levels of the excited state are in thermal equilibrium. Since the excitation of the crystal will generally result in an initial non-equilibrium distribution of excited states, the scintillation may be characterized by short-lived components until such time that thermal equilibrium is established. From then on, the pulse will be describable as a single relatively long

time constant exponential. Multiple long components are indicative of the presence of a number of different types of centres.

For the simple case of the system in fig. 5·8, let w be the energy difference between the minima of the configuration coordinates for the radiative state D and the metastable state A, with the latter lying lower. If the populations of D and A are x(t) and y(t) respectively, then the total number of excited states at any time, $n(t) = x(t) + y(t)$.

Then: $$\frac{dn}{dt} = -\alpha_1 x$$

and: $$\frac{dx}{dt} = \frac{dn}{dt} \cdot \frac{x}{n} = -\frac{\alpha_1 x}{(1 + y/x)}$$

Invoke a Boltzmann distribution at all times (neglecting any initial non-equilibrium distribution) i.e.

$$y(t)/x(t) = \exp(w/kT).$$

The emission intensity will then be given by

$$I(t) = \frac{n_0 \alpha_1}{1 + \exp(w/kT)} \exp(-t/\tau)$$

where:

(5.20) $$\tau = \frac{1 + \exp(w/kT)}{\alpha_1}$$

Equation (5.20) is quoted by Plyavin' (1959) for the case under discussion here.

This form of kinetics analysis thus predicts that the straight line portion of the $\ln(\tau)$ vs. $1/T$ graph will have a slope determined by w. This differs from the interpretation given earlier in equation (5.14) where the factor ε is the energy barrier between the two states. The Russian

analysis interprets the term α_1 not as a frequency factor but rather as the decay probability of the radiative state. For example, in the table 5.2 for crystal H5, this form of analysis would yield a radiative state life time of about 5 ns (the reciprocal of the frequency factor for component seven).

It is doubtful that this thermal equilibrium model can be applied successfully to the complex time behaviour that is indicated in this study of NaI(Tl). Looking first at the initial behaviour of the scintillation, the strong negative amplitude component at room temperature would have to be associated with an initial nonequilibrium distribution of states or, alternatively, with energy transport time to the thallous ion centre. The time constant involved was shown to range from 40 to 65 ns, which is improbably high for the latter possibility. This then suggests that time constants for thermal redistribution are of the order of 50 ns. It is implicit in the thermal equilibrium model that these nonradiative transition probabilities be much larger than the radiative probability, α_1, so that the Boltzmann distribution can be first achieved and then maintained. There is a contradiction since the radiative life time according to the Russian analysis is determined above to be about 5 ns. What is probably a stronger argument against the thermal equilibrium model is that it predicts but one long time constant exponential in the emission pulse for a given type of luminescent centre. Components six and seven are fairly definitely to be associated with the same centre and at temperatures just below 0°C contribute to two long time constant exponentials.

The Russian thermal equilibrium model for the intracentre kinetics of the thallous ion does not seem to apply in the case of NaI(Tl). There does not seem to be any obvious reason why the kinetics

should differ radically from a NaI host crystal to, say, a KI matrix. It is suggested that a scintillator such as KI(Tl) be studied using the photon sampling technique of this work. The resultant order of magnitude improvement in time and amplitude information would supplement the disputed interpretation given by Illingworth (1964) who was only able to estimate roughly decay times less than 300 ns and could not measure at all life times less than 50 ns.

5.6 Concluding Comments

The application of the photon sampling technique to the investigation of the luminescence of NaI(Tl) has been shown to result in a considerably more detailed description of the time processes involved than had been previously available. In addition to confirming some of the earlier measurements of the life times present in the scintillation, the technique has not only indicated hitherto unobserved components, but has also yielded the amplitudes of the various decay components.

Although the complexity revealed in the case of gamma excitation is difficult to resolve completely, some aspects of the kinetics involved in the luminescence have been made apparent. In the interpretation of the kinetics it has been suggested that the pulse shape changes that result from varying the crystal temperature are due in part to a change in the method of energy transport to the luminescent centres. Preliminary work which has been done on alpha stimulation has suggested that a rather larger fraction of the room temperature energy transfer is due to excitons than is the case when the crystal is gamma excited.

Further study is required to resolve the observed pulse shape dependence on thallium concentration. With the data that have been collected, it would seem that a model of the scintillator based on the

assumption of a dilute thallium impurity may be inappropriate for Tl concentrations of 0.1% and higher. Interactions between Tl^+ ions may be required to obtain a satisfactory explanation.

APPENDIX A - 1

AVALANCHE TRIGGER CIRCUIT

In the accompanying figure:

1. All capacitors in microfarads unless otherwise noted.
2. Transistor type 2N709 (selected) by RCA.
3. V_{cc} ranges from 35 to 45 volts depending on the particular transistor. V_{cc} is chosen equal to BV_{CBO} for the transistor as measured on a curve tracer.
4. Transistor base must be less positive than about 50 mV otherwise circuit is oscillatory.
5. Minimum trigger input required is approximately +0.25 V.
6. Adjust for a minimum trigger of 0.5 V.
7. Output pulse is approximately -0.7 V on a terminated RG58A cable.

Avalanche Trigger Circuit

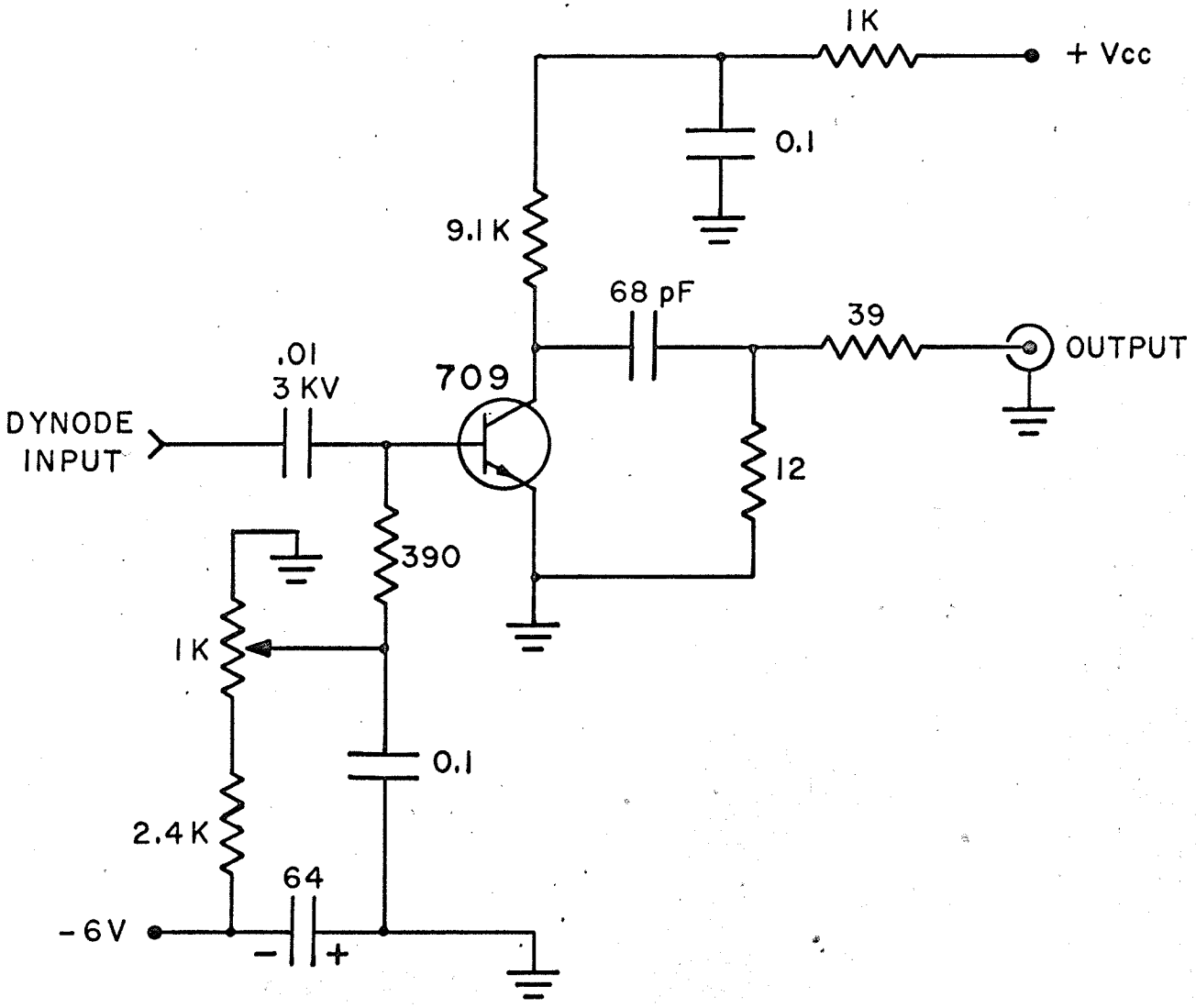

APPENDIX A - 2

PHOTOMULTIPLIER DIVIDER CHAIN

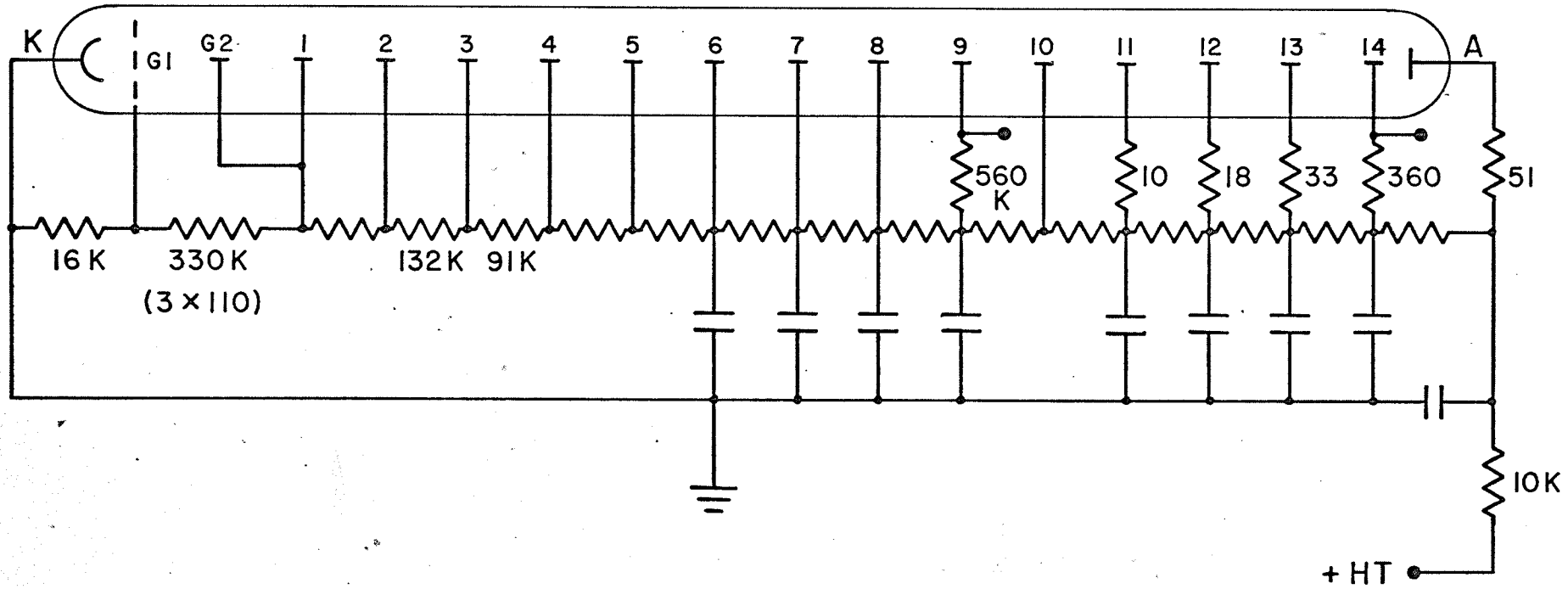

Notes:

1. All dynode resistors 1 Watt, 5%.
2. Unmarked dynode resistors 110 K.
3 All capacitors 0.01 μF, 3 KV.

APPENDIX A - 3

TEMPERATURE CONTROLLER

Temperature control below 0°C is achieved by liquid nitrogen coolant which is added to the interior of the insulated box as determined by a rise in temperature of the crystal thermocouple. The e.m.f. of the thermocouple is monitored by a Rubicon potentiometer and light-spot galvanometer. A photoresistor is mounted behind the galvanometer scale to intercept the light beam when the crystal temperature rises. The increased current through the photoresistor when it is illuminated is detected by a galvanometer relay which connects a resistor R, in parallel with one of the arms of the bridge in the Bayley temperature controller. The Bayley controller supplies 110 V, 15 A, to a power plug if its thermistor probe indicates a temperature below a preset limit. The arm of the bridge with which R is put in parallel is chosen such that the resultant bridge unbalance is interpreted by the bridge as a drop in temperature at the thermistor probe. The 110 V plug is then energized. This plug powers a small pump which supplies air pressure to a liquid nitrogen dewar, resulting in a flow of coolant to the insulated box. Because of the large thermal mass of the crystal chamber it is necessary to interrupt the liquid nitrogen flow to prevent excessive temperature swings. This is achieved by the simple expedient of connecting a 150 Watt light bulb in parallel with the air pump. This lamp is placed next to the bridge thermistor probe, acting as a heater. As soon as the thermistor temperature rises above the temperature determined by the bridge resistances and the shunt R, power will be removed from the 110 V plug. There results a periodic activation of the air pump the characteristics

of which are adjustable over a fairly wide range of frequency and duty cycle. Pumping ceases entirely as soon as the light spot drifts off the photoresistor. With some care, the system can be adjusted to yield a temperature oscillation at the crystal thermocouple of ± 0.1°C. More usual operating fluctuations were ± 0.5°C. Liquid nitrogen consumption when controlling at -90°C was about 20 liters in 24 hours.

APPENDIX A - 4

PRECISION CABLE LENGTH MEASUREMENT

One section of a multifunction pulse generator that has been constructed was designed for the precision measurement of the electrical length of coaxial cables.

In the accompanying schematic, the tunnel diode monostable can be converted into an oscillator by connecting cable to the BNC connector A. If the other end of the cable is an open circuit, and a momentary signal is injected into the tunnel diode (by simply turning on the power supply), the diode will trigger, the resulting pulse will propagate down the cable and be reflected back down the line to re-trigger the diode. The period of the oscillation will be approximately twice the length of the coaxial line. Output B is buffered from the tunnel diode by an emitter follower, while output C is a simple amplifier stage used to drive a high speed scaler.

The oscillation period can be determined either through an oscilloscope at B for rough work, or by counting the number of pulses in a known time interval at C. A difference technique is used to circumvent problems associated with the switching time of the diode and the fact that reflections occur at the open end of the cable. The period for a ballast cable, about 200 ns long, is first determined. Then the unknown cable is connected to A with the ballast at its far end. The new period is measured. The length of the unknown is half the difference in periodic times.

Precisions of the order of a few hundredths of a nanosecond are possible for cables as long as 200 ns. Longer cables can be measured by putting another tunnel diode trigger circuit at the open circuit end of the reflection cable.

Tunnel Diode Monostable

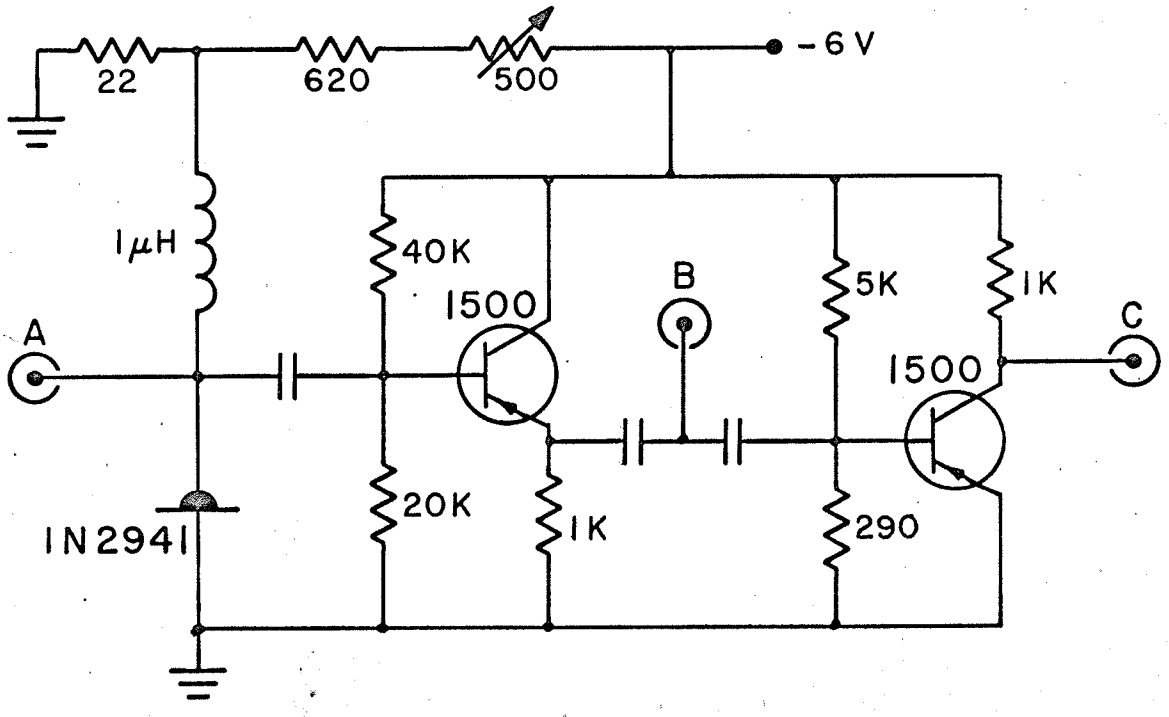

all capacitors 1 KpF

APPENDIX A - 5

OPTICAL FILTER TRANSMISSION CHARACTERISTICS

In the accompanying figure:

(a) Corning No. 9863.

(b) Glass window used in crystal containers.

(c) Corning No. 7380.

(d) Corning No. 3850.

For comparison, the relative response of the 56AVP photomultiplier is shown in curve (e).

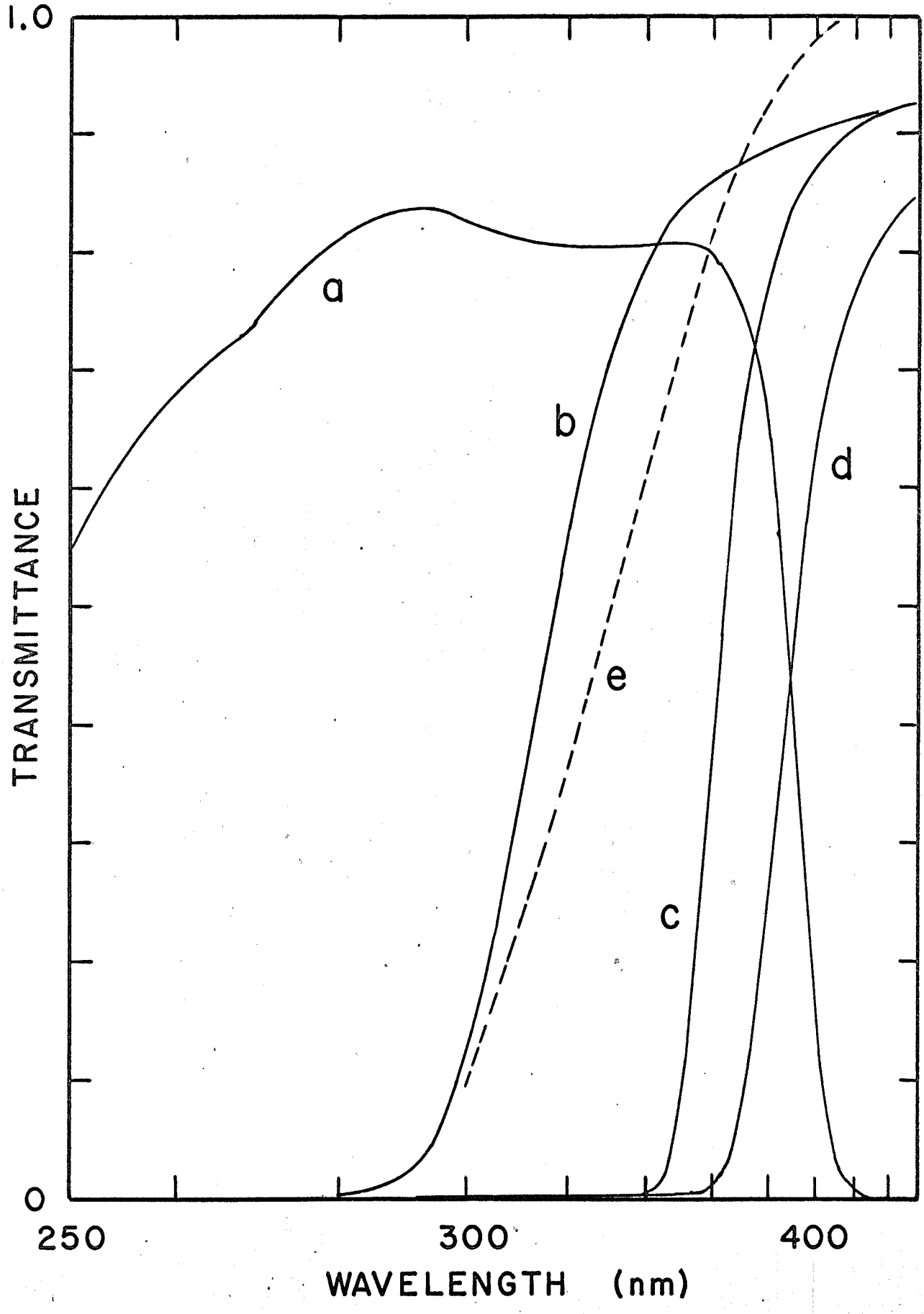
1.0
0
TRANSMITTANCE
250
300
400
WAVELENGTH (nm)
a
b
c
d
e

REFERENCES

Abramowitz, M. and Stegun, I. 1965. "Handbook of Mathematical Functions" (Dover Publications, New York), pp. 941, 985.

Bergsøe, P., Hansen, P. G. and Jacobsen, C. F. 1962. Nucl. Instr. Meth. 17, 325.

Birks, J. B. 1964. "The Theory and Practice of Scintillation Counting" (Macmillan Co., New York).

Bittman, L., Furst, M. and Kallmann, H. 1952. Phys. Rev. 87, 83.

Bollinger, L. M. and Thomas, G. E. 1961. Rev. Sci. Instr. 32, 1044.

Bonanomi, J. and Rossel, J. 1951. Helv. Phys. Acta 24, 310.

Bonanomi, J. and Rossel, J. 1952. Helv. Phys. Acta 25, 725.

Brody, S. S. 1957. Rev. Sci. Instr. 28, 1021.

Cameron, J. F., Clayton, C. G. and Spackman, R. A. 1962. "Nuclear Electronics" 1, 95 (I.A.E.A., Vienna).

Chase, R. L. and Higinbotham, W. A. 1957. Rev. Sci. Instr. 28, 488.

Chornii, Z. P. and Lyskovich, A. B. 1965. Opt. Spectry. 19, 248.

Cooke, I. and Palser, R. 1964. IEEE Trans Nucl. Sci. NS - 11, No. 3, 15.

Curie, D. 1963. "Luminescence in Crystals" (John Wiley and Sons, New York).

Cziffra, P. and Moravcsik, M. J. 1959.

Univ. of Calif. Radiation Lab Report, UCRL - 8523 Rev.

Delbecq, C. J., Hayes, W. and Yuster, P. H. 1961.

Phys. Rev. 121, 1043.

Delorme, R. and Perrin, F. 1929.

J. Phys. Rad. 10, 177.

Der Mateosian, E., McKeown, M. and Muehlhause, C. O. 1956.

Phys. Rev. 101, 967.

Dexter, D. L. and Knox, R. S. 1965.

"Excitons", (John Wiley and Sons, New York).

Eby, F. S. and Jentschke, W. K. 1954.

Phys. Rev. 96, 911.

Edgerton, R. 1965.

Phys. Rev. 138, A85.

Edgerton, R. and Teegarden, K. 1963.

Phys. Rev. 129, 169.

Edgerton, R. and Teegarden, K. 1964.

Phys. Rev. 136, A1091.

Emigh, C. R. and Megill, L. R. 1954.

Phys. Rev. 93, 1190.

Falk, W. R. and Katz, L. 1962.

Can. Jour. Phys. 40, 978.

Fowler, W. B. 1968. "Physics of Color Centres"

edited by W. B. Fowler (Academic Press, New York).

Gaviola, E. 1926.

Zeit. f. Phys. 35, 748.

Gold, R. 1965.

Rev. Sci. Instr. 36, 784.

Gwin, R. and Murray, R. B. 1963.

Phys. Rev. 131, 508.

Halling, H., Mayerhofer, S., Nabielek, H. and Ujlaki, E. 1967.

Nucl. Instr. Meth. 50, 22.

Helmer, R. G. and Heath, R. L. 1967.

Nucl. Instr. Meth. 57, 46.

Herb, G. K., Fontana, M. P. and Van Sciver, W. J. 1968.

Phys. Rev. 168, 1000.

Herget, W. F., Deeds, W. E., Gailan, N. M., Lovell, R. J. and Nielsen, A. H.

1962. J. Opt. Soc. Am. 52, 1113.

Hersh, H. N. and Hadley, W. B. 1963.

Phys. Rev. Letters 10, 437.

Hofstadter, R. 1949.

Phys. Rev. 75, 796.

Illingworth, R. 1964.

Phys. Rev. 136, A508.

Jablonski, A. 1933.

Nature 131, 839.

Johnson, P. D. and Williams, F. E. 1960.

Phys. Rev. 117, 964.

Johnson, R. P. 1939.

J. Opt. Soc. Am. 29, 283, 387.

Kabler, M. N. 1964.

Phys. Rev. 136, A1296.

Kirkbride, J., Yates, E. C. and Crandall, D. G. 1967.

Nucl. Instr. Meth. 52, 293.

Koch, L., Koechlin, Y., Mougin, B. and Tregeur, L. 1959.

"Nuclear Electronics" 1, 53 (I.A.E.A., Vienna).

Knox, R. S. 1959.

Phys. Rev. 115, 1095.

Knox, R. S. and Dexter, D. L. 1956.

Phys. Rev. 104, 1245.

Knox, R. S. and Teegarden, K. J. 1968. "Physics of Colour Centers"

ed. W. B. Fowler (Academic Press, New York), p.1.

Koechlin, Y. 1964.

Trans. N. Y. Acad. Sci. 27, 227.

Kristofel', N. N. 1960.

Opt. Spectry. 9, 324.

Kristofel', N.N. and Zavt, G. S. 1966.

Opt. Spectry. 20, 373.

Kuchnir, F. T. and Lynch, F. J. 1968.

IEEE Trans. Nucl. Sci. NS - 15, No. 3, 107.

Lanczos, C. 1956. "Applied Analysis"

(Prentice-Hall, New Jersey) p. 272.

Lefevre, H. W. and Russel, J. T. 1959.

Rev. Sci. Instr. 30, 159.

Lundby, A. 1950.

Phys. Rev. 80, 477.

Lynch, F. J. 1966.

IEEE Trans. Nucl. Sci. NS - 13, No. 3, 140.

Lynch, F. J. 1968.

IEEE Trans. Nucl. Sci. NS - 15, No. 3, 102.

McGuire, R.L. Yates, E.C., Crandall, D.G. and Hatcher, C.R.

1965. IEEE Trans. Nucl. Sci. NS - 12, No. 1, 24.

Meessen, A. 1958.

J. Phys. Rad. 19, 437.

Meyer, A. and Murray, R.B. 1962.

Phys. Rev. 128, 98.

Moore, R.H. and Zeigler, R.K. 1959.

Los Alamos Scientific Lab. Report, LA - 2367.

Murray, R.B. and Keller, F.J. 1965.

Phys. Rev. 137, A942.

Murray, R.B. and Keller, F.J. 1967.

Phys. Rev. 153, 993

Murray, R.B. and Meyer, A. 1961.

Phys. Rev. 122, 815

Nyberg, D.W. and Colbow, K. 1967.

Can. J. Phys. 45, 3333.

Orear, J. 1958. Univ. of Calif. Radiation Lab Report.

UCRL - 8417.

Owen, R.B. 1959. "Nuclear Electronics" 1, 27

(I.A.E.A., Vienna).

Payen de la Garanderie, H. and Curie, D. 1962.

"Luminescence of Organic and Inorganic Materials."

edited by H.P. Kallmann and G.M. Spruch.

(John Wiley and Sons, New York) p.334.

Perrin, F. 1926.

J. Phys. Rad 7, 390.

Perrin, F. 1929.

Ann. Phys. (Paris) 12, 169.

Pertsev, A. N., Pisarevskii, A. N. and Soshin, L. D. 1965.

Opt. Spectry. 18, 366.

Phillips, H. B. and Swank, R. K. 1953.

Rev. Sci. Instr. 24, 611.

Plyavin', I. K. 1958.

Opt. i Spektroskopiya 4, 266.

Plyavin', I. K. 1959.

Opt. i Spektroskopiya 7, 71.

Potekhina, N. D. 1960.

Opt. Spectry. 8, 437.

Rautian, S. G. 1958.

Uspekhi Fiz. Nauk 66, 475.

Robertson, J. C. and Lynch, J. G. 1961.

Proc. Phys. Soc. 77, 751.

Rollett, J. S. and Higgs, L. A. 1962.

Proc. Phys. Soc. 79, 87.

Seitz, F. 1938.

J. Chem. Phys. 6, 150.

Seitz, F. 1954.

Rev. Mod. Phys. 26, 7.

Singer, S., Neher, L. K. and Ruehle, R. A. 1956.

Rev. Sci. Instr. 27, 40.

Startsev. V.I. Baturicheva. Z.B. and Tsirlin, Yu, A. 1960.

Opt. Spectry. 8. 286.

Stoddart, L.C. and Berger, R.L. 1965.

Rev. Sci. Instr. 36, 85.

Stokes, G.Q. 1852.

Phil. Trans. Roy. Soc. London A142, II, 463.

Storey, R.S., Jack, W. and Ward, A. 1958.

Proc. Phys. Soc. 72, 1.

Swank, R.K. and Brown, F.C. 1963.

Phys. Rev. 130, 34.

Taylor, J.W. and Hartman, P.L. 1959.

Phys. Rev. 113, 1421.

Trinkler, M.F. and Plyavin', I.K. 1965.

Phys. Stat. Sol. 11, 277.

Van Sciver, W.J, 1956.

IRE Trans Nucl. Sci. NS - 3, No. 4, 39.

Van Sciver, W.J. 1958.

"Nuclear Electronics" 1, 37 (I.A.E.A., Vienna).

Van Sciver, W.J. 1960.

Phys. Rev. 120, 1193.

Van Sciver, W.J. 1964.

Phys. Letters 9, 97.

Van Sciver, W.J. 1966.

IEEE Trans. Nucl. Sci. NS - 13, No. 3, 138.

Van Sciver, W.J. and Bogart, L. 1958.

IRE Trans. Nucl. Sci. NS - 5, No. 3, 90.

Van Sciver, W. J. and Hofstadter, R. 1955.

Phys. Rev. 97, 1181.

Vitol, I. K. and Plyavin', I. K. 1960.

Opt. Spectry. 9, 189.

Wall, W. R. 1956.

Thesis, University of Manitoba.

Wall, W. R. and Roulston, K. I. 1965. Cong. Can. Assoc. Phys.,

abstracted Phys. in Canada 21, 34.

Wall, W. R. and Roulston, K. I. 1966.

Bull. Am. Phys. Soc. 11, 478.

Wall, W. R. and Roulston, K. I. 1968.

IEEE Trans. Nucl. Sci. NS - 15, No. 3, 153.

Watts, H. V., Reiffel, L. and Oestreich, M. D. 1962.

"Nuclear Electronics" 1, 3. (I.A.E.A., Vienna).

Weber, W., Johnstone, C. W. and Cranberg, L. 1956.

Rev. Sci. Instr. 27, 166.

Wenzelburger, H. 1967.

Nucl. Instr. Meth. 48, 341.

Williams, F. E. 1951.

J. Chem. Phys. 19, 457.

Williams, F. E. and Hebb, M. H. 1951.

Phys. Rev. 84, 1181.

Wood, R. F. 1966.

Phys. Rev. 151, 629.

Yuster, P. H. and Delbecq, C. J. 1953.

J. Chem. Phys. 21, 892.

Zecchi. 1652. in "Luminescence of Inorganic Solids" p. 4.

Ed. P. Goldberg (Academic Press, New York, 1966).